UNIVERSITY OF NAPLES "FEDERICO II"

FACULTY OF ENGINEERING

DEPARTMENT OF INDUSTRIAL ENGINEERING
AEROSPACE DIVISION

A THESIS SUBMITTED FOR THE DEGREE OF
DOCTOR OF PHILOSOPHY

PHD SCHOOL OF AEROSPACE, NAVAL AND QUALITY ENGINEERING

Numerical implementation of damage and fracture models for progressive damaging simulation in composite material structures

SCHOOL COORDINATOR:
Prof. Luigi De Luca

TUTOR:
Prof. Leonardo Lecce

CANDIDATE:
Ing. Leandro Maio

2013

Contents

INTRODUCTION

Recent developments in the aviation industry to improve fuel efficiency and extent of the flight autonomy have accelerated the interest in the use of advanced composites as primary structural materials. Composite materials offer the possibility to design stiffness and strength characteristics of the final structure by suitably selecting the type of reinforcing fibers and the distribution of the reinforcing directions and allow to adapt these features as a function of the applied loads and structural requirements.

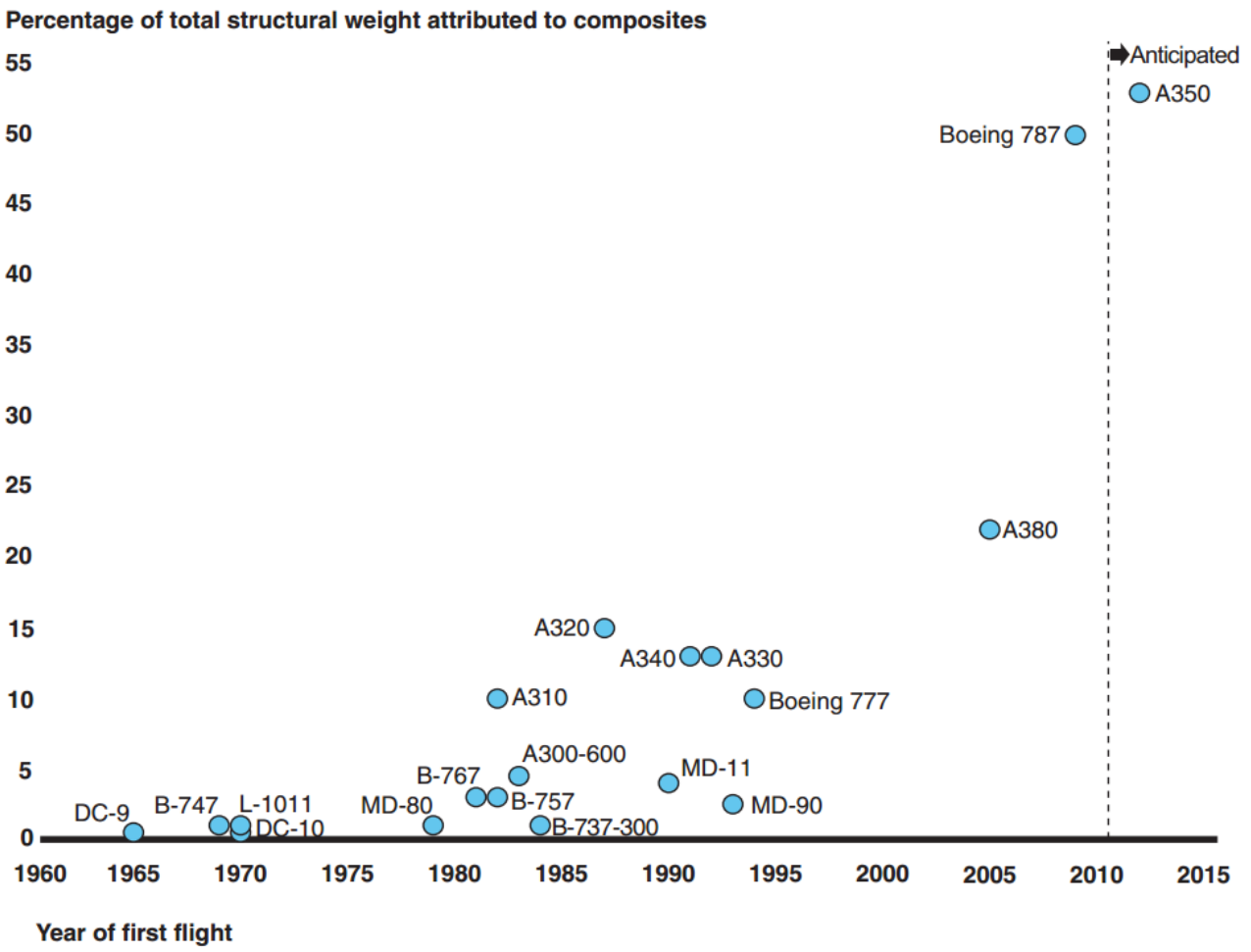

Sources: GAO analysis of information from FAA (GAO-11-849, Sep. 21, 2011), NASA, Boeing Company, "Jane's All the World's Aircraft" and "Jane's Aircraft Upgrades".

They are being used for decades in transport airplane components. Prior to the mid-1980s, composite materials were used in transport category airplanes in secondary structures (e.g. wing edges) and control surfaces. The A320, introduced by Airbus in 1988, was the first airplane in production with an all-composite tail section; afterwards, in 1995, the commercial airplane 777, introduced by Boeing Company, was also with a composite tail section. In recent years, manufacturers have expanded the use of composites to the fuselage and wings because these materials are typically lighter and more resistant to corrosion than metallic materials that have been used traditionally in airplanes. In 2009, the Boeing 787 Dreamliner has become the first mostly composite large transport airplane in commercial service; it is about 50 percent composite by weight (excluding the engines); this airplane will be probably followed soon by the Airbus A350, having composite material roughly in the same proportion as its Boeing competitor (see Jackson PA, Hunter J, Daly M, *Jane's All the World's Aircraft* 2012/2013, Jane's 626 Information, Group, 2012). Some concerns have been raised related to the use of large proportion of composite on an airplane structure. These concerns mainly originated from the state of the science underpinning the expanded use of composite materials in commercial transport category airplanes, and the lack of experience with such design.

The Government Accountability Office (GAO) studied how the US Federal Aviation Administration (FAA) and the European Aviation Safety Agency (EASA) certificated the 787. The GAO in the report *Status of FAA's Actions to Oversee the Safety of Composite Airplanes* (GAO-11-849, Sep. 21, 2011) identified four concerns:

- *limited information*: these regard the composite airframe structure behavior when they are damaged and as they age. The concerns are due to the limited in-service experience with composite materials used in the commercial aircraft structure and to the limited available information on the behavior of these materials compare to information on the metal behavior. Damage prediction is very important because it help form the basis for a new

airplane's design or maintenance program but the limited amount of in-service performance data available to use as inputs to the models may create challenges for airplane designers.

- *technical concerns*: these regard the challenges in detecting and characterizing damage in composite structures, as well as making adequate composite repairs. The damage in composites subjected to impact loading is unique and it may not be visible or may be barely visible, making it more difficult for a technician to detect than damage to metallic structures. In addition, the ability of composite nondestructive inspection techniques to adequately detect damage depends on the composite's construction and the type of damage (e.g., delamination, disbonding, or water infiltration). Thus, damage may not be detected sufficiently or properly if repair technicians do not use or apply the correct nondestructive inspection technique. Furthermore, the strength of a bonded composite repair after it is completed can't be measured by a nondestructive inspection technique. Composite repairing is also a concern partly because composite repairs are more susceptible to human error than metal repairs and because the quality (i.e., achieving the anticipated strength) of a composite repair is highly dependent on the process used.

- *limited standardization*: composite materials and repair techniques are less standardized than metal materials and repairs and this can be attributed to business proprietary practices and the relative immaturity of the application of composite materials in airframe structures

- *level of training and awareness*: these concerns regard repair technicians, designees, airport workers, FAA aviation safety inspectors receive that have worked with metal materials for decades generally may not be as familiar with composite materials, whose application in airplanes is relatively recent and whose unique characteristics are associated with technical challenges. Thus, repair technicians, designees, FAA agents, need adequate training about composites.

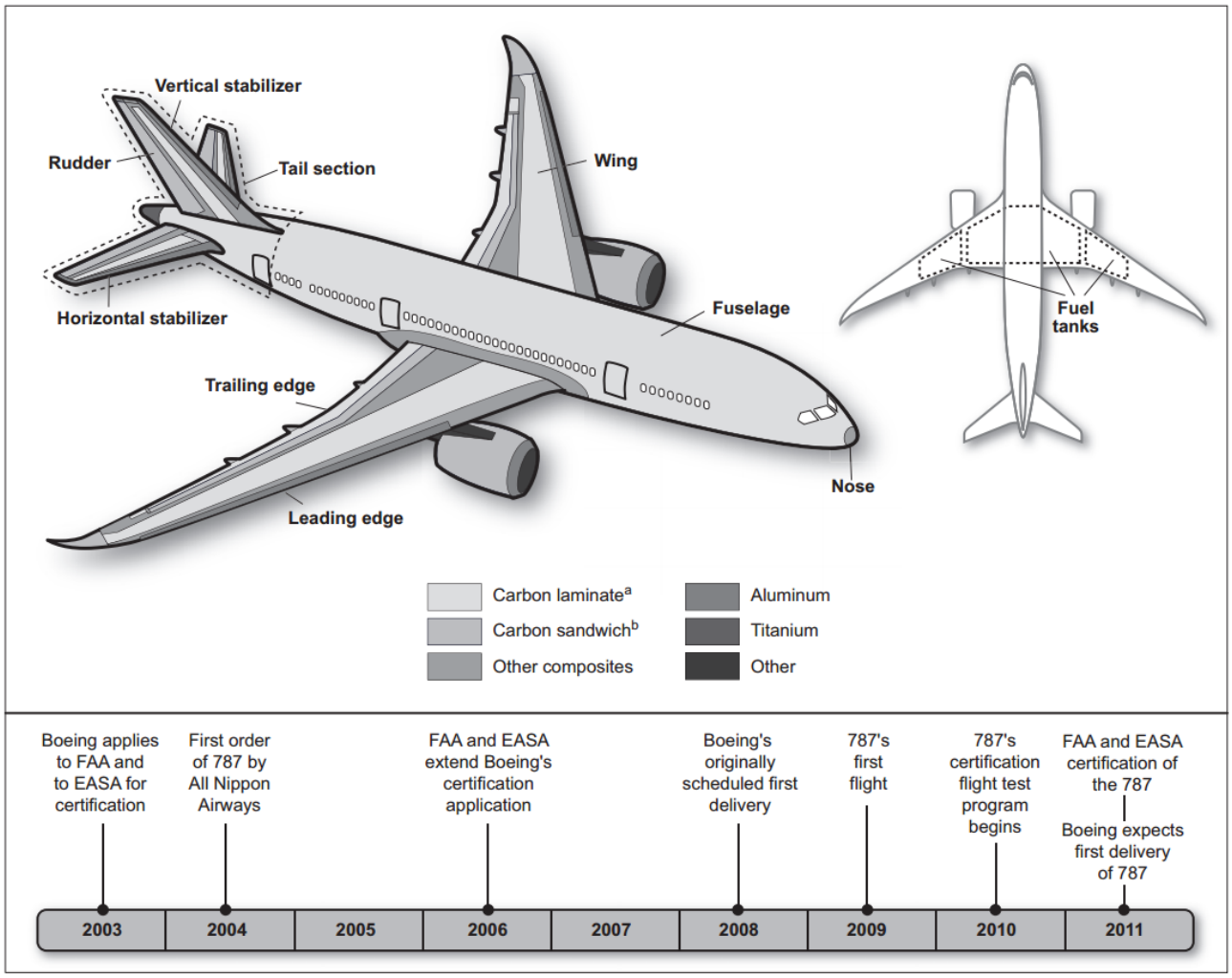

Source: GAO presentation of Boeing Company information (GAO-11-849, Sep. 21, 2011).

a. Carbon laminate is a composite structure produced by layering sheets of carbon fiber materials one on top of the other until the product meets a specified thickness.

b. Carbon sandwich is a composite structure involving the layering of carbon fiber sheets on top of a honeycomb structure.

Among the above identified problems resulting from the use of composite materials, the damaging and its prediction are the focus of this work. The reason for this choice is that there is a need to better understand the complex and multiple mechanisms of damage in composite structures and to develop failure theories and damage prediction model more reliable. In this context, the damage prediction tools have become increasingly important because composite structural testing is very expensive for industry. One of the most powerful computational methods for the composite structure analysis is the finite element method. In this research are examined and developed some of the most recent studies in the field of damage prediction and it will describe the issues associated to

the application of these methods to composite structures. In detail the objective of the conducted research program is to enhance the damage prediction model capabilities for unidirectionally reinforced continuous carbon fiber reinforced polymers (CFRP). For this purpose, a cohesive-frictional model for the prediction of interlaminar damage (delamination) and a non-local constitutive model for intralaminar progressive damage simulation in composite laminated structures were defined. The proposed constitutive models were developed for explicit solver of commercial finite element software ABAQUS which has demonstrated to be a powerful tool for implementation of FORTRAN Vectorized User-Material (VUMAT) and for the simulation of discontinuous and unstable events.

CHAPTER 1

THE COMPOSITE MATERIALS

1.1 Introduction to composite materials

The term *composite material* signifies that two or more distinct materials are combined on a macroscopic scale to form a useful third material. While each component material retains its identity, the new composite material displays macroscopic properties better than its parent constituents, particularly in terms of mechanical properties and economic value. Therefore the advantage of composite materials is that their variable composition enables the engineer to design the final material itself which gives the design an additional degree of freedom; if well designed, they usually exhibit the best qualities of their constituents and often some qualities that neither constituent possesses.

Applications of composites include aerospace, aircraft, automotive, marine, energy, infrastructure, armor, biomedical and recreational (sports) applications. The high-stiffness, high-strength and low-density characteristics make composites highly desirable in primary and secondary structures of both military and civilian aircraft. The strongest sign of acceptance of composites in civil aviation is their use in the new Boeing 787 "Dreamliner" and the world's largest airliner, the Airbus A380. The Boeing 777, for example, uses composite materials, such as carbon/epoxy and graphite/titanium, for approximately 50% of the weight of the Boeing 787, including wings, fuselage, horizontal and vertical stab, wing/body fairing, and most of the interior partitions and stow bins. Another good example of a composite in the flying world is the B-2 or Stealth Bomber, see Fig. 1.1. The body is engineered to deflect radar away from detection and the body and parts of the wings are covered in a radar absorbing composite material, making it virtually undetectable to radar.

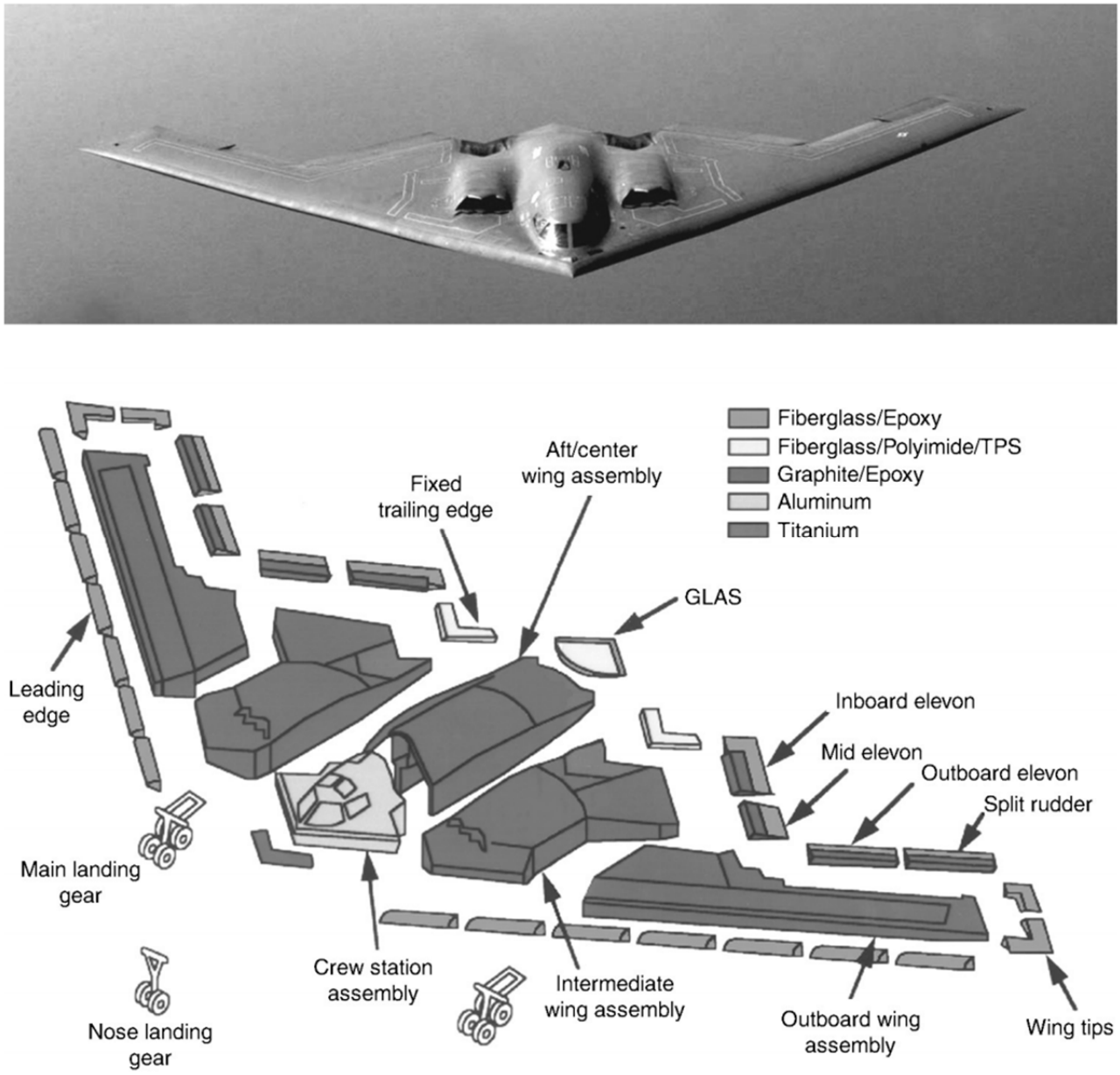

Fig. 1.1 - The U. S. Air Force B-2 advanced “stealth” bomber, which is constructed to a large extent of advanced composite materials. Source: D. B. Miracle, S. L. Donaldson, Introduction to Composites, Air Force Research Laboratory.

In contrast to metallic alloys, in a composite material each constituent retains its separate chemical, physical, and mechanical properties. The constituents are a reinforcement and a matrix. The fibers can be made of metals, organic materials, carbon and glass, while the matrix materials are often polymers, metals, ceramics, carbon, etc. The composites can be classified according to matrix material. They can also be classified according to the shape of the filler [1].

If the composite is classified according to the matrix the distinction is the following:

- polymer matrix composites, PMC: materials with high specific mechanical properties;
- metal matrix composite, MMC: improved resistance to high temperature;
- ceramic matrix composites, CMC: to improve the toughness.

If the composite is classified according to the filler the distinction is the following:

- composites with particulate inclusions;
- composites with fiber inclusions:
    - short fibers;
    - long fibers.

Overall, the properties of the composite are determined by [2]:

1. the properties of the fiber:
2. the properties of the matrix;
3. the ratio of fiber to matrix in the composite (*fiber volume fraction*);
4. the geometry and orientation of the fibers in the composite.

However the ratio of the fiber to matrix derives largely from the manufacturing process used to combine matrix with fiber and weakly from the design of composite. In addition, the manufacturing process used to combine fiber with matrix leads to varying amounts of imperfections and air inclusions that reduce the performance of the material. In the following sections the constituent materials used in composite processing will be presented individually.

1.2 The fiber reinforcement

The good mechanical properties of composites are obtained through a suitable subdivision of the mechanical roles of reinforcement and fibers, in order to minimize the global weight [3].

The reinforcement is usually a fiber or a particulate. Particulate may be spherical, platelets, or any other regular or irregular geometry. Particulate composites tend to be much weaker and less stiff than continuous fiber composites, but they are usually much less expensive. The most familiar example of the particulate composite materials is concrete used in a lot of construction work. Concrete is formed by bonding particles of sand and gravel together in a cement matrix, which has chemically reacted with water and hardened. As regards the fibers, instead, they can be particles, short fibers with a random orientation or continuous fibers. A fiber has a length and its diameter; the length-to-diameter ratio is known as the *fiber aspect ratio* and it can vary greatly. Continuous fibers have long aspect ratios, while discontinuous fibers have short aspect ratios. Continuous-fiber composites normally have a preferred orientation, while discontinuous fibers generally have a random orientation. Examples of continuous reinforcements include unidirectional, woven cloth, and helical winding (Fig. 1.2a), while examples of discontinuous reinforcements are chopped fibers and random mat (Fig. 1.2b) [4].

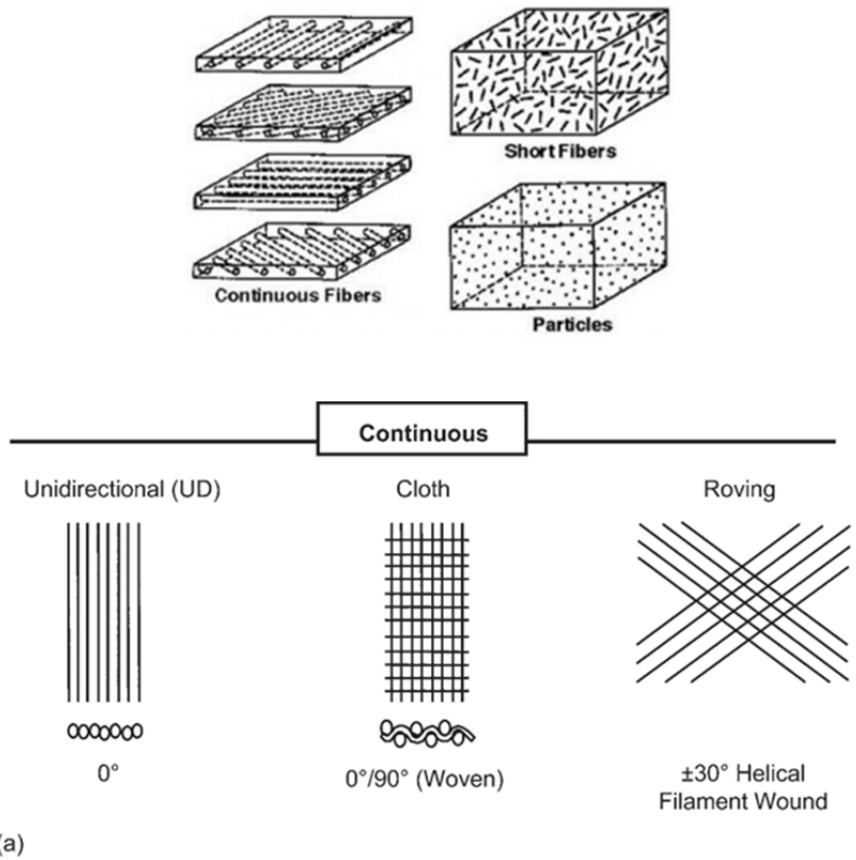

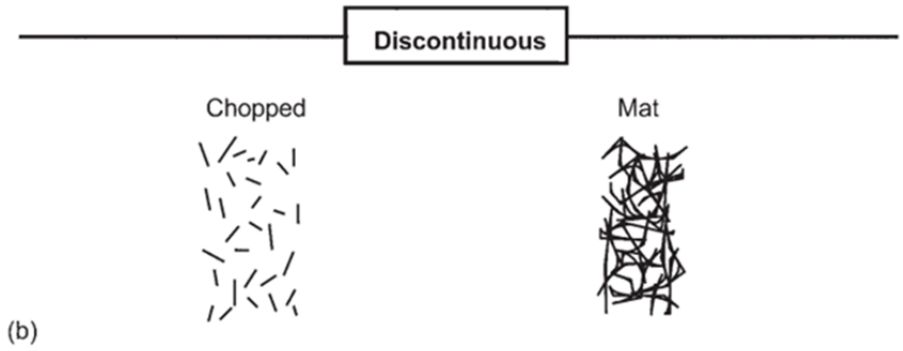

Fig. 1.2 - Reinforcement types [4]: unidirectional, woven cloth, and helical winding (a); chopped fibers and random mat (b).

However continuous-fiber composites are often made into laminates by stacking single sheets of continuous fibers in different orientations to obtain the desired strength and stiffness properties with fiber volumes as high as 60 to 70 percent.

Fibers produce high-strength composites because of their small diameter; they contain far fewer defects (normally surface defects) compared to the material produced in bulk. As a general rule, the smaller the diameter of the fiber, the higher its strength, but often the cost increases as the diameter becomes smaller. In addition, smaller-diameter high-strength fibers have greater flexibility and are more amenable to fabrication processes such as weaving or forming over radii [5].

In general, since the mechanical properties of most reinforcing fibers are considerably higher than those of un-reinforced matrix systems, the higher the fiber volume fraction the higher will be the mechanical properties of the resultant composite material. Therefore the mechanical properties of the fiber/matrix composite are dominated by the contribution of the fiber to the composite. However in practice there are limits, since the fibers need to be fully coated in matrix to be effective, and there will be an optimum packing of the generally circular cross-section fibers.

The fiber reinforcement give the stiffness and resistance to the composite material. The mechanical load is taken by the fibers and these can be oriented to provide properties in directions of primary loads; their role is, therefore, of fundamental importance to obtain good overall mechanical properties. The major importance characteristics of most reinforcing fibers are, therefore, high

strength, high stiffness, and low density. Most fibers show behavior which can be defined as elastic brittle, i.e., the stress–strain response is linear elastic until the fiber breaks [3]. Although many textile yarns fibers can be used for the matrix reinforcement only four principal classes dominate; they are:

- glass fibers;
- carbon (graphite) fibers (high modulus or high strength);
- aramid fibers (very light);
- boron fibers (high modulus or high strength).

Others fiber types include natural polymers such as cellulosics (jute, flax and cotton) and synthetic polymers (polyamide, polyethylene, polypropylene) but these are less used. Typical values of the mechanical properties of fibers are shown in Tab. 1.1.

The glass fibers are the most commonly used in low to medium performance composites due to their low cost. This fiber type shows isotropic behavior. The glass fibers have good tensile strength and low cost, but unfortunately their stiffness is not very high and they suffer from low fatigue endurance and property degradation due to severe hygrothermal conditions.

The carbon fibers are used in high-performance composites; they have high stiffness, high tensile strength, low weight, high chemical resistance, high temperature tolerance but low compressive strength and low thermal expansion and these properties make them very popular in aerospace, civil engineering, military, and motorsports, along with other competition sports. However, they are relatively expensive when compared to similar fibers, such as glass fibers. Values of stiffnesses and strengths vary depending on the processing temperature and usually the increase in stiffness is obtained at the expense of strength. Unlike the glass type, carbon fibers are highly anisotropic; in fact, the stiffness of the fiber in axial direction is much higher than that in radial direction, usually the transverse modulus, perpendicular to the fiber axis, is 3–10% of the axial modulus [3]. As already said, carbon fibers have also high resistance to temperature; they can be heated above

2000°C retaining their properties, of course this relevant property cannot be exploited in polymer matrix composites, due to the limited resistance to temperature of most matrices, but it can be exploited advantageously in carbon/carbon composites.

Other kinds of fibers, less used, are quoted here, such as aramid and boron. Aramid fibers are organic; they have high stiffness and tensile strength and high moisture absorption and they show an anisotropic behavior. Thanks to their toughness aramid fibers are used where high impenetrability is required, e.g. bulletproof vests; however, their high water absorption, and their difficult post-processing do not allow a wide use of these fibers. Boron fibers have high stiffness and high cost. Their strengths often compare with those of glass fibers, but their tensile modulus is high, almost four to five that of glass. The technology of the boron fibers is very expensive, factor that together with its high density, it has led to a substantial abandonment.

	Specific weight, γ (kN/m^3)	Young's modulus, E (GN/m^2)	Specific modulus E/γ (Mm)	Tensile strength σ^R (MPa)
Al	26.3	73	2.8	500
Ti	46.1	115	2.5	1500
Steel	76.6	207	2.7	
Glass S	24.4	86	3.5	3500
Carbon (high strength)	18	228-262	14	3000-4500
Carbon (high modulus)	18	353-393	21	2500

Tab. 1.1 - Mechanical properties of fibers and metal alloys. It is observed that the fibers have high structural efficiency: high strength and high elastic modulus with minimum weight.

1.3 The matrix phase

The matrix in a composite material has the task of acting as filling material. Initially in the state of viscous fluid in order to fill all the spaces and perfectly adhere to the reinforcement, it undergoes a process of solidification which allows to give stability and geometry to the structure. Therefore the

matrix is the component that holds the reinforcement together to form the bulk of the material. It has the function to support and protect the reinforcement phase and to provide a means of transmitting the loads between the filler. The filler or reinforcement is the material that has been impregnated in the matrix to lend its advantage (usually strength) to the composite. In a fiber-reinforced composite, the matrix (continuous phase) performs several critical functions, including mainly the maintenance of the fibers in the proper orientation and spacing and protecting them from abrasion and the environment; moreover, keeping the fibers separated decreases cracking and redistributes the load equally among all fibers. Thus, the matrix contributes greatly to the properties of the composites. The ability of composites to withstand heat, or to conduct heat or electricity depends primarily on the matrix properties since this is the continuous phase. Therefore, the matrix selection depends on the desired properties of the composite being constructed. There are three main types of matrices: polymer, metal, and ceramic. In polymer and metal matrix composites that form a strong bond between the fiber and the matrix , the matrix transmits external loads from the matrix to the fibers through shear stress at the interface [4]; indeed in ceramic matrix composites, the objective is often to increase the toughness rather than the strength and stiffness; therefore, a low interfacial strength bond is desirable.

The plastic composites, the ones whose matrix consists of a plastic material, are without doubt the most famous and popular both for their application modes within everyone's means who don’t have sophisticated technologies and decreasing costs. They have supplanted other materials in a wide range of applications, and today they come to use in real structural elements. Polymer matrices can be subdivided into two main classes: thermosetting and thermoplastic. Main types of thermosetting matrices for composite materials are: phenolics; unsatured polyesters; epoxies; polyimides and bismaleimides. Indeed the main types of thermoplastic matrices for composite materials are: polyolefins (PE, PP); thermoplastic polyesters (PET, PBT, LCP); polyamides (PA6, PA66); polyaryl ethers (PEEK); thermoplastic polyimide (PEI, PAI, LARC); polyaryl sulphides (PPS).

As general distinctive properties thermosetting matrices can be used approximately for temperatures below, they have good strength, and low fracture toughness. Thermosetting resins are the most used in engineering applications, among them it's possible to find polyester and epoxy matrices, the latter being standard for aerospace applications. The thermoplastic matrices are more expensive, they can be used for temperatures higher than 2001, have good strength, and high toughness.

Typical values of the mechanical properties of polymer matrices, taken from Ref. [3,6] are shown in Tab. 1.2.

Matrix	*Density* (Mg/m^3)	*Young's modulus* (GPa)	*Poisson's ratio*	*Tensile strength* (GPa)	*Failure strain* (%)
Thermoset epoxy resin	1.1–1.4	3.0–6.0	0.38–0.40	0.035–0.1	1.0–6.0
Thermoplastic PEEK	1.26–1.32	3.6	0.30	0.17	50.0

Tab. 1.2 - Mechanical properties of thermosetting and thermoplastic matrices. It is important to note that the these properties are significantly lower than those of the reinforcement.

From the data in Tab. 1.2 it can be appreciated that the main difference between thermosets and thermoplastic matrices is the value of failure strain; in fact, as previously observed, thermoset matrices are brittle materials, while thermoplastic ones can undergo plastic deformation (permanent deformation). Furthermore, another important difference between thermosetting and thermoplastic matrices concerns their resistance to high temperatures, which is much higher in thermoplastic polymers [3].

1.4 Laminated composites

One of the most popular composites are the so called continuous fiber reinforced composite materials (sometimes referred to as long fiber reinforced composites). This type of materials consist of reinforcing continuous fibers of certain orientation which are embedded in a matrix system. In this combination the fibers give the material outstanding strength and stiffness while the matrix

allows for the force transmission between fibers. The type and quantity of the reinforcement determine the final properties. In Fig. 1.3 it's shown that the highest strength and modulus are obtained with continuous-fiber composites. There is a practical limit of about 70 volume percent reinforcement that can be added to form a composite [3]. At higher percentages, there is too little matrix to support the fibers effectively.

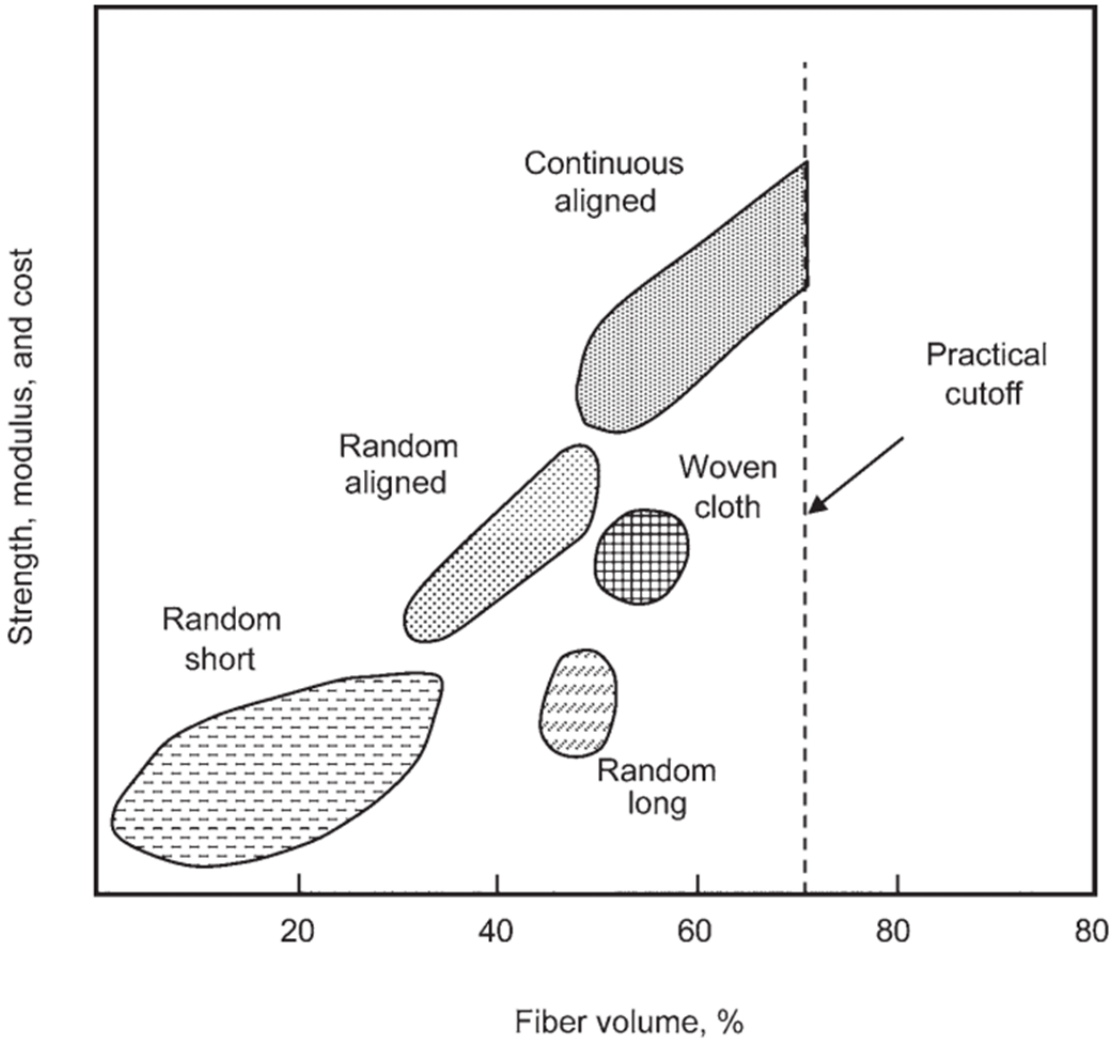

Fig. 1.3 - Influence of reinforcement type and quantity on composite performance [4].

Since reinforcing fibers are designed to be loaded along their length, and not across their width, the orientation of the fibers creates highly 'direction-specific' properties in the composite. This

"anisotropic" feature of composites can be used to good advantage in designs, with the majority of fibers being placed along the orientation of the main load paths.

Composites are usually built up of separate thin layers of fibers and matrix, called *ply* or *lamina*. A single lamina with only one orientation of the fibers is called unidirectionally (UD) reinforced. Often laminas of different fiber orientations are stuck together to form a laminate. So, laminated composite materials or simply a *laminate* consist of layers of various materials (stacked plies). Because the fiber orientation directly impacts mechanical properties, it seems logical that the stacking sequence of laminas is optimised thus giving the laminate the desired stiffness and strength for a given application.

In forming fiber reinforcement, the assembly of fibers to make fiber forms for the fabrication of composite material can take the following forms:

- unidimensional: unidirectional tows (consist of thousands of filaments, each filament having a diameter of between 5 and 15 micrometers), yarns, or tapes;
- bidimensional: woven or nonwoven fabrics (felts or mats);
- tridimensional: fabrics (sometimes called multidimensional fabrics) with fibers oriented along many directions (more than two directions).

Among the possible configurations, unidirectional (0°) laminae, for example, are extremely strong and stiff in the 0° direction. However, they are very weak in the 90° direction because the load must be carried by the much weaker polymeric matrix [4].

From what has been said so far, it is clear that the heterogeneous composition of composites leads to direction dependent material properties. In order to distinguish the different material directions, a material coordinate system (1,2,3) is typically introduced as illustrated in Fig. 1.4. For unidirectional laminated composite, direction 1 (longitudinal dir.) refers to the orientation of the reinforcing fibers, direction 2 (transvers dir.) is defined by the direction normal to direction 1 and

in-plane of the fiber reinforcement, whilst direction 3 usually points in the through thickness direction if the lamina is embedded in a laminate, so it is normal to the lamina.

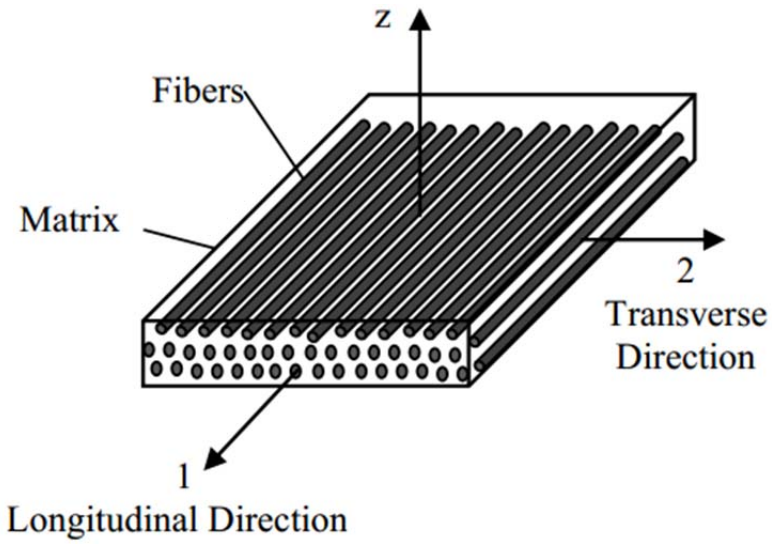

(a)

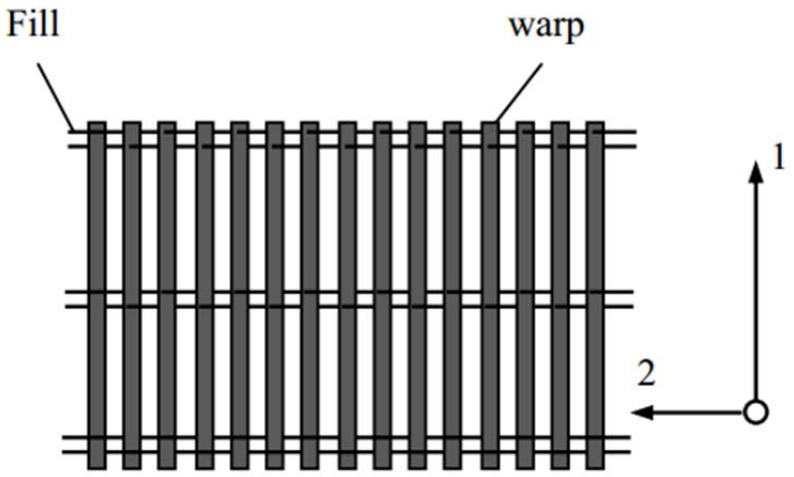

(b)

Fig. 1.4 - Orientations in composite layers [7]: unidirectional ply (a); woven fabrics (b). The fabrics are made of fibers oriented along two perpendicular directions, one is called the warp and, the other is called the fill (or weft) direction.

The continuous fiber reinforced composite materials are the focus of this study. Especially the combination of carbon fiber and epoxy resin will be investigated due to the high relevance in industrial applications.

1.5 Stress-strain relationships

Material behavior is mathematically characterized by the so-called *constitutive equations*, also called *material laws*. There is a very wide range of materials used for structures, with drastically different behavior. In addition the same material can go through different response regimes: elastic, plastic, viscoelastic, cracking, fracture. However, here, the attention is restricted to a very specific material class and response regime by making the following behavioral assumptions [8]:

1. Macroscopic Model. The material is mathematically modeled as a continuum body; therefore its features at the micro and nano scales (fiber, molecules, atoms etc.) are ignored.
2. Elasticity. In physics, elasticity is a physical property of materials which return to their original shape after they are deformed; in other words, it completely recovers its form when applied forces are removed; this means the stress-strain response is reversible and consequently the material has a preferred natural state. This state is assumed to be taken in the absence of loads at a reference temperature.
3. Linearity. The relationship between strains and stresses is linear.
4. Small Strains. Deformations are considered so small that changes of geometry are neglected as the loads are applied. Violation of this assumption requires the introduction of nonlinear relations between displacements and strains. This is necessary for highly deformable materials such as rubber (more generally, polymers). Inclusion of nonlinear behavior significantly complicates the constitutive equations and is therefore left for advanced courses.

Therefore, assuming a initial linear elastic behavior of the material and infinitesimal deformations, the generalized 3-D Hooke's law in tensorial form is:

$$\boldsymbol{\sigma} = \boldsymbol{C} : \boldsymbol{\varepsilon} + \boldsymbol{\sigma}^0 \qquad (1.1)$$

In the Eqn. 1.1, $\boldsymbol{\sigma}$ is the stress tensor, $\boldsymbol{\varepsilon}$ denotes the strain tensor, $\boldsymbol{C}$ is a forth order tensor of called *elasticity tensor* which contains material elastic parameters and $\boldsymbol{\sigma}^0$ are the initial stresses. For the general case of anisotropic or triclinic material, because the material has not plane of symmetry, a total of 21 independent material constants is needed to describe the stress-strain behavior. If the anisotropic material has three mutually orthogonal planes of symmetry then the constitutive law involves only 9 independent material constants and the material is said *orthotropic*.

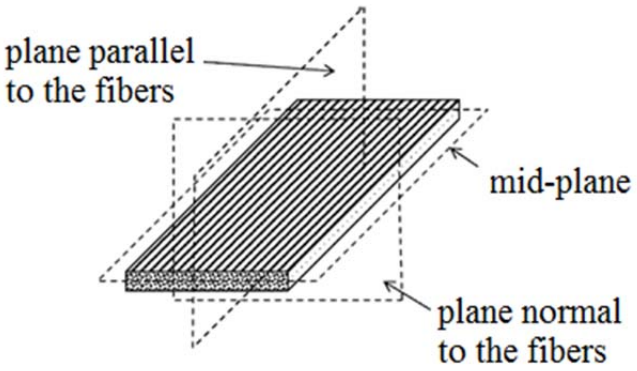

Fig. 1.5 - The three planes of symmetry of the orthotropic material.

Unidirectional plies are often treated as orthotropic because they exhibit three planes of material symmetry, the 1-2 plane, the 1-3 plane and the 2-3 plane (see Fig 1.5). As a result the Eqn. 1.1 in matrix form becomes:

$$\begin{pmatrix} \sigma_{11} \\ \sigma_{22} \\ \sigma_{33} \\ \sigma_{12} \\ \sigma_{23} \\ \sigma_{13} \end{pmatrix} = \begin{bmatrix} C_{11} & C_{12} & C_{13} & 0 & 0 & 0 \\ C_{12} & C_{22} & C_{23} & 0 & 0 & 0 \\ C_{13} & C_{23} & C_{33} & 0 & 0 & 0 \\ 0 & 0 & 0 & C_{44} & 0 & 0 \\ 0 & 0 & 0 & 0 & C_{55} & 0 \\ 0 & 0 & 0 & 0 & 0 & C_{66} \end{bmatrix} \begin{pmatrix} \varepsilon_{11} \\ \varepsilon_{22} \\ \varepsilon_{33} \\ 2\varepsilon_{12} \\ 2\varepsilon_{23} \\ 2\varepsilon_{13} \end{pmatrix} \qquad (1.2)$$

Special care should be taken to not confuse γ with ε, see Fig. 1.6.

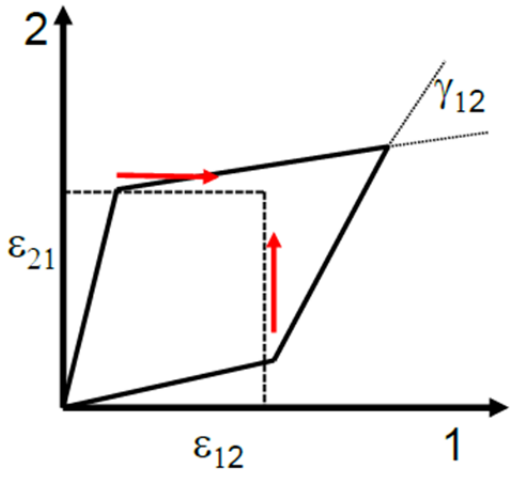

Fig. 1.6 - difference between γ and ε.

Following the assumption that the stress strain relations are invertible, from the elastic tensor the *compliance tensor* is obtained:

$$\boldsymbol{S} = \boldsymbol{C}^{-1} \qquad (1.3)$$

and the Eqn. 1.1, with zero initial stresses $\boldsymbol{\sigma}^0 = 0$, can be now rewritten as:

$$\boldsymbol{\varepsilon} = \boldsymbol{S} : \boldsymbol{\sigma} \qquad (1.4)$$

allowing S to be expressed in terms of engineering constants. The Eqn. 1.4 in engineering notation becomes:

$$\begin{pmatrix} \varepsilon_{11} \\ \varepsilon_{22} \\ \varepsilon_{33} \\ 2\varepsilon_{12} \\ 2\varepsilon_{23} \\ 2\varepsilon_{13} \end{pmatrix} = \begin{bmatrix} \frac{1}{E_1} & -\frac{\nu_{12}}{E_1} & -\frac{\nu_{13}}{E_1} & 0 & 0 & 0 \\ -\frac{\nu_{12}}{E_1} & \frac{1}{E_2} & -\frac{\nu_{23}}{E_2} & 0 & 0 & 0 \\ -\frac{\nu_{13}}{E_1} & -\frac{\nu_{23}}{E_2} & \frac{1}{E_3} & 0 & 0 & 0 \\ 0 & 0 & 0 & \frac{1}{G_{12}} & 0 & 0 \\ 0 & 0 & 0 & 0 & \frac{1}{G_{23}} & 0 \\ 0 & 0 & 0 & 0 & 0 & \frac{1}{G_{13}} \end{bmatrix} \begin{pmatrix} \sigma_{11} \\ \sigma_{22} \\ \sigma_{33} \\ \sigma_{12} \\ \sigma_{23} \\ \sigma_{13} \end{pmatrix} \qquad (1.5)$$

From Eqn. 1.5 it becomes clear that the number of elastic constants (9) that fully describes the linear elastic behavior of orthotropic material coincides with the number of engineering constants: E_1, E_2, E_3, G_{12}, G_{23}, G_{13}, ν_{12} , ν_{13} , ν_{23} .

If the anisotropic material presents infinite planes of symmetry about an axis material then the constitutive law involves only 5 independent elastic/engineering constants. In fact, assuming that the material properties are identical in any direction transverse to the fiber direction (1-direction) leads to isotropic material behavior in the 2-3 plane. This behavior is called *transversally isotropic*. For symmetry about the 1-axis the Eqn. 1.2 reduces to:

$$\begin{pmatrix} \sigma_{11} \\ \sigma_{22} \\ \sigma_{33} \\ \sigma_{12} \\ \sigma_{23} \\ \sigma_{13} \end{pmatrix} = \begin{bmatrix} C_{11} & C_{12} & C_{12} & 0 & 0 & 0 \\ C_{12} & C_{22} & C_{23} & 0 & 0 & 0 \\ C_{12} & C_{23} & C_{22} & 0 & 0 & 0 \\ 0 & 0 & 0 & C_{44} & 0 & 0 \\ 0 & 0 & 0 & 0 & \frac{1}{2}(C_{22} - C_{23}) & 0 \\ 0 & 0 & 0 & 0 & 0 & C_{44} \end{bmatrix} \begin{pmatrix} \varepsilon_{11} \\ \varepsilon_{22} \\ \varepsilon_{33} \\ 2\varepsilon_{12} \\ 2\varepsilon_{23} \\ 2\varepsilon_{13} \end{pmatrix} \qquad (1.6)$$

Within the thesis work the material is generally assumed to behave as orthotropic. Only in some exceptions transverse isotropic behavior is considered.

References

[1] D. D. L. Chung, “Composite Materials : Science and Applications”, Engineering Materials and Processes Ser., Springer, 2010.

[2] Guide to Composites, SP Systems.

[3] A. Corigliano, "Damage and fracture mechanics techniques for composite structures", Comprehensive Structural Integrity, Elsevier, 2003, 3(9).

[4] F.C. Campbell, “Structural Composite Materials”, ASM International, 2010.

[5] F. C. Campbell, “Lightweight Materials: Understanding the Basics”, ASM International, 2012.

[6] D. Hull, T. W. Clyne, “An Introduction to Composite Materials”, Cambridge University Press, Cambridge, UK, 1996.

[7] V. V. Vasiliev, E. V. Morozov, “Advanced Mechanics of Composite Materials”, Second Edition Book, Elsevier Ltd., 2007.

[8] Introduction to Aerospace Structures, Course, Department of Aerospace Engineering Sciences University of Colorado.

CHAPTER 2

DAMAGE IN COMPOSITE MATERIALS

2.1 Introduction to damage in composite materials

The increasingly more demanding mission requirements of modern aerospace vehicles and the use of non-traditional materials, such as non-metallic composites, in construction of aerospace structures lead to significant challenges [1]. In this framework, the evaluation of structural integrity and failure prediction of modern aerospace structures and flight vehicles are essential for the design and service life assessment.

The evaluation of structural integrity is an important engineering problem in structural design. In fact it is well known that structural strength may be degraded during its design life due to mechanical and/or chemical aging. Therefore, the structural design depends upon a detailed knowledge of load, physics and material which is necessary to understand and predict how structures support and resist self-weight and imposed loads. Structural loads or actions are forces, deformations, or accelerations applied to a structure or its components and they may cause stresses, deformations, and displacements in structures. Assessment of their effects is carried out by the methods of structural analysis. Depending on the structural design, material type, service loading, and environmental conditions, the cause and degree of strength degradation due to the different aging mechanisms will vary. One of the common causes of strength degradation is crack development in the structure. When cracks occur, the crack size effects and growth rate on the fracture resistance of the material and the remaining strength and the structure life need to be determined. Therefore, another important engineering problem in structural design is the evaluation of structural reliability. In reliability analysis of structural systems the main problem is to evaluate

the probability of failure corresponding to a specified reference period; so, in critical applications the reliable performance of a structure depends on ensuring that the structure in service satisfies the conditions assumed in design and life prediction analyses. Reliability assurance requires evaluation of the stress state in the structure and the material's strength allowable corresponding to a given failure criterion for a given loading condition and the availability of nondestructive testing and evaluation techniques to characterize discrete cracks according to their location, size and orientation thus leading to an improved assessment of the potential criticality of individual flaws [1].

In conclusion, excess load or overloading may cause structural failure, and hence such possibility should be either considered in the design or strictly controlled. Therefore, if the purpose of a structure is to carry loads, then a designer must assure that the structure has sufficient load-bearing capacity and if the structure is to function over a period of time, then it must be designed to meet its functionality over that period without losing its integrity [2]. These are generic structural design issues irrespective of the material used. There are, however, significant differences in design procedures depending on whether the material used is a so-called monolithic material, e.g., a metal or a ceramic, or whether it is a composite material with distinctly different constituents.

As regards to composite materials, their heterogeneous microstructure, the differences between constituent properties, the interface presence as well as directionality of reinforcement that induces anisotropy in overall properties, provide significantly different characteristics to composite materials in how they deform and fail when compared to metals or ceramics. The consequences of all damages in composite structures are changes in stiffness, strength, and fatigue properties, therefore, it is imperative to understand the damaging mechanisms and to be able to predict them.

The term *damage* refers to a collection of all the distributed irreversible changes brought about in a material by a set of energy dissipating chemical or physical processes, resulting from the application of thermomechanical loadings and it may inherently be manifested by atomic bond breakage [2]. Examples of damage in composites are multiple fiber-bridged matrix cracking in a unidirectional composite, multiple intralaminar cracking in a laminate, local delamination

distributed in an interlaminar plane, and fiber/matrix inter-facial slip associated with multiple matrix cracking. These damage mechanisms will be explained in detail in the following paragraphs. Another term typically used is “failure” and it should not be confused with term “damage”. The *failure* is the inability of a material system (and consequently, a structure made from it) to perform its design function. In reality, the failure event in a composite structure is preceded and influenced by the progressive occurrence and interaction of various damage mechanisms. Fracture is one example of a possible failure; but, generally, a material could fracture (locally) and still perform its design function. Upon suffering damage, e.g., in the form of multiple cracking, a composite material may still continue to carry loads and, thereby, meet its load-bearing requirement but fail to deform in a manner needed for its other design requirements, such as vibration characteristics and deflection limits. In the following paragraph the main damage mechanisms in composite materials will be discussed.

2.2 Interfacial debonding

The interface between the fiber and the matrix play a central role in the mechanical behavior of composite materials; it must transfers the load from matrix to fiber in order to allow a correct behavior of the whole composite. Many important phenomena may take place at the interface between fiber and matrix which tend to promote plastic deformation of the matrix and can influence the onset and nature of failure. The adhesion bond at the interfacial surface affects the macroscopic mechanical properties of the composite. In general terms, to have high modulus and high strength one needs a good adhesion between matrix and fiber. For instance, if the fibers are weakly held by the matrix, the composite starts to form a matrix crack at a relatively low stress. However, if the fibers are strongly bonded to the matrix, the matrix cracking is delayed and the composite fails catastrophically because of fiber fracture as the matrix cracks. The resistance of adhesion is mainly

due to van der Waals forces and can be influenced by many factors such as the electrostatic attraction, the interdiffusion and the chemical reactions [3]. Controlling interfacial properties can thus provide a way to control the performance of a composite structure. In order to improve the resistance to *fiber–matrix debonding*, surface treatment can be applied to the fibers, and the use of silane coupling agents can strongly improve the adhesion.

One way to measure the interface resistance is promote a debonding process between fiber and matrix by moving the fiber with respect to the matrix. In the literature a number of tests have been proposed to do it as the single fiber pull-out and the single fiber push-out [4,5,6].

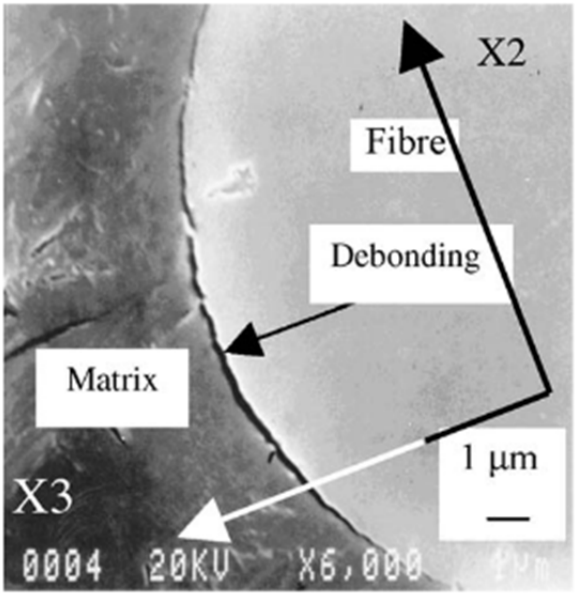

Fig. 2.1 – Partial debonding at the fiber matrix interface detected by scanning electronic microscope [7].

2.3 Matrix microcracking/intralaminar (ply) cracking

In composite materials the matrix must transfer stresses between fibers, stabilize fibers when loaded in compression, increase the resistance to impact damage. However, the properties of these materials in the directions dominated by matrix, as the transverse direction to the fibers in a unidirectional composite, are generally low precisely due to its presence because it is weak and

compliant (having a low stiffness) and in many cases the first form of damage which develops in laminate composites concerns just matrix. Considering a single ply under transversal tension, i.e. with a load direction at 90° with respect to the reinforcement direction (fibers), the lamina behavior is matrix-dominated and the failure occurs due to transverse matrix cracking. The matrix also dominates the behavior of single laminas loaded in plane shear, i.e., with a load direction at 45° with respect to the fiber direction.

When the matrix is damaged, its function, discussed above, cannot be accomplished properly and the mechanical resistance of the composite material can be seriously altered. However, the existence of damage in the matrix does not necessarily mean catastrophic failure of the composite as it can be present only in certain plies (usually those transverse to the main loading direction) and while the fibers (which carry most of the load) remain intact. The terms *matrix microcracks*, *transverse cracks*, *intralaminar cracks*, and *ply cracks* are invariably used to refer to matrix damage. Such cracks are found to be caused by tensile loading, fatigue loading, see Fig. 2.2, as well as by changes in temperature or by thermal cycling. They can originate from fiber/matrix debonds or manufacturing-induced defects such as voids and inclusions. Although as already said above matrix cracking does not cause structural failure by itself, it can result in significant degradation in the thermomechanical properties of the laminate including changes in all effective moduli, Poisson ratios, and thermal expansion coefficients. Furthermore it can also induce more severe forms of damage, such as delamination and fiber breakage, which are the reason of complete failure of the composite structural member [8] and give pathways for entry of fluids [3].

The appearance of transverse cracks and their growth in the inner-ply of a cross-ply laminate $[0_m/90_n]_s$ under tension represent a classical problem, which has been known and studied for a long time [9,10,11,12]. First, some cracks appear in the direction orthogonal to the loading (transverse cracking), in the inner-ply for a certain strain, see Fig. 2.3. Next some interface cracks appear when transverse cracks reach the interface (or before reaching) between the inner and outer plies. Finally,

coalescence of the different interface cracks occurs leading to macroscopic interfacial damage (*delamination*).

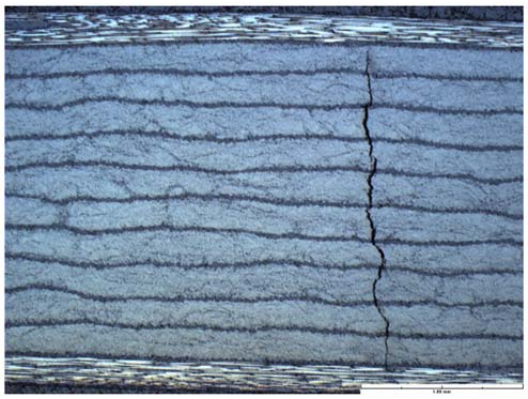

Fig. 2.2 – Transverse matrix cracking in cross-ply laminates resulting from fatigue loading: the horizontal bands are carbon fiber laminas. There are ten 90 degree laminas in the middle of this layup and 0 degree lamina on the "top" and "bottom" of the layup. Source: Justin M. Ketterer , "Fatigue crack initiation in cross-ply carbon fiber laminates", Thesis, Georgia Institute of Technology, 2009.

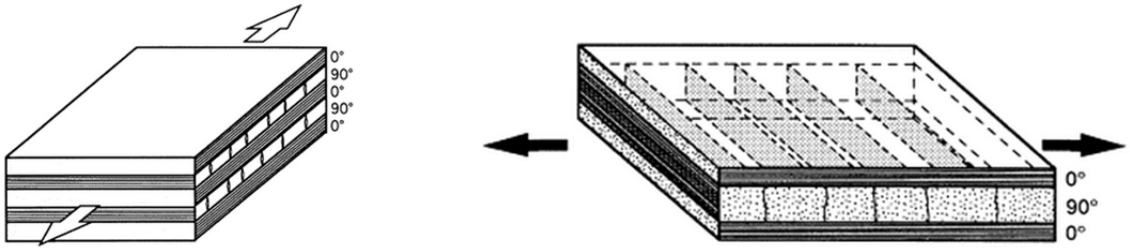

Fig. 2.3 – Transverse matrix cracking in cross-ply laminates [11].

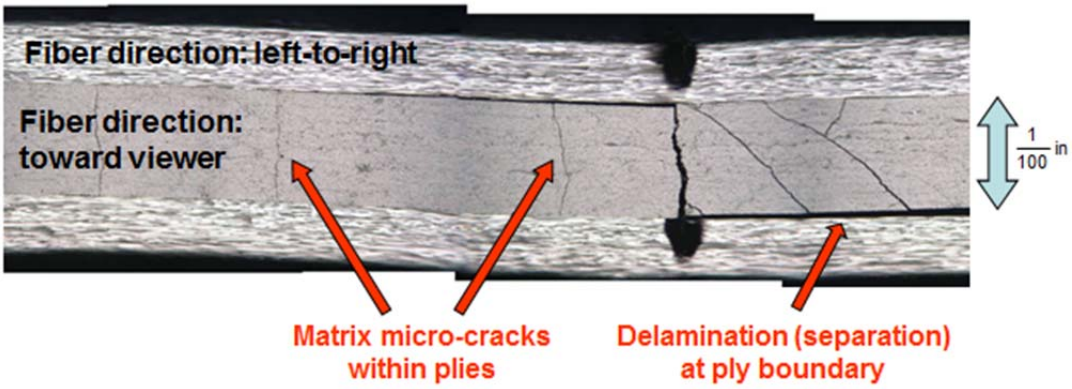

Fig. 2.4 – Photograph (David Hsu, Dan Barnard) showing damage in a 4-ply laminated: cracking of the matrix material within a ply and delaminations at the boundary between plies.

Therefore, the importance of matrix cracking is due to the fact that generally it triggers other damage mechanisms, such as delamination, , see Fig. 2.4, which are the reason of complete failure of the composite structural member [13].

The usual tests for matrix microcracking are uniaxial tension on single laminas or laminate or the bending tests in which 90° layer are on the tension side of the laminate. More information concerning the behavior of matrix materials and their damage processes can be found, e.g., in Corigliano [3] and Kelly et al. [14].

2.4 Fiber microbuckling

Fiber reinforced composite materials under compression loading may develop different types of failure mechanisms: microbuckling leading to kinking, delamination, and matrix damage. These different modes of failure occur either separately or simultaneously depending on the loading which affects the global response of the laminate. Therefore, it is of importance to study the interaction between these different types of failure mechanisms [15]. In most cases, the weakness under compression of fibrous composites severely limits the structural efficiency of the system and leads to under-utilization of the true material properties [16]. When a unidirectional composite is loaded in compression, the failure is governed by a mechanism known as *microbuckling* of fibers. The microbuckling is the buckling of fibers embedded in matrix foundation. So it is of fundamental importance to distinguish between the tensile and compressive behavior of fibers. Most fiber reinforced polymer matrix composites have a compressive strength less than their tensile strength. Therefore in many engineering applications, the compressive strength is a design limiting feature. Fiber strength in tension can be considered as a real fiber property; on the contrary, fiber strength in compression is highly limited by the risk of buckling of the load bearing fibers aligned with the loading direction. The buckling phenomenon is strongly affected by the initial imperfections of the

composite that were introduced during the manufacturing process including associated defects such as fiber misalignment, rich resin, and porosity [16]. Over the past ten years significant improvements have been made to tensile strength, but, unfortunately, compressive strength has shown little concomitant improvement. In general, it can be observed that the fiber strength in compression will depend on geometrical properties like the fiber aspect ratio (L/d), where L is the fiber length and d its diameter, and on mechanical properties of the fiber and of the matrix which have an influence on the local stiffness of the fiber during bending [3]. Usually, the phenomenon of local fiber buckling is accompanied by the formation of *kink bands* in the part of the fiber that has compressive stresses; it occurs mostly in the case of aramid fibers.

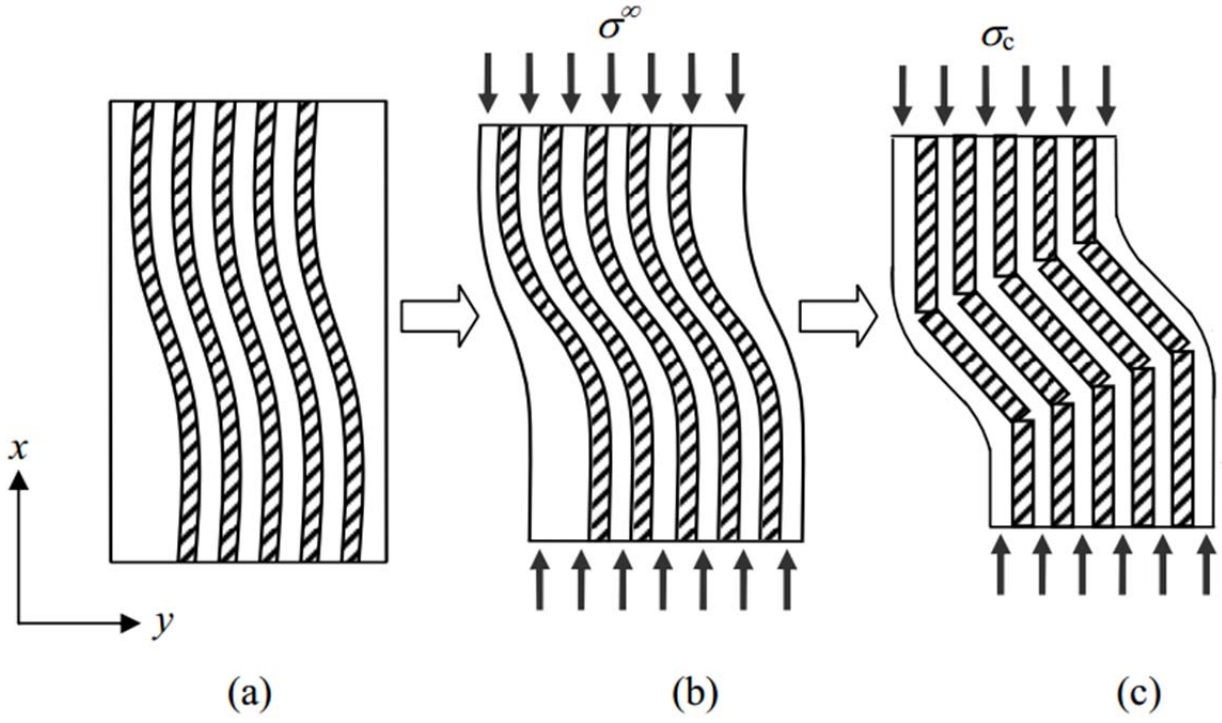

Fig. 2.5 – The schematic diagram showing the formation of kinking failure mode in UD laminate: (a) fibers with an initial fiber misalignment, (b) deformation of fibers via fiber microbuckling mechanism when it is loaded in compression σ∞ and (c) fibers kinking phenomena causing laminate catastrophic fracture [18].

Kinking is highly localized fiber buckling. It is only occurs after microbuckling has already developed after the attainment of a peak compressive load when the region between breaks is deformed plastically; therefore kinking in polymer composites is a direct consequence of localised

plastic microbuckling coupled with low failure strain of the reinforcing material [17,18], see Fig. 2.5 and Fig. 2.6.

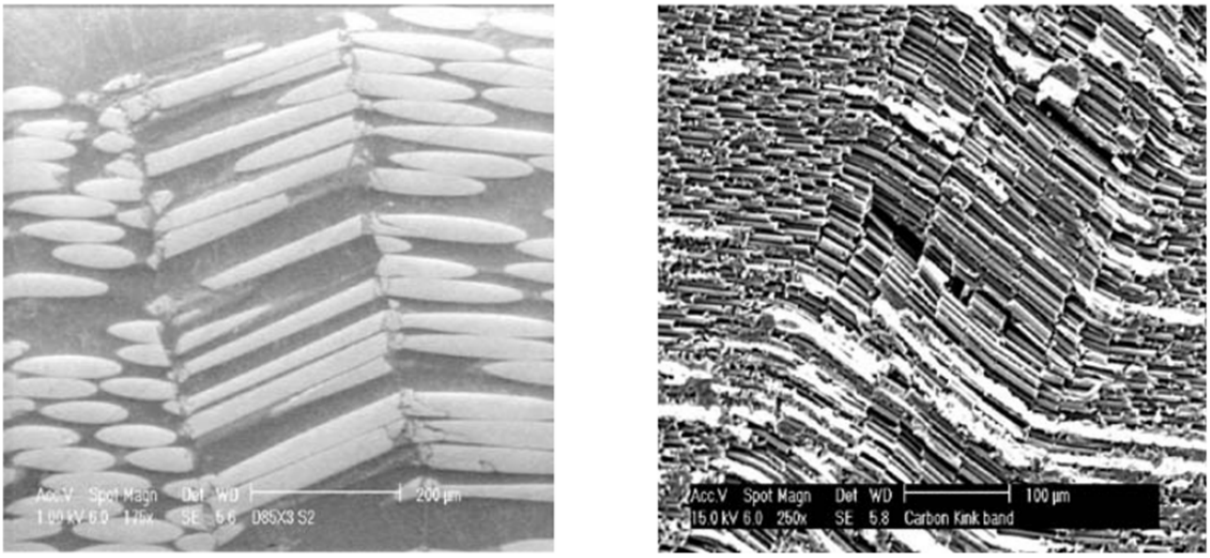

Fig. 2.6 – Typical kink bands in various laminae. Note the broken fiber demarcating the kink band [19].

More information concerning the behavior of composite materials under compression loading and their damage processes can be found, e.g., in Ref. [18,19,20,21].

2.5 Fiber breakage

The failure of a composite reinforced with long brittle fibers ultimately is due to fiber breakage, see Fig. 2.7 and Fig. 2.8. In the broken fibers the stress is zero while in intact fibers it is recovered (stress redistribution between fibers and matrix) as axial distance increases from each break, affecting other fibers in the local vicinity of the broken fibers and possibly breaking some. In fact the fiber/matrix interface transfers the stress from the broken fiber back to the fiber at a certain distance, making another fiber break possible if the strength is exceeded by the stress. The important parameters describing stress transfer are the stress concentrations in the neighboring fibers around the broken fiber and the longitudinal ineffective length over which the broken fiber

recovers its load-carrying capacity [22]. More information concerning the fiber breakage can be found, e.g., in Ref. [2,3,22].

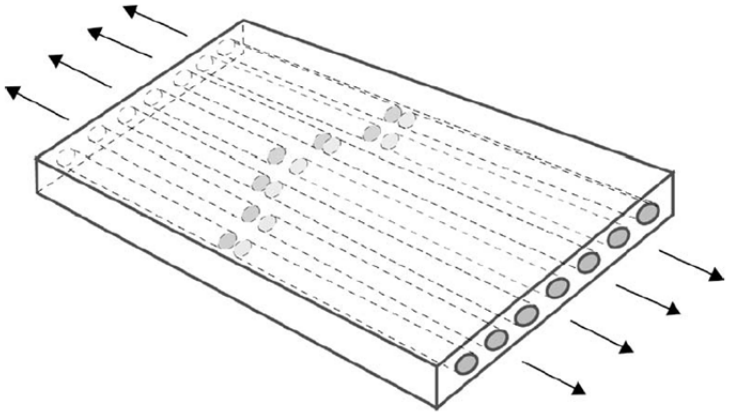

Fig. 2.7 – Ply loaded in longitudinal tension: rupture of fibers [3].

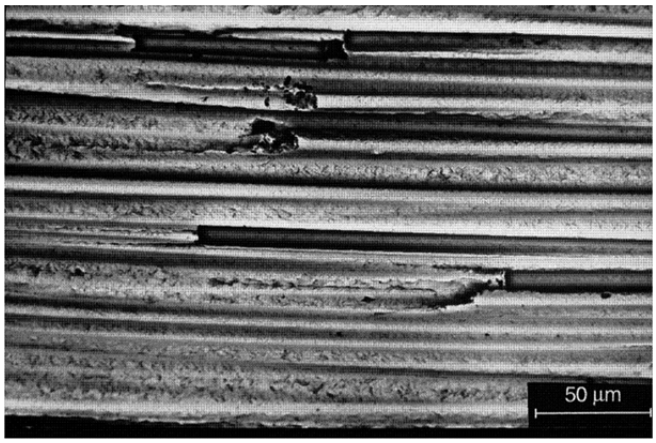

Fig. 2.8 – Scanning electron micrograph photography of random fiber breakage in $[0]_{16}$ tensile test specimen of different magnifications: (a) global view [22].

2.5 Interlaminar Fracture: the delamination

Interlaminar fracture or *delamination* is a typical failure mode of laminated composite materials and it is one of the major problems for fiber reinforced composites. It strongly influences structural

performance of composite structure because its occurrence greatly reduces the structure stiffness, leading to failure during service. Therefore, the delamination can be a substantial problem in designing composite structures as it can diminish the role of strong fibers and make the weaker matrix properties govern the structural strength. It is due to the low resistance of the thin resin-rich interface existing between adjacent layers, under the action of impacts, transversal loads or free-edge stresses. Internal defects can propagate due to delamination which can be activated even by compressive loading and subsequent local buckling of the delaminated area; so, this form of damage is of particular concern in primary compression-loaded structures, since internal interfacial damages may result in dramatic reductions in compressive strength, even when undetectable by visual inspection of the laminate surface. In contrast to metals, in polymer composite laminates delamination can occur below the surface of a structure under a relatively light impact, such as that from a dropped tool, while the surface appears undamaged to visual inspection, see Fig. 2.9. In composite laminates, delamination can even occur at cut (free) edges, such as at holes, or at an exposed surface through the thickness. In the presence of free edges, delamination starts mainly due to tensile loading and propagates from the edge toward the interior of the laminate [3].

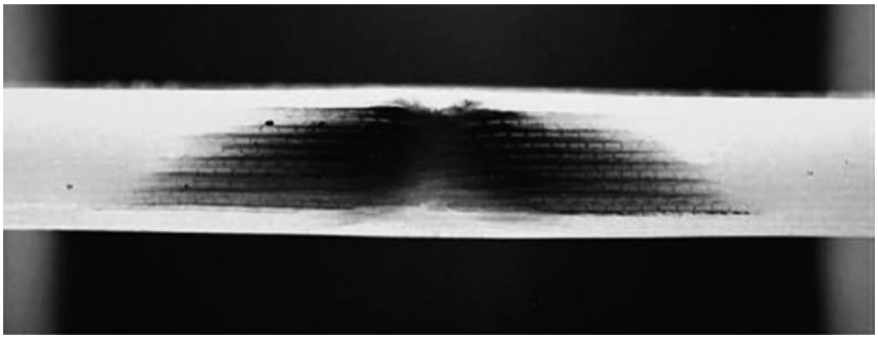

Fig. 2.9 – Section view of a impacted composite material sample: delaminations without damage to the surface [23].

Delamination occurs with fracture at an interface when adjacent plies have different orientations and they are subjected to interlaminar normal and shear stresses. Apparently, interlaminar shear

stress and in-plane transverse tensile stress are the dominant stresses causing the critical matrix cracking. Such interlaminar stresses become significant and affect the overall performance where geometrical and material discontinuities exist. Interlaminar stresses in turn arise due to mechanical properties mismatch between adjacent layers. The delamination phenomenon can be explained by considering two laminas loaded in tension, the first in the direction orthogonal to the fibers, the second in the fiber direction. Due to Poisson's ratio mismatch, being the lateral contraction of the first lamina governed by the fiber stiffness unlike the other, when the laminas are glued together to form a laminate, interlaminar shear stresses must arise for tension loading in order to preserve geometrical compatibility. The critical material property which gives rise to delamination is the interlaminar strength, which is determined by the matrix. Once the interlaminar cracks are formed, their growth is determined by the interlaminar fracture toughness, which is also governed by the matrix. If delamination is viewed as decohesion of the cohesive zone between the separating plies, then both the matrix strength and the fracture toughness act as material parameters. As a design approach, delamination can be reduced either by improving the interlaminar strength and fracture toughness or by modifying the fiber architecture to reduce the driving forces for delamination.

Finally, it is important to note that after the onset of delamination, the fracture can propagate in different modes, as shown in Fig. 2.10. These failure modes can be classified as mode I, which is the opening component, mode II, the shear component perpendicular to the delamination front and mode III, which is the shear component parallel to the delamination front.

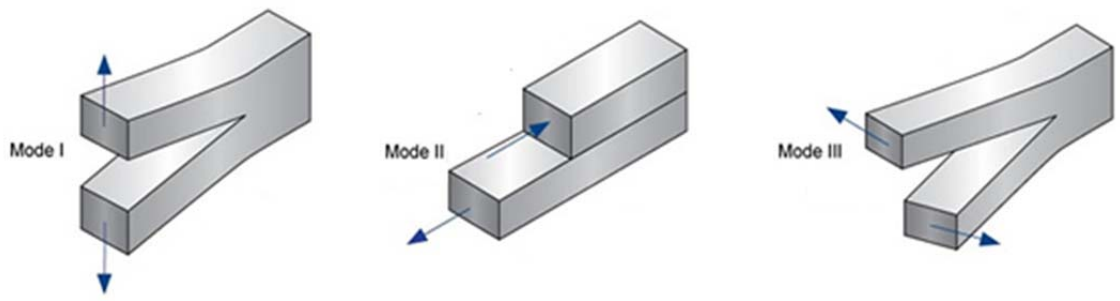

Fig. 2.10 – Mode I, mode II and mode III crack propagation modes. Source: NDT – Resource Center.

A fracture not necessarily propagates as a single fracture mode but it can do it as a combination of them. When more than one mode of fracture is present, this is known as *mixed mode*.

Due to the importance of delamination in the assessment of structural composite resistance, many attempts have been made in order to enhance interlaminar fracture properties in laminate composites. High-performance composites have been produced with enhanced delamination resistance by means of the introduction of some devices which create a direct connection between laminas in the transverse direction. Z-pinning and fiber stitching [24] are among the most effective. Further information on the delamination processes can be obtained from Ref. [25].

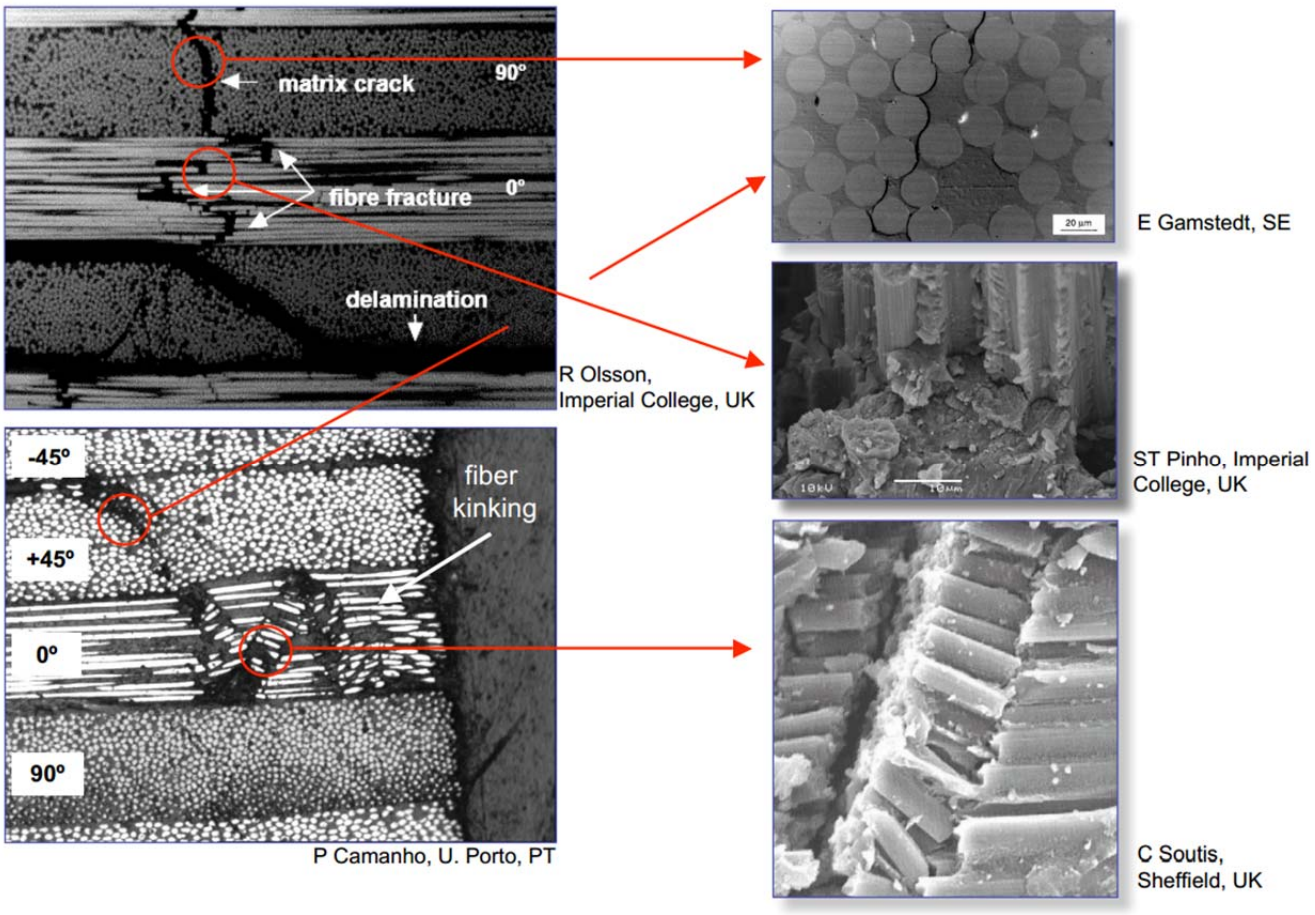

Fig. 2.11 – Figurative summary of damaging mode of a composite laminate. Source: C. G. Dàvila, C. A. Rose, P. P. Camanho, P. Maimì, A. Turon, Progressive Damage Analysis of Composites, Aircraft Aging and Durability Project, Nasa

References

[1] S. Y. Ho, “Structural Failure Analysis and Prediction Methods for Aerospace Vehicles and Structures”, Defence Science and Technology Organisation, 2010.

[2] R. Talreja, C. V. Singh, “Damage in composite materials”, Cambridge University Press, 2012.

[3] A. Corigliano, "Damage and fracture mechanics techniques for composite structures", Comprehensive Structural Integrity, Elsevier, 2003, 3(9).

[4] J. K. Wells, P. W. R. Beaumont, “Debonding and pull-out processes in fibrous composites”, Journal of Materials Science, 1985, 20(4):1275-1284.

[5] C. DiFrancia, Thomas C. Ward, Richard O. Claus, “The single-fibre pull-out test. 1: Review and interpretation”, Composites Part A: Applied Science and Manufacturing, 1996, 27(8):597–612.

[6] T. P. Weihs, W. D. Nix, "Experimental Examination of the Push-Down Technique for Measuring the Sliding Resistance of Silicon Carbide Fibers in a Ceramic Matrix", Journal of the American Ceramic Society, 1991, 74(3):524–534.

[7] Y. Ricotti, D. Ducret, R. El Guerjouma, P. Franciosi, “Anisotropy of hygrothermal damage in fiber/polymer composites: Effective elasticity measures and estimates”, Mechanics of Materials, Elseiver, 2006, 38(12):1143–1158.

[8] M. N. Tamin, “Damage and Fracture of Composite Materials and Structures”, Springer, 2012.

[9] I. G. Garcìa, “Application of coupled stress and energy criterion to the analysis of crack initiation and growth in composites at micro and mesoscales”, Master Thesis, University of Seville, 2010.

[10] J. Berthelot, “Transverse cracking and delamination in cross-ply glass-fiber and carbon-fiber reinforced plastic laminates: Static and fatigue loading”, Applied Mechanics Reviews, 2003, 56(1):111-147.

[11] J. M. Berthelot, J. F. Le Corre, “Modelling the transverse cracking in cross-ply laminates: application to fatigue”, Composites Part B: Engineering, 1999, 30(6):569–577.

[12] J. Zhang, J. Fan, C. Soutis, “Analysis of Multiple Matrix Cracking in [±θm/90n]s Composite Laminates – Part 2: Development of Transverse Ply Cracks,” Composites, 1992, 23(5):299-304.

[13] J. Wang, B. L. Karihaloo, “Cracked composite, laminates least prone to delamination”, Proc. Roy. Soc.London, 1994, 444(1920):17-35.

[14] A. Kelly, C. Zweben, “Comprehensive Composite Materials”, Elsevier, Oxford, UK, 2000:1–6.

[15] P. Prabhakar, W. H. Ngy, A. M. Waasz, R. Raveendrax, “Investigation of failure mode interaction in laminated composites subjected to compressive loading”, Proceedings of the 52nd AIAA/ASME/ASCE/AHS/ASC Structures, Structural Dynamics, and Materials Conference, Denver, Colorado, USA, 2011,1792.

[16] Y. Zhang, H. Fu, Z. Wang, “Better predictions of airfoil strength”, Society of Plastics Engineers, 2011.

[17] N. K. Naik, R. S. Kumar, “Compressive strength of unidirectional composites: evaluation and comparison of prediction models”, Composite Structures, 1999, 46(3):299-308.

[18] A. Jumahata, C. Soutisa, F.R. Jonesb, A. Hodzica, “Fracture mechanisms and failure analysis of carbon fibre/toughened epoxy composites subjected to compressive loading”, Composite Structures, 2010, 92(2):295–305.

[19] C. Yerramalli, “A mechanism based Modeling approach to failure in fiber reinforced composites”, Ph.D. thesis, Aerospace Engineering Department, University of Michigan, Ann Arbor, 2003.

[20] S. Basu, A. M. Waas, D. R. Ambur, “Compressive failure of fiber composites under multi-axial loading”, Journal of the Mechanics and Physics of Solids, 2006, 54(3):611–634.

[21] T. Yokozeki, , T. Ogasawara, T. Ishikawa, “Nonlinear behavior and compressive strength of unidirectional and multidirectional carbon fiber composite laminates”, Composites Part A: Applied Science and Manufacturing, 2006, 37(11):2069–2079.

[22] H. Li, Y. Jia, G. Mamtiminc, W. Jiang, Lijia An, “Stress transfer and damage evolution simulations of fiber-reinforced polymer–matrix composites”, Materials Science and Engineering A, 2006, 425:178–184.

[23] T. W. Shyr, Y. H. Pan, “Impact resistance and damage characteristics of composite laminates”, Composite Structures, 2003, 62:193–203.

[24] A. P. Mouritz, “Review of z-pinned composite laminates”, Composites Part A: Applied Science and Manufacturing, 2007, 38(12):2383–2397.

[25] S. Sridharan, “Delamination behaviour of composites”, 2008, Washington University in St. Louis, USA.

CHAPTER 3

FAILURE CRITERIA

3.1 Damage onset prediction in composite materials

In general it is said that a laminate may fail in one of the following types of failure modes: 1) *first-ply failure* (FPF); *ultimate laminate failure* (ULF) and 3) *inter-laminar failure* [1]. The first-ply failure indicates the failure of the laminate with the failure of the first layer. ULF is defined as the failure of the laminate when ultimate load capacity is reached following failure of all the plies. Intra-laminar failure is defined as the failure resulting from the separation of adjacent layers though the individual lamina remains intact. However the catastrophic failure of a structure in composite material rarely occurs at the load corresponding to the initial or first-ply failure. So the first-ply failure does not mean that the ultimate capacity of the laminate has been reached. In fact, when the first ply fails, other plies may remain intact but with the failure of the first ply, a redistribution of stresses takes place in the remaining plies. The structure ultimately fails due to the propagation or accumulation of local failures (or damage) as the load is increased.

In general, laminated composites may fail by fiber breakage, matrix cracking, or by delamination of layers. The mode of failure depends upon the loading, stacking sequence, and specimen geometry.

In order to correctly identify the damage onset in an anisotropic material, failure criteria need to be defined. Failure criteria compare the loading state at a point (stress or strain) with a set of values reflecting the strength of the material at that point (often referred to as the material allowables). Both loading and strength values should be reflected in the same material coordinate system. For unidirectional materials, this is typically in the direction of the fibers. However, for woven and

knitted fabrics, this direction is not obvious and might change as the material is formed to shape. In general, the load is represented by a full stress or strain tensor having six independent components:

$$\sigma_{11}, \sigma_{22}, \sigma_{33}, \tau_{12}, \tau_{23}, \tau_{31} \qquad (3.1)$$

$$\varepsilon_{11}, \varepsilon_{22}, \varepsilon_{33}, \gamma_{12}, \gamma_{23}, \gamma_{31} \qquad (3.2)$$

As mentioned in the previous chapter, a standard unidirectional composite ply coordinate system aligns the 1-axis with the fiber direction (1-axis coincides with the warp direction in fabric) and the 2-axis orthogonal, i.e. rotated 90 deg., to the fiber direction in the plane of the composite ply (2-axis coincides with the fill direction in fabric), while the 3-axis is normal to the plane of the lamina.

Failure criteria for composite materials are significantly more complex than yield criteria for metals because composite materials can be strongly anisotropic and tend to fail in a number of different modes depending on their loading state and the mechanical properties of the material. In metallic materials, strength and stiffness are independent of the direction; so, a failure criterion (e.g. Von Mises) can be expressed by defining:

- a function of the stress state of stress;
- a limit value based on experimental tests;

$$f(\sigma_{11}, \sigma_{22}, \sigma_{33}, \tau_{12}, \tau_{23}, \tau_{31}) \leq \sigma_0 \qquad (3.3)$$

In composites the situation is generalized by defining one or more functions of the stress or strain state and a series of parameters that are generally expressible as a function of a set of limit values obtained from experimental data:

$$\begin{Bmatrix} f_1(\sigma_{11}, \sigma_{22}, \sigma_{33}, \tau_{12}, \tau_{23}, \tau_{31}, parameters_1) \leq 0 \\ f_2(\sigma_{11}, \sigma_{22}, \sigma_{33}, \tau_{12}, \tau_{23}, \tau_{31}, parameters_2) \leq 0 \\ .... \end{Bmatrix} \qquad (3.4)$$

The parameters, typically strengths, can be identified on the basis of mechanical characterization tests. The strength of the material can therefore be represented by seven independent variables:

- tensile strength along the 1or X axis: X_T
- compressive strength along the 1 or X axis: X_C
- tensile strength along the 2 or Y axis: Y_T
- compressive strength along the 2 or Y axis: Y_C
- shear strength in the 12 or XY plane: S_{xy}
- shear strength in the 23 or YZ plane: S_{yz}
- shear strength in the 13 or XZ plane: S_{zx}

Therefore, it's possible written as follows:

$$parameters(X_T, Y_T, Z_T, X_C, Y_C, Z_C, S_{xy}, S_{yz}, S_{zx}) \qquad (3.5)$$

In general the parameters are a function of a set of allowables. Design allowables are statistically determined materials property values derived from experimental test data. They are limits of stress, strain, or stiffness that are allowed for a specific material, configuration, application, and environmental condition. The selection of appropriate design allowables for structures composed of composite materials is essential for the safe and efficient use of these materials [3].

Failure mechanisms in composite materials are significantly complex, resulting in a large number of criteria. A large number of such criteria exists but no one criterion being universally satisfactory. The mechanism that lead to failure in composite materials are not yet fully understood [4]. The inadequate understanding of the damage mechanisms and the difficulties in developing tractable models of the failure modes explains the generally poor predictions by most participants in the World Wide Failure Exercise [5,6] (WWFE), an international activity conceived and conducted by Hinton and Soden concerning the assessment of the status of currently available theoretical methods for predicting material failure in fiber reinforced polymer composites. The results of the WWFE indicate that the predictions of most theories differ significantly from the experimental

observations, even when analyzing simple laminates under general load combinations that have been studied extensively over the past forty years [6].

In order to introduce the failure criteria a single ply is considered. The lamina to be a regular array of parallel continuous fibers perfectly bonded to the matrix. In general, there are five basic modes of failure of such a ply: longitudinal tensile or compressive, transverse tensile or compressive, or shear. Each of these modes would involve detailed failure mechanisms associated with fiber, matrix or interface failure. In the following the strengths in the principal material axes (parallel and transverse to the fibers) are assumed as the fundamental parameters defining failure. When a ply is loaded at an angle to the fibers, as it is probably part of a multidirectional laminate, the stresses in the principal directions must be determined and compared with the fundamental values.

Failure criteria for composite materials are often classified into two groups: namely, *non-interactive failure criteria* (associated with failure modes) and *interactive failure criteria* (associated with failure modes and not). In the following sections, both types will be discussed.

3.2 Non-interactive failure criteria

A non-interactive failure criterion or *limit criterion* is defined as one having no interactions between the stress or strain components. In detail, it means that the failure criterion evaluates failure based on a single stress component and does not take into consideration a multi-axial stress state in a structure and how the combination of different stress components affect the failure initiation in a composite ply; therefore, this fact typically leads to errors in the strength predictions. These criteria, sometimes called *independent failure criteria*, compare the individual stress or strain components with the corresponding material allowable strength. The maximum stress and maximum strain criteria belong to this category.

The *Maximum Stress Criterion* for orthotropic laminae was apparently first suggested in 1920 by Jenkins [7] as an extension of the Maximum Normal Stress Theory (or Rankine's Theory) for isotropic materials. It consists of five sub-criteria, or limits, one corresponding to the strength (or allowable) in each of the five fundamental failure modes [8]. If any one of these limits is exceeded, by the corresponding stress expressed in the principal material axes, the material is deemed to have failed. In mathematical terms it say that failure has occurred if the following set of inequalities is satisfied:

$$\sigma_{11} \geq X_T \ , \ \sigma_{11} \leq X_C \ , \ \sigma_{22} \geq Y_T \ , \ \sigma_{22} \leq Y_C \ , \ \left|\tau_{12}\right| \geq \left|S_{12}\right| \qquad (3.6)$$

The inequalities in 3.6 can be merged to obtain the failure criterion in the following form:

$$\text{max. absolute value of} \left(\frac{\sigma_{11}}{X_T}, \frac{\sigma_{11}}{X_C}, \frac{\sigma_{22}}{Y_T}, \frac{\sigma_{22}}{Y_C}, \frac{\tau_{12}}{S_{12}} \right) \geq 1 \qquad (3.7)$$

where σ_{11}, σ_{22}, τ_{12} are the applied stress aligned with fiber direction and $X_T, X_C, Y_T, Y_C, S_{xy}$ are the strengths in lamina plane. It is assumed that shear failure along the principal material axes is independent of the sign of the shear stress τ_{12}.

In 1967, Waddoups proposed the *Maximum Strain Criterion* for orthotropic laminae [9] as an extension of the Maximum Normal Strain Theory (or Saint Venant's Theory) for isotropic materials. The maximum strain criterion merely substitutes strain for stress in the five sub-criteria. As in the previous case, is a simple and direct way to predict failure of composites and no interaction between the strains acting on the lamina is considered. Therefore, the Max Strain failure criterion evaluates failure based on a single strain component and does not take into consideration a multi-axial strain state and how the combination of different strain components affect the failure initiation in a composite ply. This criterion predicts failure when any principal material axis strain

component exceeds the corresponding ultimate strain. In order, to obtain failure, the following set of inequalities must be satisfied:

$$\varepsilon_{11} \geq \varepsilon_{11}^{fail+} \ , \ \varepsilon_{11} \leq \varepsilon_{11}^{fail-} \ , \ \varepsilon_{22} \geq \varepsilon_{22}^{fail+} \ , \ \varepsilon_{22} \leq \varepsilon_{22}^{fail-} \ , \ \left|\varepsilon_{12}\right| \geq \left|\varepsilon_{12}^{fail}\right| \qquad (3.8)$$

The inequalities in 3.8 can be merged to obtain the failure criterion in the following form:

$$\text{max. absolute value of} \left(\frac{\varepsilon_{11}}{\varepsilon_{11}^{fail+}}, \frac{\varepsilon_{11}}{\varepsilon_{11}^{fail-}}, \frac{\varepsilon_{22}}{\varepsilon_{22}^{fail+}}, \frac{\varepsilon_{22}}{\varepsilon_{22}^{fail-}}, \frac{\varepsilon_{12}}{\varepsilon_{12}^{fail}} \right) \geq 1 \qquad (3.9)$$

where ε_{11}, ε_{22}, ε_{12} are the applied stress aligned with fiber direction and $\varepsilon_{11}^{fail+}, \varepsilon_{11}^{fail-}, \varepsilon_{22}^{fail+}, \varepsilon_{22}^{fail-}, \varepsilon_{12}^{fail}$ are each obtained from the ratio between the resistance in a certain direction and respective elastic modulus.

Both discussed failure criteria indicate the type of failure mode. The failure surfaces for these criteria are rectangular in stress and strain space, respectively [10].

3.3 Interactive failure criteria

Interactive failure criteria involve interactions between stress or strain components. The objective of this approach is to allow for the fact that failure loads when a multi-axial stress state exists in the material may well differ from those when only a uniaxial stress is acting. Interactive failure criteria are mathematical in their formulation. Interactive failure criteria fall into three categories: (1) polynomial theories, (2) direct-mode determining theories, and (3) strain energy theories. The polynomial theories use a polynomial based upon the material strengths to describe a failure surface [11]. The direct-mode determining theories are usually polynomial equations based on the material strengths and use separate equations to describe each mode of failure. Finally, the strain energy theories are based on local strain energy levels determined during a nonlinear analysis. Most of the interactive failure criteria are polynomials based on curve-fitting data from composite material tests.

The interactive failure criteria proposed to predict lamina failure could be divided in two main groups: failure criteria not associated with failure modes and failure criteria associated with failure modes. In the following sections, both types will be discussed.

3.3.1 Failure criteria not associated with failure modes

This group includes all polynomial and tensorial criteria, using mathematical expressions to describe the failure surface as a function of the material strengths. Generally, these expressions are based on the process of adjusting an expression to a curve obtained by experimental tests. The most general polynomial failure criterion for composite materials is Tensor Polynomial Criterion proposed by Tsai and Wu [12]. The Tsai and Wu (1971) failure criterion is a phenomenological criterion, i.e. based on observation rather than derived from fundamental theories. It was derived in an attempt to predict the failure of a material by its stress invariants. As such, a single polynomial expression is used to express the advent of failure. This criterion does not identify the failure type nor the direction. The Tsai-Wu criterion remains one of the most widely used failure criterion for composite material. The Tsai-Wu criterion for composite lamina may be expressed in tensor notation as:

$$F_i\sigma_i + F_{ij}\sigma_i\sigma_j + F_{ijk}\sigma_i\sigma_j\sigma_k \geq 1 \qquad i, j, k = 1, ..., 6 \qquad (3.10)$$

where F_i, F_{ij} and F_{ijk} are components of the lamina strength tensors in the principal material axes. The usual contracted stress notation is used except that $\sigma_4 = \tau_{23}$, $\sigma_5 = \tau_{13}$ and $\sigma_6 = \tau_{12}$. However, the third-order tensor F_{ijk}, is usually ignored from a practical standpoint due to the large number of material constants required [12]. Then, the general polynomial criterion reduces to a general quadratic criterion given by:

$$F_i\sigma_i + F_{ij}\sigma_i\sigma_j \geq 1 \qquad i, j = 1, ..., 6 \qquad (3.11)$$

or in explicit form:

$$F_1\sigma_1 + F_2\sigma_2 + F_3\sigma_3 + 2F_{12}\sigma_1\sigma_2 + 2F_{13}\sigma_1\sigma_3 + 2F_{23}\sigma_2\sigma_3 + F_{11}\sigma_1^2 + F_{22}\sigma_2^2 + F_{33}\sigma_3^2 + F_{44}\sigma_4^2 + F_{55}\sigma_5^2 + F_{66}\sigma_6^2 \geq 1 \quad (3.12)$$

Considering that the failure of the material is insensitive to a change of sign in shear stresses (shear strengths are the same for positive and negative shear stress), all terms containing a shear stress to first power must vanish: $F_4 = F_5 = F_6 = 0$. This single mathematical expression for failure cannot be justified physically. Laminated composites fail according to different mechanisms depending on the orientation of loading. Other popular quadratic failure criteria include those by Tsai-Hill [13,14], Azzi and Tsai [15], Hoffman [16], and Chamis [17] can be represented in terms of the general Tsai-Wu quadratic criterion and are summarized in Fig. 3.1.

	Quadratic Polynomial Failure Criteria				
	Tsai-Wu	Tsai-Hill*	Azzi-Tsai*	Hoffman	Chamis*†
F_1	$\frac{1}{X_T}-\frac{1}{X_C}$	0	0	$\frac{1}{X_T}-\frac{1}{X_C}$	0
F_2	$\frac{1}{Y_T}-\frac{1}{Y_C}$	0	0	$\frac{1}{Y_T}-\frac{1}{Y_C}$	0
F_3	$\frac{1}{Z_T}-\frac{1}{Z_C}$	0	0	$\frac{1}{Z_T}-\frac{1}{Z_C}$	0
F_{12}	$-1/2\sqrt{X_TX_CY_TY_C}$	$-\frac{1}{2}\left(\frac{1}{X^2}+\frac{1}{Y^2}-\frac{1}{Z^2}\right)$	$-\frac{1}{X^2}$	$-\frac{1}{2}\left(\frac{1}{X_TX_C}+\frac{1}{Y_TY_C}-\frac{1}{Z_TZ_C}\right)$	$-\frac{K_{12}}{XY}$
F_{13}	$-1/2\sqrt{X_TX_CZ_TZ_C}$	$-\frac{1}{2}\left(\frac{1}{Z^2}+\frac{1}{X^2}-\frac{1}{Y^2}\right)$	0	$-\frac{1}{2}\left(\frac{1}{X_TX_C}+\frac{1}{Z_TZ_C}-\frac{1}{Y_TY_C}\right)$	$-\frac{K_{13}}{XZ}$
F_{23}	$-1/2\sqrt{Y_TY_CZ_TZ_C}$	$-\frac{1}{2}\left(\frac{1}{Y^2}+\frac{1}{Z^2}-\frac{1}{X^2}\right)$	0	$-\frac{1}{2}\left(\frac{1}{Z_TZ_C}+\frac{1}{Y_TY_C}-\frac{1}{X_TX_C}\right)$	$-\frac{K_{23}}{YZ}$
F_{11}	$\frac{1}{X_TX_C}$	$\frac{1}{X^2}$	$\frac{1}{X^2}$	$\frac{1}{X_TX_C}$	$\frac{1}{X^2}$
F_{22}	$\frac{1}{Y_TY_C}$	$\frac{1}{Y^2}$	$\frac{1}{Y^2}$	$\frac{1}{Y_TY_C}$	$\frac{1}{Y^2}$
F_{33}	$\frac{1}{Z_TZ_C}$	$\frac{1}{Z^2}$	0	$\frac{1}{Z_TZ_C}$	$\frac{1}{Z^2}$
F_{44}	$\frac{1}{R^2}$	$\frac{1}{R^2}$	0	$\frac{1}{R^2}$	$\frac{1}{R^2}$
F_{55}	$\frac{1}{S^2}$	$\frac{1}{S^2}$	0	$\frac{1}{S^2}$	$\frac{1}{S^2}$
F_{66}	$\frac{1}{T^2}$	$\frac{1}{T^2}$	$\frac{1}{T^2}$	$\frac{1}{T^2}$	$\frac{1}{T^2}$

Fig. 3.1 – Quadratic Polynomial Failure Criteria [18].

In Fig. 3.1, X, Y, and Z are lamina strengths in the x, y, and z directions, respectively, and R, S, and T are the shear strengths in the yz, xz, and xy planes, respectively. The subscripts T and C in X, Y, and Z refer to the normal strengths in tension and compression. X, Y, and Z are either X_C, Y_C, and Z_C or X_T, Y_T, and Z_T depending upon the sign of σ_1, σ_2 and σ_3 respectively. Finally, K_{12}, K_{13}, and K_{23} are the strength coefficients depending upon material.

The failure surfaces for these quadratic criteria are elliptical in shape, see Fig. 3.2. This class of criteria is nevertheless convenient, as only one criterion needs to be implemented, which explains why it has been programmed in numerous FEM codes. One of the disadvantages of these quadratic failure criteria is that they predict the initiation of failure but say nothing about the failure mode or how the composite fails.

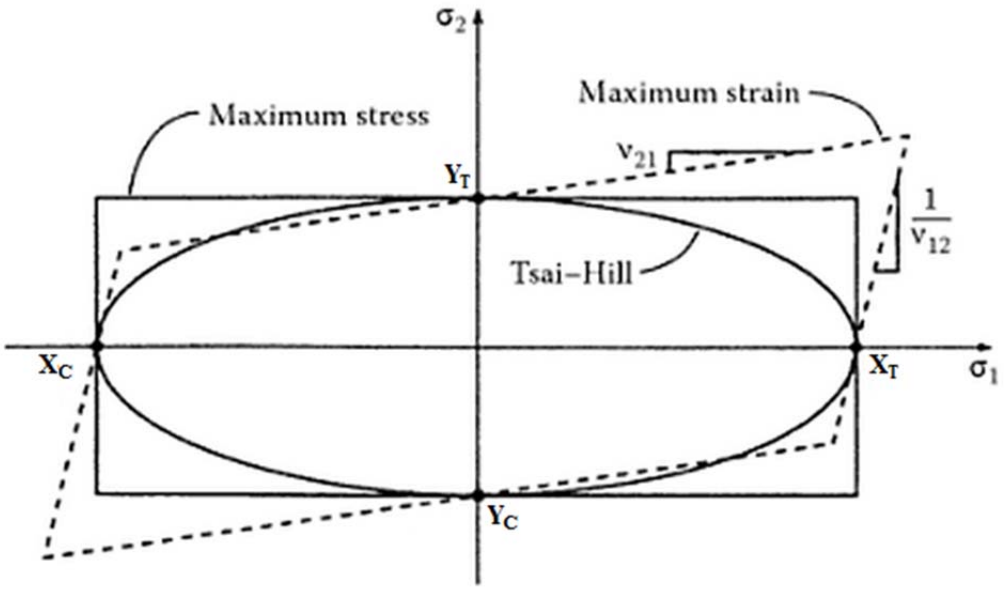

Fig. 3.2 – Maximum stress, maximum strain and Tsai-Hill failure surfaces in σ_1-σ_2 space. Source: Ronald F. Gibson, Principles of Composite Material Mechanics, Third Edition.

3.3.2 Failure criteria associated with failure modes

These criteria consider that the non-homogeneous character of composites leads different failure modes of the constituents. They are established in terms of mathematical expressions using the

material strengths and they have the advantage of being able to predict different failure modes, being therefore adequate to be used in a progressive damage analysis. The majority of the criteria proposed identify the following failure modes: fiber fracture; transverse matrix cracking; shear matrix cracking, etc. The origin of these criteria can be attributed to Hashin [19] which stated that the Tsai-Wu theory had an intrinsic problem since it could not distinguish among the various different failure modes of the composite material. He instead proposed a quadratic failure criterion in piecewise form based on material strengths, where each smooth branch represents a failure mode. According to the theory of Hashin, in unidirectional composites, there are two primary failure modes: a fiber mode and a matrix mode subdivided into either tension or compression failure. In the fiber mode, the lamina fails due to fiber breakage in tension or fiber buckling in compression. In the matrix mode, failure is due to matrix cracking.

The model proposed by Hashin and Rotem (1973) [19] is one of the first widely used failure models specifically for unidirectional composite lamina. Whereas the maximum stress criteria are fully decoupled failure criteria, the Hashin-Rotem criteria are partially coupled, i.e. failure can involve normal and shear stresses. This failure model involves two failure mechanisms, one associated with fiber failure and the other with matrix failure, distinguishing between tension and compression:

- tensile fiber failure occurs if: $\sigma_{11} \geq X_T \qquad (\sigma_{11}, X_T > 0)$
- compressive fiber failure occurs if: $-\sigma_{11} \geq X_C \qquad (\sigma_{11} < 0, X_c > 0)$
- tensile matrix failure occurs if: $\left(\frac{\sigma_{22}}{Y_T}\right)^2 + \left(\frac{\sigma_{12}}{S}\right)^2 \geq 1 \quad (\sigma_{22} > 0) \qquad (3.13)$
- compressive matrix failure occurs if: $\left(\frac{\sigma_{22}}{Y_C}\right)^2 + \left(\frac{\sigma_{12}}{S}\right)^2 \geq 1 \quad (\sigma_{22} < 0)$

where:

- σ_{11} is the nominal stress in the lamina in the direction of the fibers;
- σ_{22} is the nominal stress in the lamina in the transverse direction to the fibers;
- σ_{12} is the nominal shear stress in the plane of the lamina;
- X_T is the tensile strength of the fibers;
- X_C is the compressive strength of the fibers;
- Y_T is the tensile strength in the transverse direction of the fibers;
- Y_C is the compression strength in the transverse direction of the fibers;
- S is the shear strength.

Therefore, based on observations of specimen failure in tension with different orientations of the fibers, the authors of this proposal failure model conclude that there are only two mechanisms of failure: fiber or matrix failure. With reference to the second, they do not distinguish whether the failure is exactly at the interface or inside the matrix and thus propose that both and contribute to the appearance of the failure (the proposal is in quadratic form). The historical importance of this proposal is that it initiates a different way of approaching the generation of composites failure criteria. The authors first set out to recognize modes of failure, then to recognize the variables associated with these modes and propose an interaction between them. The idea seems adequate for the type of materials under consideration, although it may be argued that not all failure modes that can appear in fibrous composites are covered in the proposal.

Hashin later proposed a failure criterion for fibrous composites under a three-dimensional state of stress [20]. The Hashin criteria are a modification to the Hashin-Rotem criteria to account for the beneficial influence of compressive stresses on the matrix strength (Hashin, 1980). For the matrix failure mode, a quadratic approach was chosen because a linear criterion underestimates the material strength, and a polynomial of higher degree would be too complicated to deal with. Furthermore, the effect of the shear stress is now taken into account in the tensile fiber mode:

- stress tensile fiber failure criterion: $\left(\frac{\sigma_{11}}{X_T}\right)^2+\left(\frac{\sigma_{12}}{S_{12}}\right)^2\geq 1$

- compressive fiber failure remains unchanged: $\left(\frac{\sigma_{11}}{X_C}\right)^2\geq 1$ (3.14)

- tensile matrix failure is also unchanged and occurs if: $\left(\frac{\sigma_{22}}{Y_T}\right)^2+\left(\frac{\sigma_{12}}{S_{12}}\right)^2\geq 1$

- compressive matrix failure now incorporates an additional term, taking the form:

$$\left(\frac{\sigma_{22}}{2S_{23}}\right)^2+\left[\left(\frac{X_C}{2S_{23}}\right)^2-1\right]\left(\frac{\sigma_{22}}{X_C}\right)+\left(\frac{\tau_{12}}{S_{12}}\right)^2\geq 1$$

Numerous failure theories are available for fiber-rein-forced composites to date but not all are discussed here. Therefore, for further information, it is recommended the reading of Ref. [5].

References

[1] M. Mukhopadhyay, “Mechanics of Composite Materials and Structures”, Universities Press, 2005.

[2] G. Sala, “Criteri di resistenza per materiali compositi con rinforzo a fibre continue”, Corso di Tecnologie e materiali aerospaziali, Politecnico di Milano.

[3] C. Boshers, “Design Allowables”, ASM Handbook Volume 21, Composites (ASM International), 2001.

[4] C. G. Davila, P. P. Camanho, C. A. Rose, “Failure Criteria for FRP Laminates”, Journal of Composite Materials February, 2005, 39(4):323-345.

[5] P. D. Soden, M. J. Hinton, A. S. Kaddour, “A Comparison of the Predictive Capabilities of Current Failure Theories for Composite Laminates, Composites Science and Technology”, 1998, 58:1225-1254.

[6] M. J. Hinton, A. S. Kaddour, P. D. Soden, “A Comparison of the Predictive Capabilities of Current Failure Theories for Composite Laminates, Judged against Experimental Evidence”, Composites Science and Technology, 2002, 62:1725-1797.

[7] C. F. Jenkins, “Report on materials of construction use in aircraft engines”, Great Britain Aeronautical Research Committee, London, HMSO.

[8] S. K. Gaggar, L. J. Broutman, “The development of a damage zone at the tip of a crack in a glass fiber reinforced polyester resin”, International Journal of Fracture, 1974, 10:606-608.

[9] S. C. Kunz, P. W. R. Beaumont, “Microcrack growth in graphite fiber-epoxy resin systems during compressive fatigue”, in J. R. Hancock ed., Fatigue of Composite Materials, ASTM STP,1975, 569:71-91.

[10] J. N. Reddy, A. K. Pandey, “A First-Ply Failure Analysis of Composite Laminates” Computers and Structures, 1987, 25:371-393.

[11] W. P. Lin, H. T. Hu , ”Nonlinear Analysis of Fiber-Reinforced Composite Laminates Subjected to Uniaxial Tensile Load”, Journal of Composite Materials, 2002, 36(12):1429-1450.

[12] S. W. Tsai, E. M. Wu, “A General Theory of Strength for Anisotropic Materials”, Journal of Composite Materials, 1971, 5:58-80.

[13] S. W. Tsai, “Strength Characteristics of Composite Materials”, NASA CR-224, 1965.

[14] R. Hill, “A Theory of the Yielding and Plastic Flow of Anisotropic Metals”, Proceedings of the Royal Society of London, Series A, 1948, 193: 281-297.

[15] V. D. Azzi, S. W. Tsai, “Anisotropic Strength of Composites. Experimental Mechanics”, 1965, pp. 283-288.

[16] O. Hoffman, “ The Brittle Strength of Orthotropic Materials” Journal of Composite Materials, 1967, 1: 200-206.

[17] C. C. Chamis, “ Failure Criteria for Filamentary Composites. Composite Materials: Testing and Design”, STP 460, American Society for Testing and Materials, Philadelphia, 1969, pp. 336-351.

[18] D. W. Sleight, “Progressive Failure Analysis Methodology for Laminated Composite Structures”, NASA/TP-1999-209107.

[19] Z. Hashin, A. Rotem, “A Fatigue Failure Criterion for Fiber Reinforced Materials. Journal of Composite Materials”, 1973, 7:448-464.

[20] Z. Hashin, “Failure Criteria for Unidirectional Fiber Composites”, ASME Journal of Applied Mechanics, 1980, 47:329-334.

CHAPTER 4

COHESIVE-FRICTIONAL MODEL

4.1 Introduction to cohesive bond

The development of new and advanced materials leads to new challenges on the production technology and this is especially true when different materials must be joined together to make composites so as to preserve the beneficial properties of the individual components. In this perspective, the choice of joining techniques is often as important as the materials themselves. In industrial manufacturing, the structural adhesives are used to create connections (joints) representing a solution to assembly of a mechanical system. The adhesive bonding is the technique for connecting parts of a structure (or better yet their respective substrates), essentially similar or different materials, by means of adhesive. The "material-adhesive-material" system is called *bonded joint*. In a bonded joint, it is possible to distinguish three regions [1]:

- an *adhesion zone*, where is established the contact between the adhesive material and the substrate of material to be bonded. The adhesion phenomenon is the result of molecular interactions between the substrate surface and the adhesive. These interactions can be divided into: weak intermolecular interactions (e.g. van der Waal forces, hydrogen bonds) and strong chemical bonds (e.g. covalent, metallic and ionic bonds);
- a *transition zone* that separates the adhesive area from the cohesive area; in this zone the structure, the composition and the macroscopic properties of the adhesive are constantly changing;
- a *cohesion zone*, where there is the adhesive inherent strength (just called *cohesion*), in which the adhesive is present in its normal state.

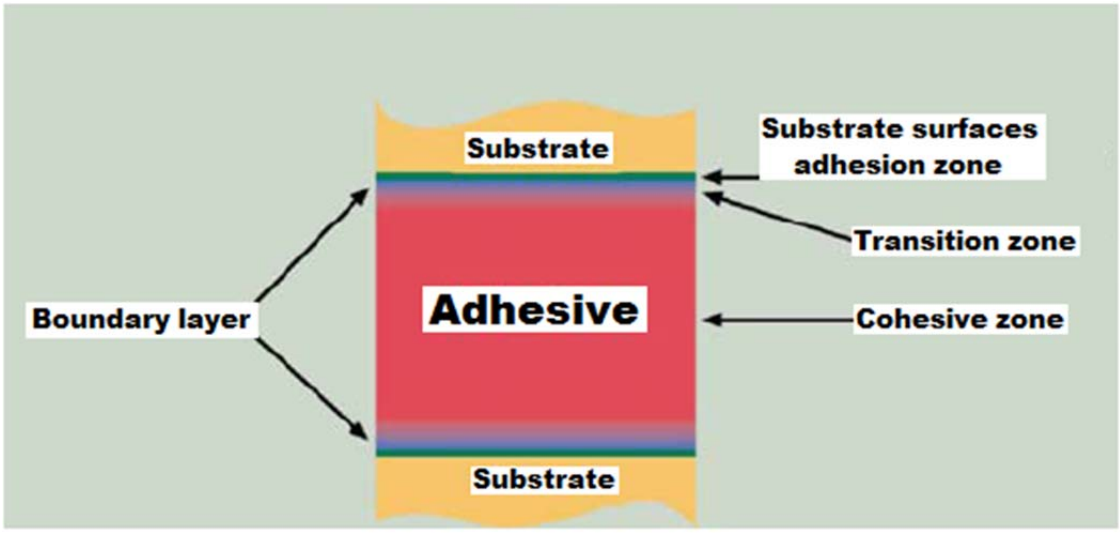

Fig. 4.1 – Joint section [1].

The adhesive bond have several advantages in comparison of mechanical fasteners such as high resistance to fatigue and corrosion and superior resistance properties that often allow the structures which are mechanically more durable (or equivalent) than conventional assemblies to be made with cost and lower weight. However adhesively bonded joints inevitably contain defects such as: voids; poor adhesion between adhesive and adherend; crack presence; these defects can evolve triggering the *decohesion* and the fracture formation.

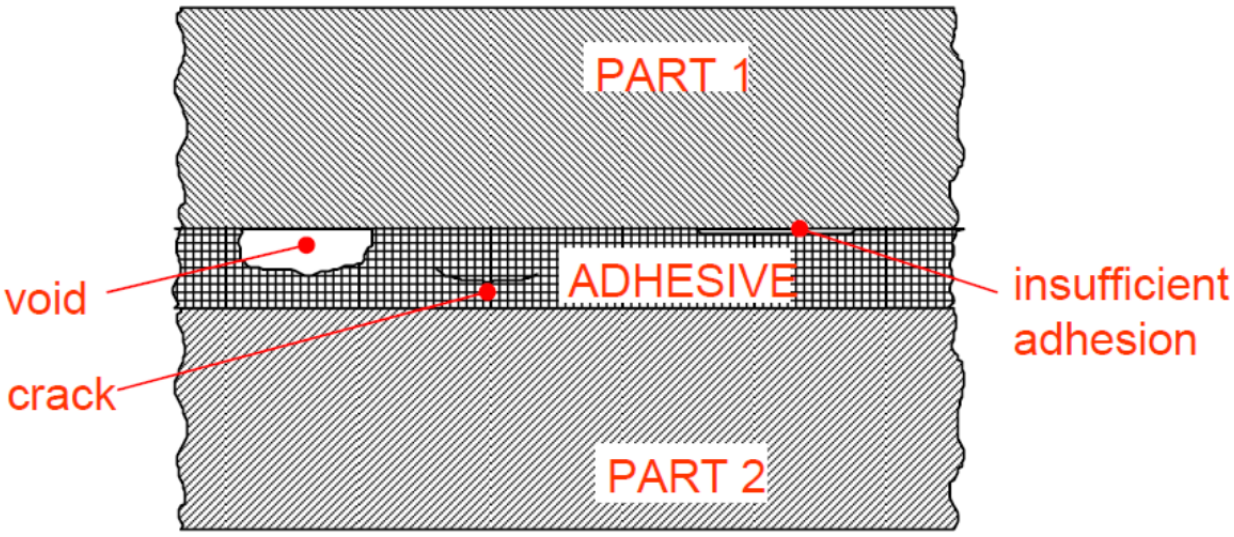

Fig. 4.2 – Defects in the joint.

4.2 Mechanical integrity evaluation approaches

The evaluation of the mechanical integrity of each structure with defects requires the development of approaches. Two types of approach have been developed for these purposes. The first called *macromechanical approach* is essentially based on the LEFM (linear elastic fracture mechanics) and EPFM (elastic plastic fracture mechanics) theories. The basic assumption is that the fracture strength can be measured in terms of a single parameter (energy fracture G_c, intensity factor K_c or J-integral) [2]. This approach is very practical, but it clashes with certain limitations, especially in presence of large plasticity scale. The major disadvantage of the approaches based on the fracture mechanics is that the size and the position of the initial crack must be known, that is, the crack is supposed already existing (pre-existing crack – e.g. defects or notches), not allowing to simulate opening processes of the crack (e.g. it does not allow to predict the onset of delamination). Moreover, in the LEFM, the fracture process is considered to be concentrated at the end of the crack; therefore it does not provide a detailed description of what happens in the *fracture process zone* (FPZ). In reality, the area in front of the crack tip is a region of material degradation which is damaged and characterized by the presence of reclosing forces; this region is called *cohesive zone* and the forces which are opposed to propagation of the macrofracture in evolution are essentially cohesion forces (e.g. intermolecular forces of electrostatic nature or van ser Waals forces).

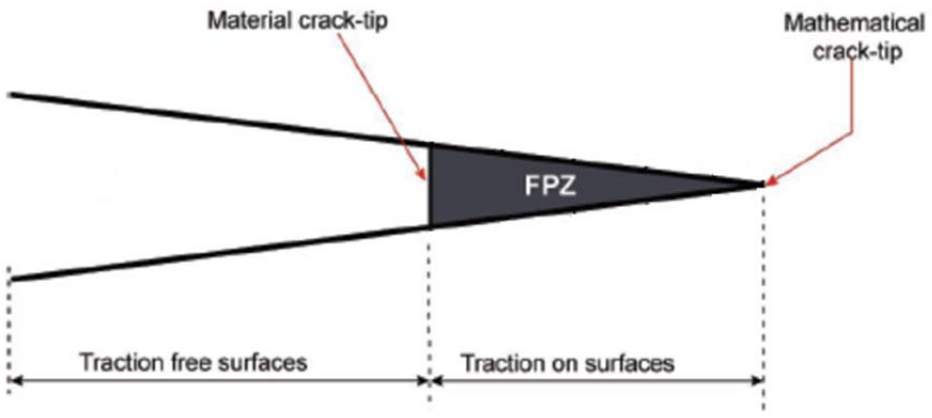

Fig. 4.3 – The fracture process zone.

Another approach available sometimes erroneously called *micromechanical approach* has developed over the last thirty years and it is based on continuum damage mechanics theory; among the models that are based on this, the cohesive zone model has been mainly used for the adhesive joints. The idea of cohesive zone was originally introduced by Dugdale [3] and Barenblatt [4] which essentially postulated the existence of a process zone in front of the crack tip and divided the area of crack propagation (or crack simply) in a region affected by tractions and a region free from tractions thus eliminating the singularity at the crack tip, see Fig. 4.3. This new approach is based on the consideration that prior to the development of macroscopic fractures, there is a zone in a condition of progressive damage localized in front of the crack, in which occurs microscopic nonlinear and dissipative phenomena, the so-called *cohesive process zone* in which the crack is forming (that is, the material is damaging); in this zone, the material is partially damaged, because the surfaces of the fracture are still able to be transmitted tractions (*cohesive tractions* or tensile forces), so there is an interaction between the two sides of the crack.

A cohesive zone model (CZM) allows the fracture simulation of an adhesive joint without requiring any pre-recruitment on the initial crack position and size thus allowing describes the nucleation, growth and propagation of interface cracks. Therefore according to the cohesive zone model the singular region introduced by the LEFM (the crack tip) can be removed by introducing a region in which non-linear phenomena occur and wherein the fracture process is described by constitutive relations, Fig. 4.4, describing the evolution of traction generated through the crack faces [5] as a function of crack face opening displacements.

The physical phenomena behind the process zone was first proposed for concrete materials as bridging due to second phase particles and away from bridging, micro-cracking were responsible [6]. This can be characterized as micro structural linkage units may be identified with cohesive bond in brittle solids, ductile filaments in plastic solids, transverse molecular chains in polymers [7]. For composites, however, load-bearing fibers, voiding and crazing are the physical phenomena resulting in such a process zone [7].

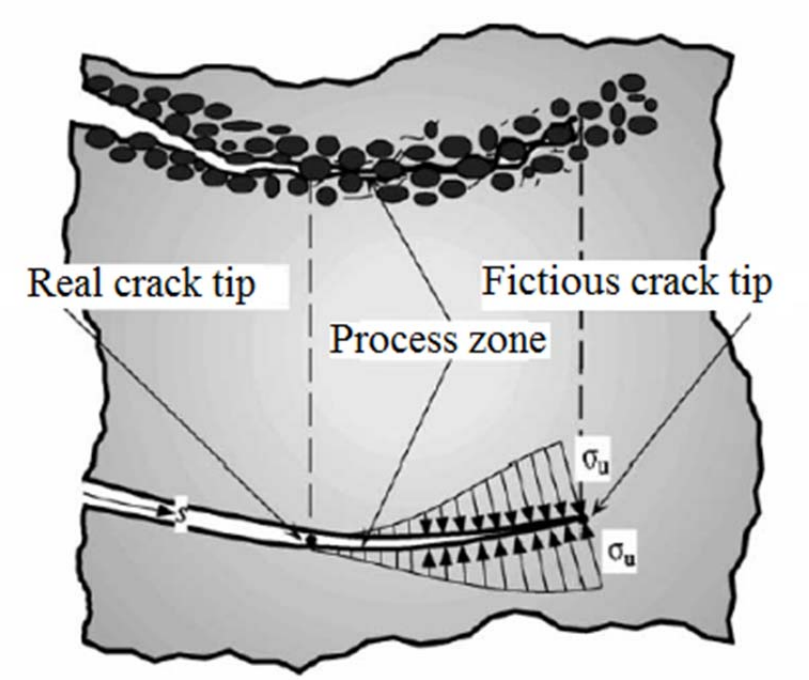

Fig. 4.4 – Process zone and cohesive tractions (without shearing stress). In the cohesive zone model the basic assumption is the formation of process zone (extension of the real crack), where the material, although damaged, is still able to transfer stresses. The point separating the real crack (region free from tractions) from the process zone, is called the *Real Crack Tip*, while the point separating the process zone from the uncracked material is referred to as the *Fictitious Crack*. The crack will propagate when stress at the crack tip reaches the material's ultimate tensile strength σ_u (or cohesive strength). At the fictitious crack tip, the stress will always be equal to the ultimate tensile strength, thus eliminating stress singularities. During crack propagation, the stresses transferred by the material are some form of decreasing functions of the crack separation [5]. All the energy dissipation takes place in the process zone, while the bulk material remains linear elastic.

4.3 Cohesive constitutive law

There are several ways to develop a constitutive law which binds the tractions to relating separation displacements and which represents the microscopic mechanism of fracture associated inelastic processes: deriving it from specific micromechanical models; by means of experimental or phenomenological way. The most constitutive laws for the cohesive zone in the literature, however, have been developed phenomenologically adopting different functions such as exponential function, trapezoidal or very commonly a bilinear function, see Fig. 4.5.

Among the various forms of cohesive laws, there is a common feature, namely the intensity of the traction typically, σ in Fig. 4.5, increases with the separation the cohesive surfaces, δ, and after that a peak value critical is reached, σ_0, the traction tends to zero with increasing separation. The descent after a peak tensile indicates the material softening within the fracture process. When the traction reaches the critical value of the displacement, δ_c, the fracture process is completed.

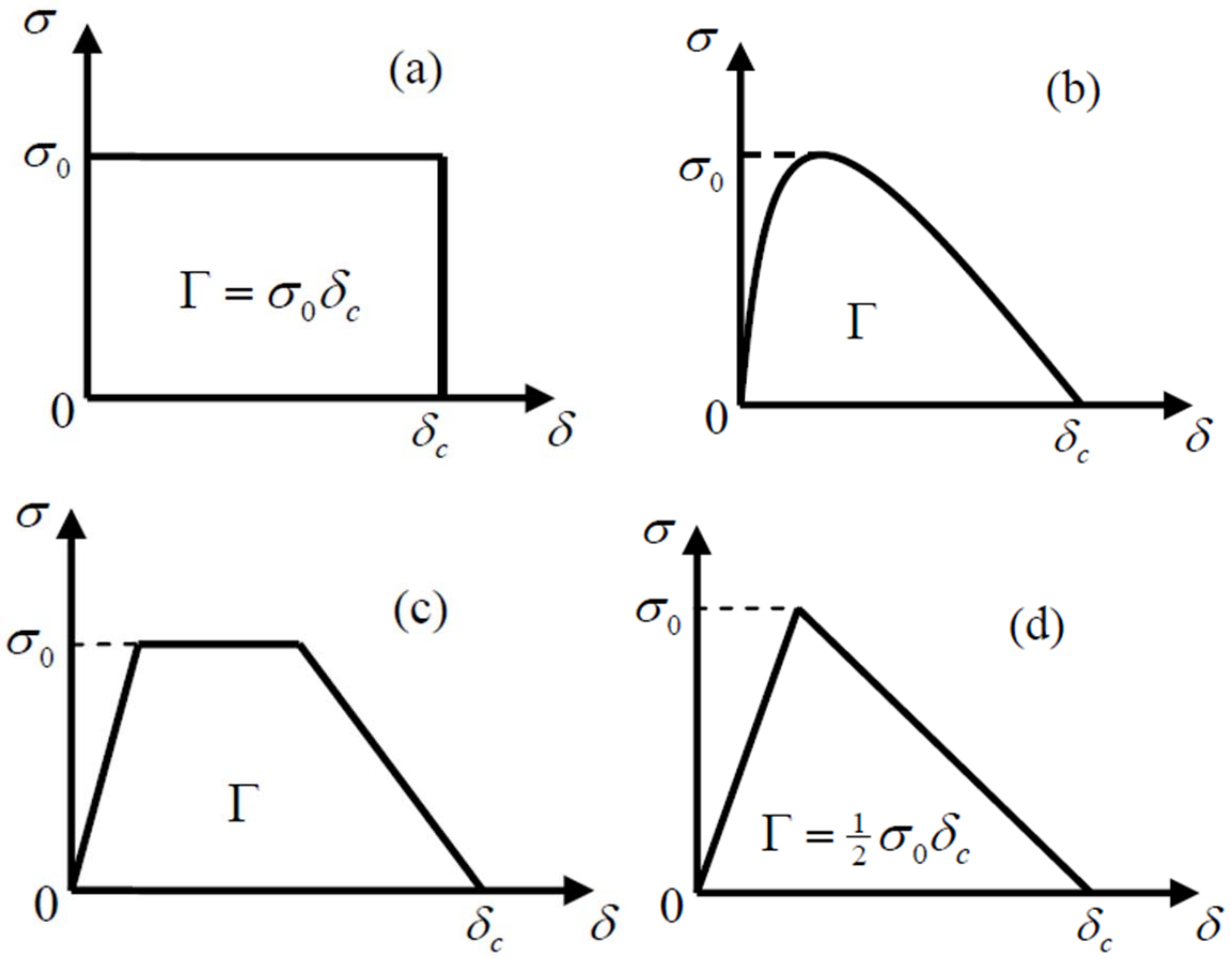

Fig. 4.5 - Examples of a traction-separation relations (constitutive laws for cohesive zone modeling): (a) constant tension for perfect plasticity, (b) regular non-linear, (c) trapezoidal, (d) bilinear or triangular [8].

A constitutive relation which describes interfacial (fracture) behavior is now discussed in detail. The constitutive law used is shown in Fig. 4.6. This law is a bilinear relationship between relative displacements and tractions.

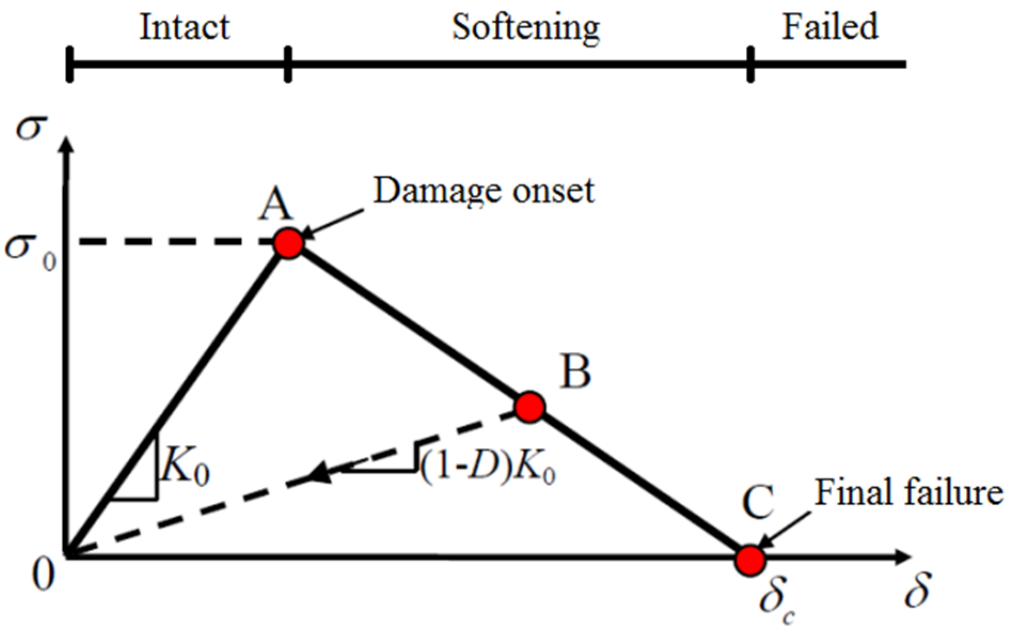

Fig. 4.6 - Illustration of the traction-separation bilinear law [8].

The interface, subjected to opening stress σ, opens first elastically with initial elastic stiffness K_0 (the first branch 0-A represents an elastic relationship) until the stress reaches the *cohesive interface strength* σ_0 (i.e. $\sigma = \sigma_0$): this represents the stress limit for the cohesive zone on the basis of the resistance of the adhesive; the achievement of this limit represents the *damage onset criterion* (i.e. when $\sigma = \sigma_0$ there is the damaging onset). A *damage parameter* D is used to describe the interface status and it evolves from 0 to 1 on the basis of a damage evolution law. When the interface is partially damaged (0<D<1), the required opening stress is linked linearly to the opening displacement in according to the following relationship:

$$\sigma = (1 - D)K_0\delta \qquad (4.1)$$

This equation is valid both during loading and unloading. During the load application, the damage parameter D increases as the opening displacement increases. When $\delta \geq \delta_c$, D = 1 and σ = 0: this condition indicates that the interface is completely broken. It is noted that during unloading (branch B-0) D remains constant; therefore, the stress decreases linearly as the opening displacement decreases with a slope $K=(1-D)K_0$ as shown by the dashed line in Fig. 4.6.

Three parameters must necessarily be known to describe the shape and the size of this triangle:

- the initial elastic stiffness K_0 (the slope of linear branch);
- the cohesive strength σ_0 / elastic energy at damage onset G_0;
- the separation critical δ_c / fracture energy G_c.

The last two parameters define respectively the curve height and width while the enclosed area represents the energy dissipated in the fracture process. As said above, the relations that describe the behavior of the cohesive interface are hence:

$$\sigma = \begin{cases} K\delta & \delta \le \delta_c \ (Before\ damage\ initiation) \\ (1-D)K\delta & \delta_c < \delta < \delta_e \ (After\ damage\ initiation) \\ 0 & \delta \ge \delta_e \ (After\ complete\ damage) \end{cases} \qquad (4.2)$$

4.4 Simulation of delamination in composites

The delamination is an interface cracking phenomenon and one of the most common damage modes in layered structures [9] such as laminated composites. It may arise under various circumstances (low velocity impacts, temperature fluctuations, bearing loads in structural joints, etc.) and its occurrence greatly reduces the stiffness of a structure, often leading to catastrophic failure during processing or in service. Furthermore this damage mode is particularly important for the structural integrity of composite structures because it is difficult to detect during inspection. Although it has been extensively investigated, the delamination mechanism of composite panels is far from fully understood. One method to understand this damage mechanism is the use of finite element analysis. The simulation of delamination using the finite element method (FEM) is normally performed by means of the Virtual Crack Closure Technique (VCCT) [10] or using cohesive finite elements [11]. However there are some difficulties when using the VCCT in the simulation of progressive delamination. The calculation of fracture parameters requires nodal variables and topological

information from the nodes ahead and behind the crack front. Such calculations are tedious to perform and may require remeshing for crack propagation. The use of cohesive finite elements can overcome some of these difficulties. They can predict both the onset and the propagation of delamination allowing to describe the non-linear behavior of the surface of interlaminar adhesion and in particular to model the complex phenomena that occur in the so-called process zone, in the vicinity of the apex of the fracture. In this work, the delamination damage resulting from low velocity impact (LVI) is examined using cohesive elements.

The application of cohesive model is performed by finite element analysis in which the candidate delamination surfaces are modeled by interface elements obeying cohesive zone constitutive relationship. As understood from the name "interface", the elements are located between the adjacent plies where the delamination occurs. They are positioned in places where they potential crack can develops, for example where there is a mismatch of material properties (discontinuitiy) across the interface as in layered structures between two adjacent plies with different fiber orientations, see Fig. 4.7, and they are characterized by a traction-relative displacement relationship (typically non-linear) which describes the evolution of the process zone and the formation of free surfaces by means of tractions.

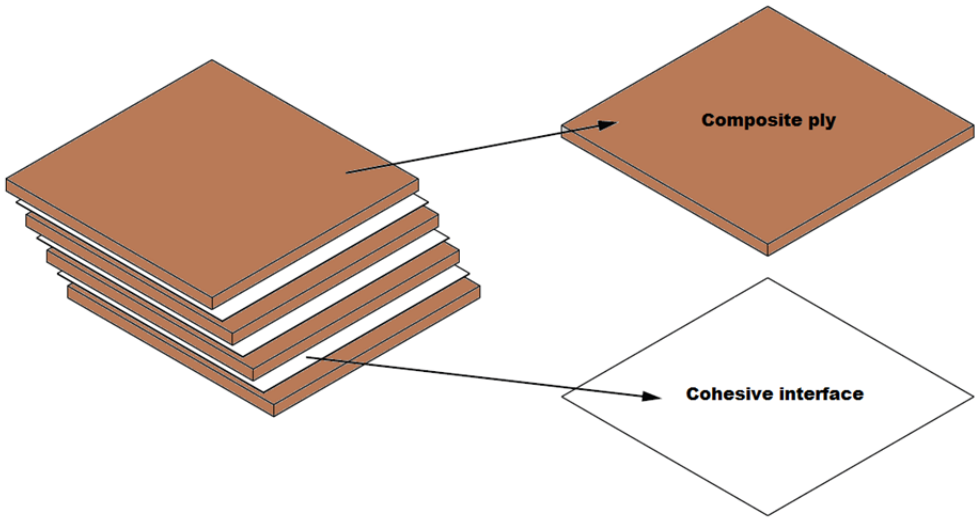

Fig. 4.7 – Cohesive interfaces between two adjacent plies.

The cohesive elements can be used to simulate the onset and growth of delaminations [12,13,14]. Cohesive finite elements can predict both the onset and the non-self-similar propagation of delamination. In general, they combine aspects of strength-based analysis to predict the onset of damage at the interface and fracture mechanics to predict the propagation of a delamination.

The interface element consists of two surfaces which are connected to adjacent solid elements; initially the two surfaces coincide, but they may be driven apart mechanically. The interface elements, in which the process zone is concentrated, are supposed to be in zero or near-to-zero thicknesses because they are located in the interfaces without affecting the real thickness of structure. This is the reason why the constitutive relations depend on displacements, not strains. The displacements in a cohesive zone model are relative displacements between the top and bottom interface surfaces which represent the adjacent delamination surfaces (in other words, the lower and upper surfaces are adjacent laminas). In order to predict the initiation and tridimensional growth of delamination, an 8-node cohesive element, available in most finite element commercial software packages such ABAQUS, see Fig. 4.8, is typically adopted.

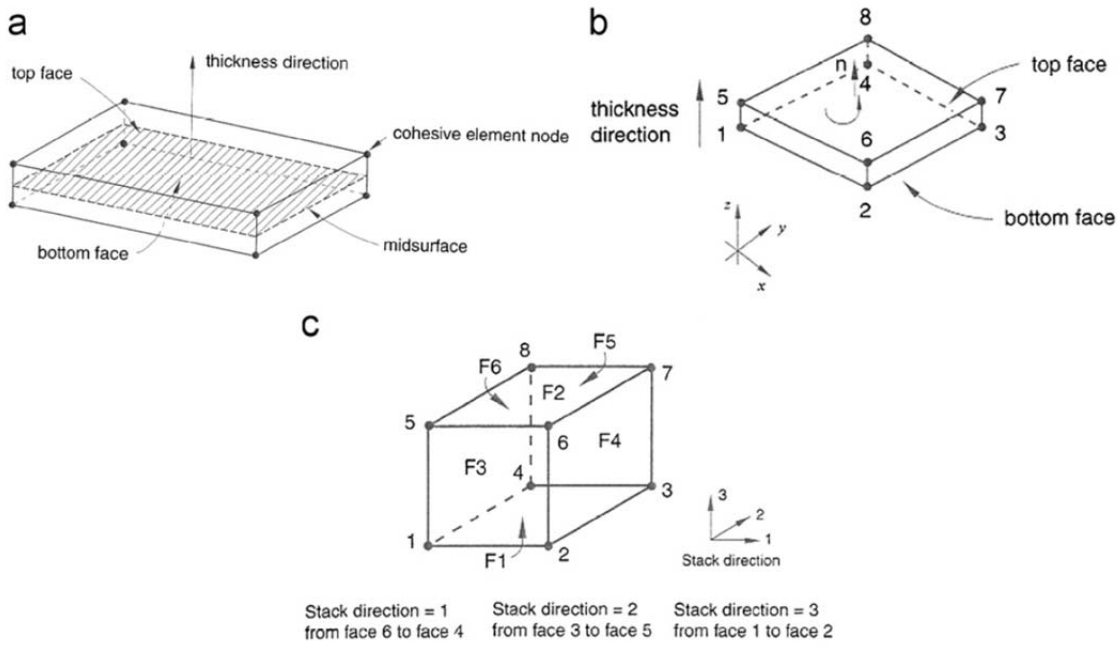

Fig. 4.8 – COH3D8 finite element characteristic available in ABAQUS: (a) representation, (b) thickness direction and (c) stack directions [15,16].

By adopting this technique, the behavior of the material is divided into two parts:

- continuous undamaged part with an arbitrary material law (modeled with standard solid elements as 3D 8-noded linear brick (hexahedral) elements);
- the cohesive interface between the elements of the continuum, which specify only the damage of the material with cohesive properties (modeled with cohesive solid elements), see Fig. 4.9.

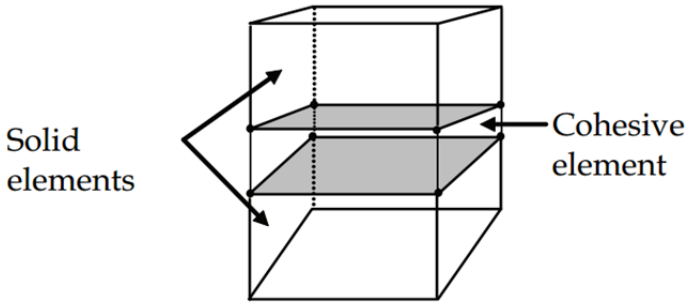

Fig. 4.9 - Eight-node cohesive and standard elements. Cohesive elements are positioned between the ones of bulk material.

Therefore, the elements of the cohesive zone does not represent any physical material, but describe the cohesive forces which occur when elements of material are pulled from opposite sides. The cohesive elements are connected with the layers above and below the interface, sharing nodes or by an interface bond (interface constraint or tie constraint). When the damage begins or grows, the cohesive elements are opened in order to simulate the crack onset or growth, see Fig. 4.10.

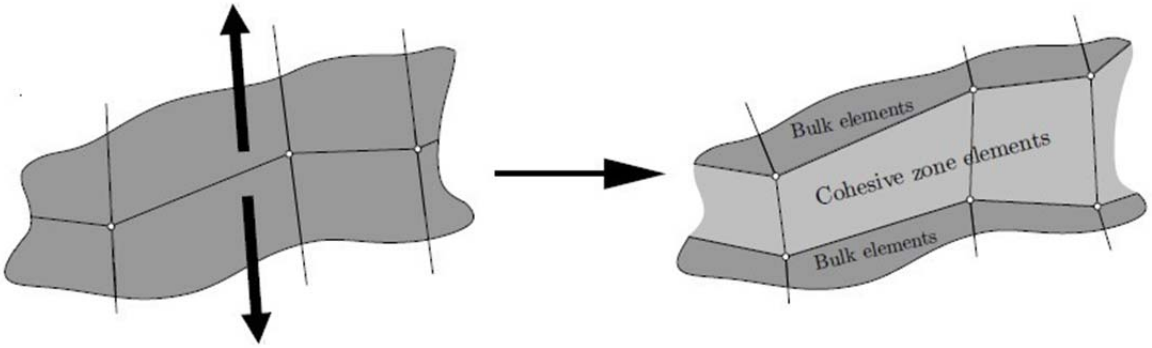

Fig. 4.10 – The opening of the cohesive element [17].

As previously anticipated, because the crack path can only follow these elements, the crack propagation direction depends on the presence (or absence) of cohesive zone elements, which means that the crack path is mesh dependent. If the crack propagation direction is not known in advance, the mesh generation must provide different possible crack paths.

4.5 The cohesive zone model

In the CZM, fracture is considered as a gradual phenomenon in which separation takes place across a cohesive zone resisted by cohesive tractions. The degradation of the material in the cohesive zone is represented by softening-type traction-separation laws which capture both strength-based bond weakening and fracture-based bond rupture.

In the following paragraph, an cohesive zone law accounting for progressive irreversible damage prior to complete separation is presented. The cohesive zone model used here is based on the model proposed in reference [18]. A brief description of the 2D model, with special focus on the constitutive damage model, is presented. Then, the model will be adapted to be used in 3D finite element applications. The cohesive interface model is formulated within the framework of damage mechanics and it is presented for the simulation of delamination in a laminated composite structure. The main features of the model are: the introduction of a single energy based damage variable for describing the damage state of the interface whose evolution is related to that of a critical damage-driving force and a treatment for the mixed-mode situation based on the definition of an equivalent energy release rate whose expression is consistently derived from the formulation. Damage onset and decohesion propagation conditions are obtained based upon two interaction criteria taken from the composite literature.

To describe the model, initially an 2D assembly consisting of two elastic bodies (adherends) joined by a plane adhesive layer is considered as reference problem. The adhesive layer thickness is

assumed to be negligible compared to both that of the joined bodies and to its in-plane dimensions; therefore the adhesive layer can be conveniently schematized as a zero-thickness surface entity (i.e. as an interface) ensuring stress transfer between the adherends. The interface will be considered as the only source of material nonlinearity; all expected dissipative phenomena are thus supposed to take place at this level only.

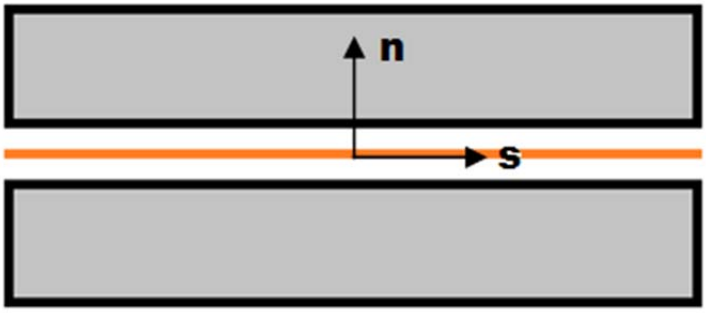

Fig. 4.11 – Interface schematization.

The energy definition of a system is very important. The cohesive zone model which will be discussed is derived from the damage theory, so from a thermodynamic approach which starts own from an expression of the free Helmholtz energy density (or stored elastic specific energy function) under isothermal condition:

$$\psi([\boldsymbol{u}],d)=\frac{1}{2}(1-d)k_n^+\left\langle[u_n]\right\rangle_+^2+\frac{1}{2}(1-d)k_s^+[u_s]^2+\frac{1}{2}k_n^-\left\langle[u_n]\right\rangle_-^2 \qquad (4.3)$$

where the subscripts n and s identify the normal and shear components respectively, see Fig. 4.11. Strictly speaking, the interfacial potential ψ describes only the energy stored in the elastic deformation of the cohesive material between microdefects such as crack or voids. The complete expression for free energy should also include a term corresponding to the surface energy of the microdefects. However, the presence of this term would be important only in coupled thermomechanical problems in which there is a substantial contribution of the mechanical

dissipation to the energy balance equation. For the present purpose, the surface energy term can be omitted.

In the interfacial potential expression above $[\boldsymbol{u}]$ is displacement jump vector while $[u_n]=[\boldsymbol{u}]\cdot\boldsymbol{n}$ and $[u_s]=[\boldsymbol{u}]\cdot\boldsymbol{s}$ are normal and sliding displacement components respectively (**n** and **s** denote the outward unit normal and the unit tangent vector to the interface respectively). The Macaulay bracket for normal displacement component takes the value zero if $[u_n]<0$ to guarantee that a pure compressive stress does not contribute to damage; d is a scalar internal damage continuous variable or damage parameter used to describe interface status; it takes on values between zero (no damage) and one (failure). The parameter can be interpreted mechanically as a measure of the microvoids which develop in the interface on micromechanical scale. k_n^+ / k_s^+ e k_n^- are the undamaged interface stiffnesses in tension and compression respectively; in particular k_n^- represents a penalty stiffness introduced to avoid the interpenetration of the fracture surfaces when $[u_n]<0$. In this model the crushing between the two fracture surfaces can not affect the quality of the cohesive zone; so the cohesive damage does not develop in compression. As stated above, only the stiffness k^+ is a model mechanical parameter and it can be estimated with good approximation by means of ultrasonic techniques.

The constitutive equations follow from standard continuum thermodynamics; deriving the function ψ with respect to the pair $([\boldsymbol{u}],d)$, the relations between this pair $([\boldsymbol{u}],d)$ and the its conjugate variables $(\boldsymbol{t},Y)$ are obtained:

$$\boldsymbol{t}=\frac{\partial\psi}{\partial[\boldsymbol{u}]}=(1-d)k_n^+\langle[u_n]\rangle_+ +(1-d)k_s^+[u_s]+k_n^-\langle[u_n]\rangle_- \text{ (the cohesive law)} \qquad (4.4)$$

$$Y_m=-\frac{\partial\psi}{\partial d}=\frac{1}{2}k_n^+\langle[u_n]\rangle_+^2+\frac{1}{2}k_s^+[u_s]^2=Y_I+Y_{II} \qquad (4.5)$$

where the subscript m is appended to the mixed-mode variables, $\boldsymbol{t}$ is the interface traction vector acting at the cohesive surface and Y_m is the work-conjugate of the damage variable. So, a constitutive relationship for the interface is given in terms of the displacement jump vector which has the meaning of interface strain, and the related traction vector, which plays the role of the stress. As regards the constitutive equation, obtained by differentiating the free energy with respect to the displacement jumps, when the interface is damaged (0<d<1) the traction is linearly related to the displacement. Instead as regards the work-conjugate of the damage variable, Y_m, which is also said *equivalent mixed-mode energy release rate*, it represents the damage driving force; in detail, it is the energy which should be stored in the interface if the interface is not damaged because in its expression the damage parameter is not present. Based on the above relationships, the equivalent, mixed-mode energy release rate Y_m can be expressed as:

$$Y_m = \frac{1}{2} k_n^+ \delta^2 \qquad (4.6)$$

where δ is an *equivalent opening displacement* given by:

$$\delta = \left(\left\langle [u_n] \right\rangle_+^2 + \alpha [u_s]^2 \right)^{\frac{1}{2}} \qquad (4.7)$$

being:

$$\alpha = \sqrt{\frac{k_s}{k_n^+}} \qquad (4.8)$$

the parameter giving different weights to the normal and sliding components depending on the relevant initial elastic stiffnesses. A mixed-mode parameter β can be defined introducing the loading angle:

$$\varphi = \arctan\left[\frac{[u_s]}{\left\langle [u_n] \right\rangle_+} \right] \in [0, \frac{\pi}{2}] \qquad (4.9)$$

So, the mixed-mode parameter is given by:

$$\beta = \alpha \tan(\varphi) \qquad (4.10)$$

The mixed-mode parameter allow to connect the pure-mode energy release rate with Y_m as follows:

$$Y_I = \frac{1}{1+\beta^2} Y_m \qquad (4.11)$$

$$Y_{II} = \frac{\beta^2}{1+\beta^2} Y_m \qquad (4.12)$$

where Y_I and Y_{II} represent the mode I (opening) and mode II (sliding) energy release rate respectively.

The two introduced equations, one for $\boldsymbol{t}$ and the other for Y_m, not define completely the interface constitutive behavior; so it is necessary to introduce a damaging criterion and a damage evolution law. As in classical internal variables theories, the damage-driving force is assumed to be bounded by a critical value. This can be characterized by means of a damaging criterion of the form:

$$\phi_m = Y_m - Y_m^* \leq 0 \qquad (4.13)$$

where Y_m^* represents an instantaneous mixed-mode energy threshold or the critical mixed-mode damage-driving force. The evolution of the threshold is governed by a monotonically increasing positive function F_m (damage function in mixed-mode condition).

The increase of variable ϕ_m is associated with the damage evolution and as such it is irreversible; this can be taken into account by specifying the damage evolution equations. The evolution law for the damage threshold and the damage variable is defined as:

$$\dot{d} = \dot{\gamma} \frac{\partial \phi_m}{\partial Y_m} \qquad (4.14)$$

$$\dot{Y}^* = \dot{\gamma} \frac{\partial F}{\partial d} \qquad (4.15)$$

where $\dot{\gamma}$ is a damage consistency parameter used to define loading–unloading conditions according to the Kuhn–Tucker relations:

$$\phi_m \leq 0 \;\; ; \;\; \dot{\gamma} \geq 0 \;\; ; \;\; \dot{\gamma}\phi_m = 0 \quad (4.16)$$

The critical damage-driving force definition for a mixed-mode model can be the following:

$$Y_m^* = \begin{cases} Y_{m0} & if \;\; d = 0 \\ F_m(d) & if \;\; d \in]0,1[\\ \max\limits_{\tau \in [0,T]} Y_m(\tau) & if \;\; d = 1 \end{cases} \quad (4.17)$$

The calculation of Y_m^* requires a relationship between the energy threshold and the damage variable d and the two parameters determination which are Y_{m0} (the damage-driving force at damage onset under mixed-mode loading) and Y_{m_f} (characteristic value of Y_m) which are based on criteria determining the damage onset and propagation of decohesion.

The damage onset, neglecting the effect of compressive, can be predicted using a Hashin-type [19,20] criterion which is a criterion using an interaction between the components of the energy release rate needs to predict damage onset; it can be conveniently written as:

$$\left(\frac{Y_I}{G_{0I}}\right)^{a_1} + \left(\frac{Y_{II}}{G_{0II}}\right)^{a_2} - 1 = 0 \quad (4.18)$$

where G_{0I} and G_{0II} are the initial pure-mode damage thresholds while the exponents a_1, a_2 are model parameters that must be selected essentially in accordance with a curve fit to experimental test data; moreover they are assumed to be both strictly positive and non-necessarily integer.

The initial mixed-mode threshold Y_{m0} can be computed from the previous equation, Eqn. 4.18, on account of :

$$Y_I = \frac{1}{1+\beta^2} Y_m \;\; , \;\; Y_{II} = \frac{\beta^2}{1+\beta^2} Y_m \quad (4.19)$$

So the damage onset criterion can be expressed in the equivalent form:

$$f_0\left(\beta, Y_m\right) = c_I(\beta)(Y_m)^{a_1} + c_{II}(\beta)(Y_m)^{a_2} - 1 = 0 \qquad (4.20)$$

$$c_I(\beta) = \left[\frac{1}{(1+\beta^2)G_{0I}}\right]^{a_1} \qquad c_{II}(\beta) = \left[\frac{\beta^2}{(1+\beta^2)G_{0II}}\right]^{a_2} \qquad (4.21)$$

Therefore, Eq. 4.20 implicitly defines Y_m as a function of the mode-mixity β; as a consequence, for a given β there is always a unique solution Y_{m0} of Eq. 4.20 and its computation only requires a local iterative scheme.

The criteria adopted to predict delamination propagation in composites under mixed-mode loading conditions are usually established in terms of the components of the energy release rate and fracture toughness. In this work, the adopted condition assumes that when the energy release rate, G, exceeds the critical value, the critical energy release rate G_c, delamination grows. In this respect the criterion used to predict delamination propagation under mixed-mode loading is a generalized ellipse-like criterion called “power law criterion”; it is normally established in terms of a linear or quadratic interaction between the energy release rates [21,22]:

$$\left(\frac{G_I}{G_{cI}}\right)^{b_1} + \left(\frac{G_{II}}{G_{cII}}\right)^{b_2} - 1 = 0 \qquad (4.22)$$

As for damage onset, under mixed-mode loading the dependence of the fracture toughness on the mode ratio has to be properly accounted for. In this respect the adopted failure condition, stemming from one of the most widely used criteria to predict the propagation of delamination, is a generalized ellipse-like criterion [22]:

$$f_c(\beta, G_T) = d_I(\beta)(G_T)^{b_1} + d_{II}(\beta)(G_T)^{b_2} - 1 = 0 \qquad (4.23)$$

where $G_T = G_I + G_{II}$ and d_I, d_{II} have the same expressions as in (4.21), with G_{0I}, G_{0II}, a_1, a_2 being replaced by G_{cI}, G_{cII}, b_1, b_2. Clearly, all the considerations developed for (4.18) apply to (4.21) as well.

Finally, the following expressions for F_m are available:

$$F_{mA}(d) = \frac{Y_{mf}^2 Y_{m0}}{\left[(Y_{m0}d + Y_{mf}(1-d)\right]^2} \text{ (bilinear model)} \tag{4.24}$$

$$F_{mB}(d) = Y_{m0} + (Y_{mf} - Y_{m0})d^{\frac{1}{N}} \ (Allix \,\&\, Ladevèze) \tag{4.25}$$

$$F_{mC}(d) = Y_{m0} + (Y_{mf} - Y_{m0})[-\log(1-d)]^N \text{ (exponential model)} \tag{4.26}$$

Further information on the model discussed can be found in reference [18].

4.6 Model changes

In the current paragraph, changes to the constitutive model for cohesive zone previously are presented. The changes consist essentially in the introduction of the third displacement component and then in the introduction of third mode energy release rate, Y_{III}, for application of the model to three-dimensional cases. The new model requires the introduction of a set of three unit vectors, orthogonal to each other, **n**, **s**, **t,** denoting respectively the outward unit normal vector to the interface, the unit tangent vector to the interface and the other unit tangent vector to the interface perpendicular to the previous ones. Normally, the shear modes II and III are represented together because their individual evaluation depends on the relative displacement between homologous nodes with respect to the crack front orientation [23]. Since at finite element scale level the crack

orientation is generally unknown, it is not possible to distinguish between modes II and III. So, the total mixed-mode relative displacement δ is defined as:

$$\delta = \left(\left\langle [u_n] \right\rangle_+^2 + \alpha [u_{shear}]^2 \right)^{\frac{1}{2}} \qquad (4.27)$$

where $[u_n]$ is the relative displacement in mode I, $\alpha = \sqrt{\frac{k_s}{k_n^+}}$ con $k_s = k_t$ (assumption), and $[u_{shear}]$ is the Euclidian norm of the relative displacements in mode II and mode III:

$$[u_{shear}] = \sqrt{[u_s]^2 + [u_t]^2} \qquad (4.28)$$

where $[u_s] = [\boldsymbol{u}] \bullet \boldsymbol{s}$ and $[u_t] = [\boldsymbol{u}] \bullet \boldsymbol{t}$.

Now the pure-mode contributions to Y_m appear to be:

$$Y_I = \frac{1}{1+\beta^2} Y_m \qquad (4.29)$$

$$Y_{shear} = \frac{\beta^2}{1+\beta^2} Y_m \qquad (4.30)$$

and:

$$Y_m = Y_I + Y_{shear} \qquad (4.31)$$

where $Y_{shear} = Y_{II} + Y_{III}$.

However, there is no mixed-mode test method available incorporating Mode III loading; so, there is no reliable mixed-mode delamination failure criterion incorporating Mode III. Therefore, most of the failure criteria proposed for delamination growth are established for Mixed-modes I and II loading only.

For the above reasons, and following Li's work [24,25], the concept of energy release rate for shear loading is used here and the criteria of damage onset and evolution are modified as follows:

$$\left(\frac{Y_I}{G_{0I}}\right)^{a_1}+\left(\frac{Y_{shear}}{G_{0shear}}\right)^{a_2}-1=0 \qquad (4.32)$$

$$\left(\frac{G_I}{G_{cI}}\right)^{b_1}+\left(\frac{G_{shear}}{G_{c_{shear}}}\right)^{b_2}-1=0 \qquad (4.33)$$

where $Y_{shear}=Y_{II}+Y_{III}$, $G_{shear}=G_{II}+G_{III}$ (it is the energy release rate for shear loading proposed in Ref. [24,25]), $G_{0shear}=G_{0II}=G_{0III}$ and $G_{c_{shear}}=G_{cII}=G_{cIII}$; the latter two conditions on G_{0shear} and $G_{c_{shear}}$ ensure that the criteria are consistent for pure mode loading cases II or III; they are very common conditions because it is difficult to obtain appropriate values of G_{0III} and G_{cIII} for mode III and typically they are considered equal to those of mode II.

4.7 Friction contact implementation

In this work, the delamination damage resulting from low velocity impact (LVI) will be examined hereinafter using cohesive elements. During low velocity impact loading, after a phase of delamination initiation principally related to mode I (opening mode) fracture characteristics, interlaminar damage propagation is mainly defined by mode II (sliding mode). Previous experimental studies [26] suggest that in the delamination mode II the friction component plays a decisive role in energy dissipation; so, it cannot be neglected and it is necessary to include frictional contribute in the modeling of local delamination. For the reasons above, in this thesis, the fracture of the interface in a composite laminate under LVI is studied using a frictional cohesive model. The model based on references [27] is founded on the assumption that the sliding resistance occurs only on the damaged part or delaminated area, in accordance with a Coulomb-like friction law.

The model in Ref. [18] and discussed in the previous paragraph is based on the assumption that the negative values of relative normal displacement $[u_n] = [\boldsymbol{u}] \cdot \boldsymbol{n} \leq 0$ (mode I) have no physical sense because the cracks are closed and no damage is produced. Indeed when compressive forces act at the interface, in presence of interfacial damage (damage finite element), the cohesive response is accompanied by a frictional contact behavior on the damaged area. The presence of friction has been demonstrated to exist in mode II delamination tests where friction effects are the primary causes of the poor reproducibility of values of the measured fracture energy G_{cII} [26] and modification of the load-deflection response.

In this work, the model developed by the authors in [18] is enriched with the introduction of the friction component in according to studies conducted by the same ones in [28]. The approach is based on the concept that under the action of compressive forces, the crack faces are subjected to the contact and possible frictional sliding. The sliding in the present context is regarded as an independent phenomenon modelled at the outset from the cohesive relationship. The frictional components are introduced via an additive decomposition of the displacement jump across the interface into an elastic and inelastic component. In detail in analogy with the elasto-plastic case, the relative displacement is additively decomposed into an elastic-like (i.e. no-slip) part and a plastic-like (i.e. full-slip) part [29]:

$$[\boldsymbol{u}] = [\boldsymbol{u}^e] + [\boldsymbol{u}^p] \qquad \text{e} \qquad [\dot{\boldsymbol{u}}] = [\dot{\boldsymbol{u}}^e] + [\dot{\boldsymbol{u}}^p] \qquad (4.34)$$

where $[\boldsymbol{u}^e]$ represents the elastic displacement jump and $[\boldsymbol{u}^p]$ is the plastic displacement jump corresponding to the inelastic sliding that may occur after complete decohesion.

A modified Coulomb law, which allows for small elastic tangential displacements during frictional sliding, is then introduced. Based on Coulomb's theory of friction, the friction function reads:

$$f(\boldsymbol{t}) = |\boldsymbol{t}_s| - \mu \langle \boldsymbol{t}_n \rangle_- \leq 0 \qquad (4.35)$$

where t_s is the shear traction in the plane of fracture, $\langle\ \rangle_-$ is the argument negative part and μ is the static friction coefficient. The condition $f(\boldsymbol{t}) < 0$ lead to *sticking* case, $f(\boldsymbol{t}) = 0$ represents the *slip condition* while the condition $f(\boldsymbol{t}) > 0$ is not admissible. The irreversible sliding occurs if the condition $f(\boldsymbol{t}) = 0$ is met and sliding takes place in the direction determined by the sign of the shear traction $\boldsymbol{t}_s$. The maximum transmissible shear traction is expressed via the slip condition.

In the case of sliding, when the friction law is violated and the initial assumption of sticking has to be neglected, the irreversible part $\left[u^p\right]$ of the total slip is computed from the evaluation of the non-associative friction rule:

$$\left[\dot{\boldsymbol{u}}^p\right] = \dot{\lambda} d_t g(\boldsymbol{t}) \qquad (4.36)$$

where g represents a suitable defined real-valued "*slip potential*" $g(\boldsymbol{t}) = |t_s| - c$ and λ is the consistency parameter obeying the loading/unloading conditions:

$$f(\boldsymbol{t}) \le 0 \qquad \dot{\lambda} \ge 0 \qquad f(\boldsymbol{t})\dot{\lambda} = 0 \qquad (4.37)$$

Using an implicit Euler scheme for integration, the sliding displacement jump increment is obtained in the following way:

$$\Delta\left[\boldsymbol{u}^p\right] = \left[\boldsymbol{u}^p\right]_{n+1} - \left[\boldsymbol{u}^p\right]_n = \lambda \begin{bmatrix} 0 \\ \dfrac{t_s}{|t_s|} \end{bmatrix} \qquad (4.38)$$

whereby no change occurs the normal force; on the contrary, the shear traction is updated according to:

$$t_{s,n+1} = t_s^{trial} - \lambda k_s^f \Delta\left[\boldsymbol{u}^p\right] \bullet \boldsymbol{s} \qquad (4.39)$$

where $t_s^{trial} = k_s^f \left(\left[\boldsymbol{u} \right]_{n+1} - \left[\boldsymbol{u}^p \right]_n \right) \bullet \boldsymbol{s}$ is the tangential traction evaluated under the initial assumption of sticking, and k_s^f is a penalization parameter used to regularize the tangential response; experimental evidence indicates that this corresponds to stiffness of the interface roughness in the contact zone [30].

For stick-slip transitions a return mapping scheme is used to restore consistency of the elastically predicted frictional forces, that are relaxed onto the Coulomb surface by allowing the increase of the inelastic part of displacement jumps according to a non-associative flow rule. The radial return-like formula yields the discrete consistency parameter λ as:

$$\lambda = \frac{f^{trial}}{k_s^f} \qquad (4.40)$$

Under compressive forces the cohesive relationship is combined with the discussed frictional model by assuming that friction acts only on the contact area (i.e. damaged portion of the interface). The resultant tangential tractions are obtained by adding up the tangential tractions:

$$t_{s,n+1} = t_s^{trial} - \lambda k_s^f \Delta \left[\boldsymbol{u}^p \right] \bullet \boldsymbol{s} \qquad (4.41)$$

to their purely adhesive counterpart:

$$t_s = (1-d) k_s \left[u_s \right] \qquad (4.42)$$

4.8 Cohesive-frictional model application

Low velocity impact is one of the most critical events for composite laminates. Indeed, laminated structures submitted to low energy impacts or small dropped objects, such as tools during assembly or maintenance operations, can undergo significant damage in terms of matrix cracks, fiber

breakage or delamination [32]. The interfacial damage is particularly dangerous because it drastically reduces the residual mechanical characteristics of the structure, and at the same time can leave very limited visible marks on the impacted surface [33].

In this section the use of cohesive interface elements for delamination damage prediction in a laminate subjected to low-velocity impact is investigated. Cohesive elements can simulate adhesion bonding failure or delamination. They play the role of interface decohesion elements which model progressive failure at interfaces when its load carrying capability is lost. The application of cohesive elements for delamination simulation is one of the key issues in this thesis. A modification of the cohesive model, including the friction effect, originally developed by authors in Ref. [18,28] was presented. The model is implemented in the explicit finite element code ABAQUS by using a vectorized user material subroutine, called VUMAT, written in Fortran [31] in order to study computationally the consequences of a low energy impact on interface between plies of dissimilar orientation. The user material is associated with the cohesive elements available in ABAQUS software library (COH2D4 for 2D problems, COH3D8 for 3D applications).

For the definition of the interface behavior, it's necessary the knowledge of the cohesive properties. The macroscopic properties of the interface material, such as the critical fracture energy in pure mode I, II and III (previously referred to as G_{cI}, G_{cII} and G_{cIII}) can be measured experimentally and used directly in the cohesive model; instead, the damage-driving force at damage onset in pure mode I, II and III may be obtained by experimental–numerical calibration procedure of model and the undamaged interface stiffnesses by means of empirical formulas. However, for the reasons presented in the paragraph 4.4, fracture modes II and III will not be distinguished and the cohesive properties associated with the Mode III will be considered the same as those relating to the mode II.

For the purposes above, the studies reported in [34] were the reference. In the following the cohesive-frictional model with interface elements discussed in the previous sections will be first calibrated with the data available from authors by means of simulations of standard fracture

toughness tests and finally employed to model the impact response of cross-ply graphite/epoxy laminated plate analyzed in the same Ref. [34].

4.8.1 Cohesive input properties

In composite structures the damage onset and evolution consist of combined inter-laminar (delamination) and intra-laminar ply damaging mechanisms. In fact the two physical damage forms are strongly coupled. Therefore it is necessary to identify experiments which isolate inter-laminar behavior (i.e., tests that result in minimal or no intra-laminar material failure) in order to use experimental data to characterize cohesive material properties. Moreover, it is necessary to identify tests test to characterize interfacial behavior which separate the normal and shear modes of delamination. In this regard the double cantilever beam (DCB) test is designed to produce pure normal mode delamination without any intra-laminar material damaging and it is commonly used for obtaining pure mode-I loading condition; while the end-notched flexural (ENF) specimen is designed to produce pure shear mode delamination without any intra-laminar material damaging and it is commonly used for obtaining pure mode-II loading condition. Utilizing experimental data to characterize cohesive behavior, the number of cohesive properties that must be determined is minimized [35]. Cohesive input properties include parameters that define the stiffness, elastic energies at damage onset and fracture energy of the cohesive material layer in each of its three deformation modes (e.g., a normal mode denoted by a subscript n), and two shear modes (denoted by subscript s and t respectively), see Tab. 4.1. In order to determining the input properties of cohesive elements that must be used in finite element models to fit numerical results of double cantilever beam (DCB) and end notched flexure (ENF) simulations with experimental ones derived from the same tests, three steps are necessary:

1. to determine mesh size;
2. to calculate cohesive stiffness:k_n, k_s;
3. to calibrate elastic energy at damage onset: G_{0I} , G_{0II}.

Normal mode:

k_n = Stiffness (MPa/mm), G_{0I} = Elastic energies at damage onset (mJ/mm^2), G_{cI} = Fracture Energy (mJ/mm^2)

Shear mode:

k_s = Stiffness (MPa/mm), G_{0II} = Elastic energies at damage onset (mJ/mm^2), G_{cII} = Fracture Energy (mJ/mm^2)

Shear mode:

k_t = Stiffness (MPa/mm), G_{0III} = Elastic energies at damage onset (mJ/mm^2), G_{cIII} = Fracture Energy (mJ/mm^2)

Tab. 4.1 - Cohesive input properties.

4.8.2 Mesh size

Initially it's necessary to create DCB and ENF finite element models with loading and dimensions that match the experimental conditions. The DCB model is used to determine the normal cohesive properties (k_n, G_{0I} and G_{cI}), and the ENF model is used to determine the shear cohesive properties (k_s, G_{0II} and G_{cII}). The cohesive properties for the mode II and III are assumed to be equal. When a finite element model is created one must be cognizant of the fact that predicted cohesive behavior is mesh-dependent, i.e., using cohesive properties across a wide range of cohesive mesh densities a considerable range of predicted delamination responses will be obtained [34,35,36]. Since cohesive solutions are mesh dependent, it is important that the meshes for the DCB and ENF specimens use cohesive elements that are approximately the same size as the cohesive elements that are anticipated to be used in subsequent progressive failure analyses of composite structural components. The influence of effect of mesh density on the simulated response of DCB and ENF tests were investigated during the first phase of the study but it will not be discussed here.

4.8.3 Cohesive stiffness

The cohesive stiffness should be determined before the elastic energy at damage onset is obtained. It is important to realize that one cannot determine a definitive value of stiffness for cohesive layers when it is used to simulate the delamination between plies. The stiffness of the cohesive layer needs to be stiff enough so that it provides adequate load transfer between the bonded layers, but if it is too stiff, then spurious stress oscillations can occur. As such, the following equation presented in Ref. [36] should be used to estimate the stiffness of the cohesive layer in the mode-I direction:

$$k_n \approx \left(\frac{\alpha E_3}{t} \right) \qquad (4.43)$$

According to the above formula, the interface stiffness is the elastic modulus of the resin per unit thickness, where E_3 is the Young's modulus of the laminate in the thickness direction, t is the larger of the sublaminate thicknesses above or below the cohesive layer, and α is a parameter that is much larger than 1 with a suggested value of 50 in Ref. [36] to obtain a stiffness of the cohesive layer which is small enough to avoid numerical problems, such as spurious oscillations of the tractions in an cohesive element, and also large enough to prevent the laminate from being too compliant in the thickness direction. Therefore, a value of α equal to 50 was used in the current study. In calculating the stiffness k_s and k_t in the shear directions associated respectively to mode II and mode III, the normal modulus of the composite material E_3 is replaced with the shear moduli G_{12} and G_{13} of the laminate, respectively.

4.8.4 Energies at damage onset

After setting the stiffness of the cohesive material, the finite element models of the DCB and ENF specimens can be used to iteratively determine the elastic energies at damage onset of the cohesive material (G_{0I} , G_{0II}=G_{0III}).

The double cantilever beam finite element model is used to calibrate G_{0I}, and the end notched flexure finite element model is used to calibrate G_{0II} (o G_{0III}).

The energy values predicted by the DCB and ENF finite element models are dependent on both the cohesive mesh density and the stiffnesses chosen for the cohesive material (previous steps), thus it is likely that the initial damage energy estimates need to be adjusted in order for the DCB and ENF models to match the experimental results obtained by the same tests.

4.8.5 Calibration of the cohesive properties

Mode I and Mode II delamination numerical simulations are now discussed. General guidelines to create finite element models of each test are given in Ref. [34]; in this are reported essential mechanical properties and geometries of testing specimens.

The dimensions of each specimen are 20 mm in width, 150 mm in length, with a total thickness of 3 mm and an initial crack (crack-like defect) of 35 mm. The elastic properties of materials and the fracture properties of interface are reported in Tab. 4.2.

Properties for composite material [34]
E_{11} = 93.7 GPa; E_{22}= E_{33} = 7.45 GPa
$G_{12} = G_{23} = G_{13}$ = 3.97 GPa
$\nu_{12} = \nu_{23} = \nu_{13}$ = 0.261
$\rho = 1.5 \cdot 10^{-9}$ ton/mm3.
Properties for cohesive interface [34]
G_{cI} = 0.520 mJ/mm^2
$G_{cII} = G_{cIII}$ = 0.970 mJ/mm^2

Tab. 4.2 - Cohesive input properties

In Tab. 4.2, E_{11}, E_{22}, E_{33}, are the Young's modules in the direction of the fibers, in direction orthogonal to fiber and situated in the lamina plan and in the direction normal to the plane of the composite lamina respectively; ν_{12}, ν_{13} and ν_{23} are the values of the Poisson's ratio and G_{12}, G_{13} and G_{23} are the shear modules; ρ is the composite material density and similar value is considered for the cohesive zone.; finally, G_{cI}, $G_{cII}=G_{cIII}$ are fracture energy associated to fracture modes obtained from experimental tests. The experimental determination of critical energy release rates was conducted by authors in [35], by means of double cantilever beam (DCB) and the end notched flexure (ENF) specimens. DCB and ENF tests are performed on unidirectional composite laminates, which means that delamination growth occurs at a [0/0] interface and crack propagation is parallel to the fiber orientation. However, this kind of delamination growth will rarely occur in real structures [37].

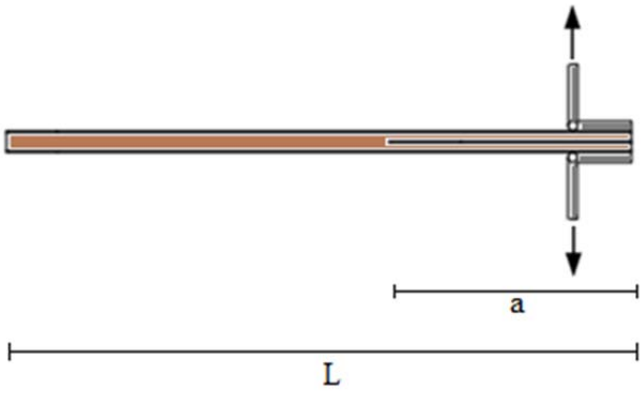

Fig. 4.12 – Double cantilever beam specimen geometry.

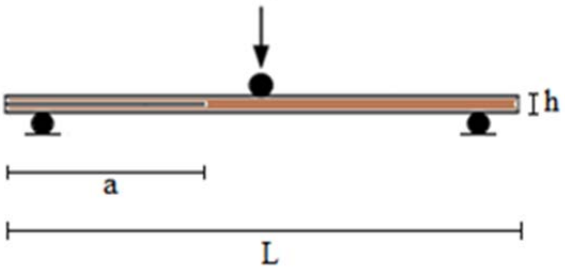

Fig. 4.13 – End-notched flexure specimen geometry.

Bidimensional finite element models are used to simulations because with this simplification a simulation produce results practically coincident with those obtained by three-dimensional models; this was noted also in [35].

The composite arms are modeled with continuum plane stress elements with four nodes and reduced formulation (CPS4R). The behavior of these elements is linear elastic without any possibility of damage. The elastic parameters for these elements are reported in Tab. 4.2. Between the two composite arms, there is the cohesive layer with the exclusion of pre-cracked zone. The interface between the sub-laminates (the cohesive zone) is modeled as a zero-thickness cohesive layer and discretized using four nodes cohesive elements (COH2D4) available in the commercial finite element code ABAQUS. Cohesive elements are formulated in terms if traction vs. relative displacement relationship. They were not introduced for all the length of the specimen FE models associated to tests, but only from the end of the crack length, where the tip of the initial crack is, until the end of the specimen. A convergence analysis was preliminary conducted to determine the appropriate element size but it will not be discussed here. The choice length of the cohesive element is 0.5 mm because with it the responses computed via finite element analyses do not exhibit false instabilities caused by coarse meshes, as reported by several authors [38,39]. Contact pair surfaces were introduced only in ENF tests, in order to avoid interpenetration of sublaminates in the pre-cracked zone (contact between composite arms and contact between bottom ply and rigid supports). Finally an appropriate displacement was prescribed at nodes of load application in according to considered experimental test.

The cohesive model with interface elements adopting a exponential cohesive law discussed in the previous section is used to simulate delamination by means of user material subroutine implemented in ABAQUS. The onset of delamination is determined based on the inter-laminar quadratic nominal stress criterion and the delamination growth is based on a critical fracture energy criterion. Damage is modeled as an irreversible process by including a damage parameter.

The first numerical results presented regard the DCB simulation. It is obtained at the end of calibration. In Fig. 4.14 it is possible to see the deformed shape of the DCB specimen captured during the simulation; moreover the process zone, in progressive damage condition and resulting from opening displacements applied to composite arms, is in evidence. In Fig. 4.15 the force-opening curve is shown and this is compared with the same curve obtained in the experimental test. There is a good agreement between the elastic branch of the curve and also the onset prediction of the crack propagation looks adequate.

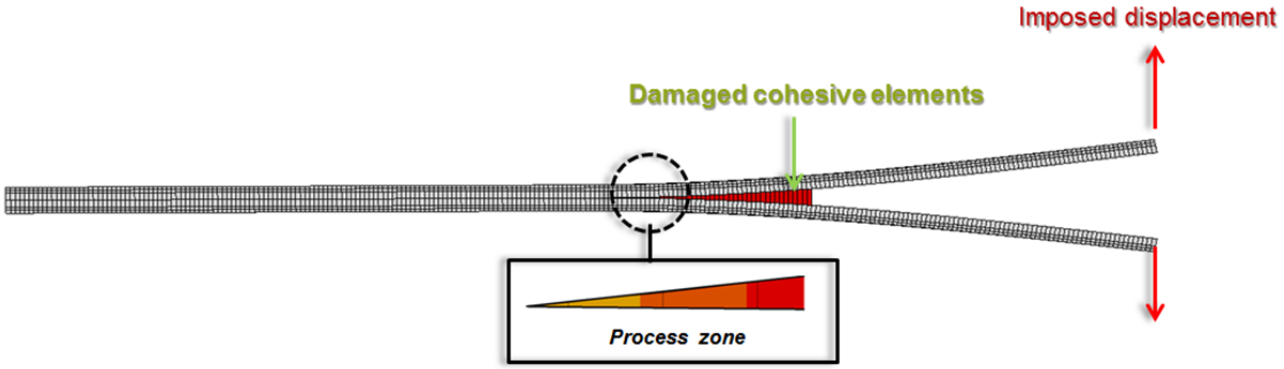

Fig. 4.14 – Deformed shape of the specimen captured during the DCB simulation test.

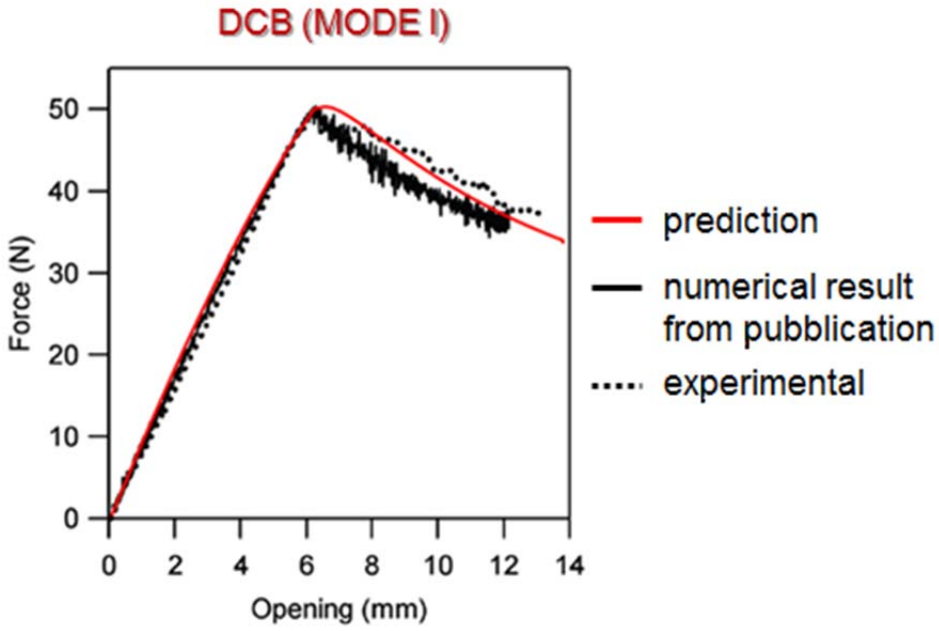

Fig. 4.15 – Calibration of the model with experimental result [35] for mode I: force vs. opening curve for the DCB test.

The second numerical results presented regard the ENF simulation. It is obtained at the end of calibration. In Fig. 4.16 it is possible to see the deformed shape of the ENF specimen captured during the simulation; moreover the contact zones between ply and rigid supports and between ply and ply in the pre-cracked region are in evidence. In these zone a contact formulation to avoid the interpenetration is necessary. In Fig. 4.17 the force-sliding curve is shown and this is compared with the same curve obtained in the experimental test. There is a good agreement between the elastic branch of the curve and also the onset prediction of the fracture propagation looks adequate.

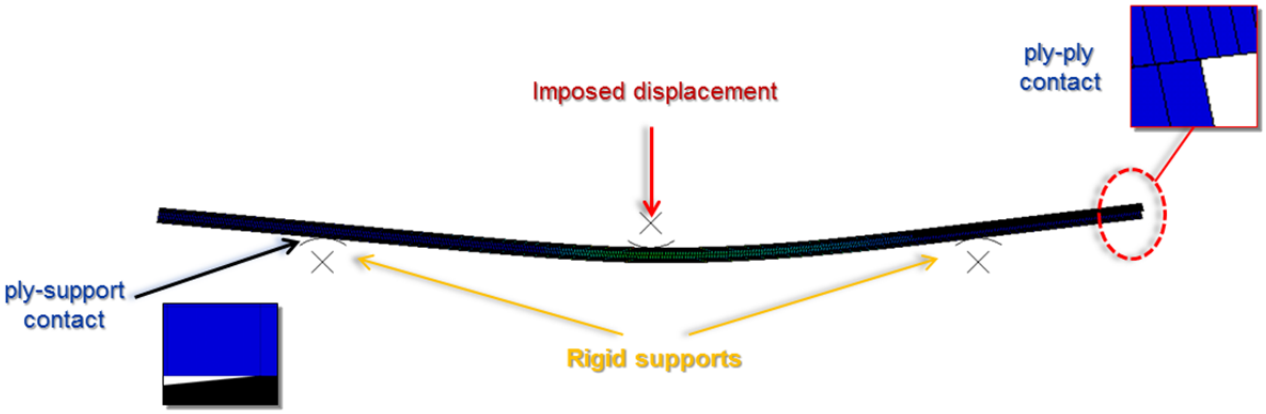

Fig. 4.16 – Deformed shape of the specimen captured during the ENF simulation test.

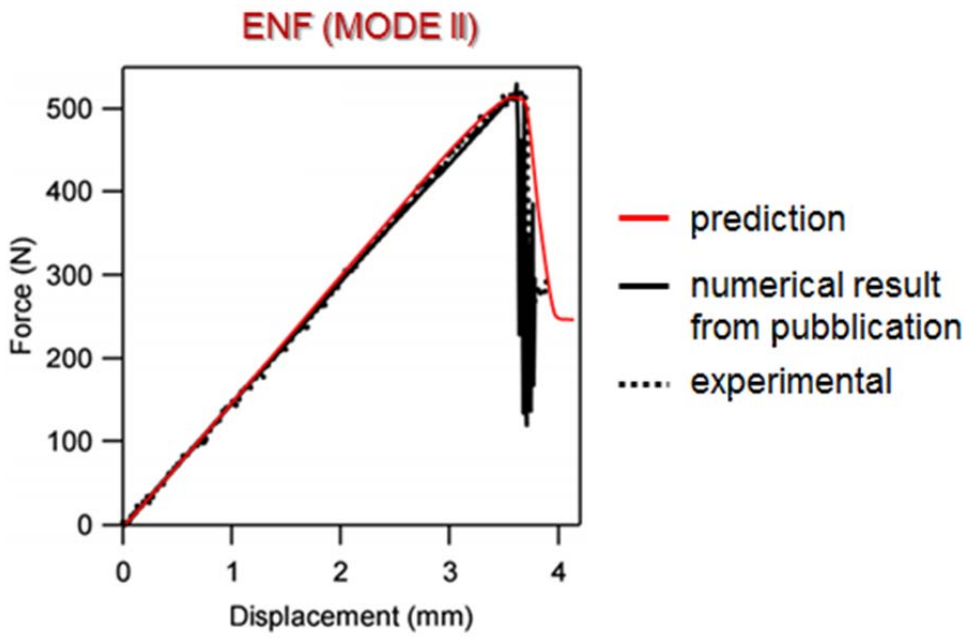

Fig. 4.17 – Model calibration with experimental result [35] for mode II: force vs. sliding curve for the ENF test.

4.8.6 Simulation of low energy impact

A numerical study was conducted to investigate the predictive capabilities of the cohesive-frictional model discussed above when applied to a practical impact problem. In the present investigation, the explicit solver of finite element software ABAQUS was used to calculate the transient response of the impact on composite laminates. The transient response of the impact was analyzed on the basis of the following assumptions: frictionless between the impactor and composite structure; neglecting the damping effect in the composite structure; ignoring the gravity force during the impact period; ignoring strain rate effect; rigid body for the impactor. Numerical simulations were carried out to test the implemented model ability to predict the interfacial damage for low velocity impact on composite plate in terms of orientation, shape and dimension of delamination. For the purposes above, the studies reported in Ref. [34,40] were the reference sources; from these are obtained geometrical data of the laminate, boundary conditions, mechanical properties of composite material and the experimental results as X radiography image of specimen after impact and resulting delamination dimensions. The authors of indicated reference conducted numerical and experimental investigations on impact-induced delamination in cross-ply composite laminate. The graphite/epoxy composite material forming the laminate (object of study) has elastic properties reported in Tab. 4.2. The plate is rectangular (45 mm x 67.5 mm) and simply supported with laminate stacking sequence of $[0_3/90_6/0_3]$; therefore, two potential interfaces for the development of delamination are present: [0/90] and [90/0]. In fact, it has been demonstrated that impact-induced delamination in composite laminates is strongly dependent on the stacking sequence: the larger the difference of fiber angles between two adjacent laminae, the larger the bending stiffness between them, and hence the larger the delamination area on the interface between them [41,40]. Moreover several additional studies have revealed the characteristic ‘‘peanut’’ shape delamination in unidirectional composite laminate [42-44]. The delamination of the peanut shape is of particular interest here and will be only considered in the present study. For Coulomb’s friction coefficient a generic value of 0.5 taken from the literature [45,46] is assumed. The impactor is a spherical body in steel of radius

6.25 mm and mass 2.3 Kg. The impactor is modeled using an analytical rigid body which means there is no deformation of the impactor. The modeling performed for each ply consists of 8-node brick elements with single integration point (C3D8R); only one element through the thickness is considered for each group of plies. Moreover, because of symmetry, only one half of the model was built and analyzed. As regards to interfaces, 8-node three-dimensional cohesive elements (COH3D8) are placed between layers with different fiber orientations. However in Ref. [35,40] only the experimental results for the bottom interface $[90_3/0_3]$ are available; therefore, only for this interface will be presented the numerical results. The introduction of cohesive elements requires partitioning of the model and this phase is shown in Fig. 4.18; in this way the cohesive layers are created.

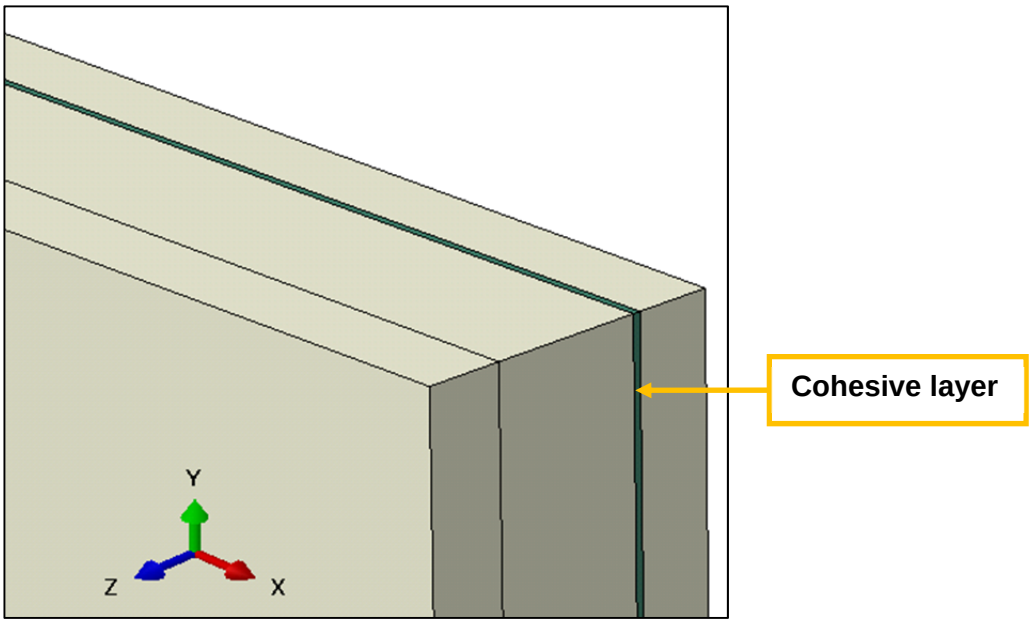

Fig. 4.18 –Model of composite plate in phase of partitioning. Initially the cohesive layer has finite thickness; after meshing the distance between the nodes on the opposite faces of the cohesive elements is reduced to zero.

After meshing, cohesive elements are assigned to the resin sections (interfaces). In order to create zero thickness cohesive elements, the collapse of the cohesive element nodes on to each other is necessary. However, it should be noted that zero thickness cohesive elements are just an

approximation. Fig. 4.19 shows the finite element mesh adopted for this study which represents a simplified model of the impact test set-up; the mesh size increased from the center toward the edges because a fine grid in the impact region of the target allows to obtain a smooth stress gradient. For proper contact definition between impactor and laminate, the "Surface-to-surface contact" formulation in ABAQUS is used.

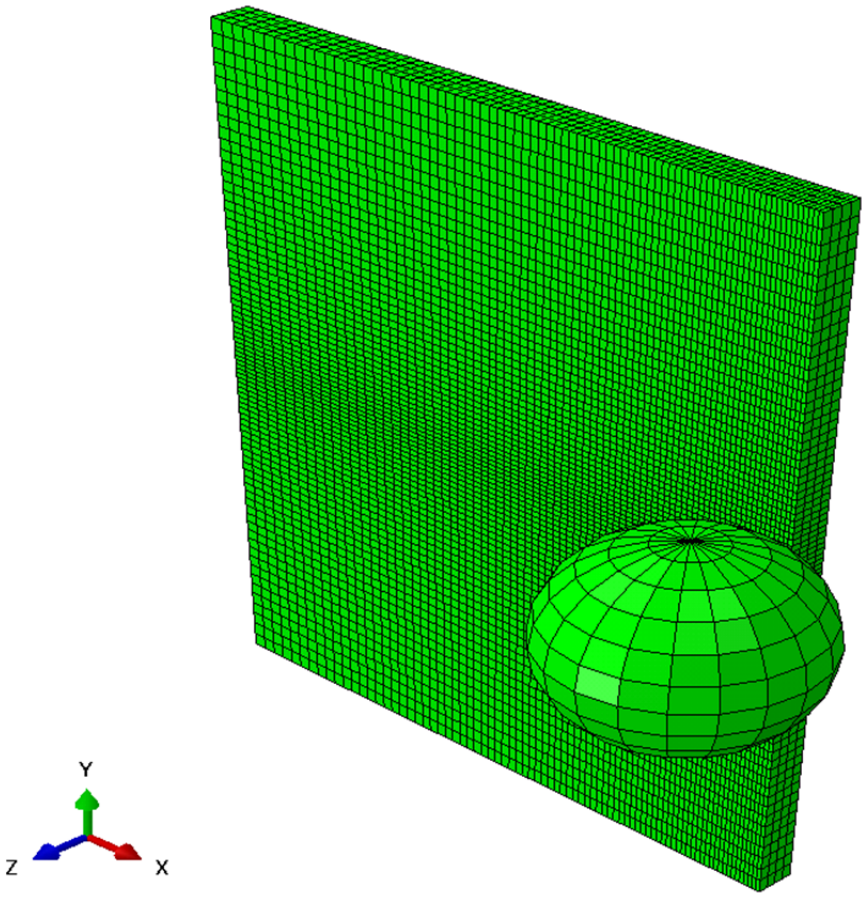

Fig. 4.19 – Structure mesh.

Impact energy levels between 1 J and 2.5 J was considered. However, the limits of this range are sufficient to show the most important results. It is natural to expect that a significant delamination occurs at the highest impact energy. In Fig. 4.20 is shown the development of the damage interface to the interface farthest from the impact area when the impactor's kinetic energy is maximum.

Several studies [43,44] have found that each delamination oriented itself along the fiber direction of the bottom ply of the delaminated interface. In the analyzed case, the damage evolution and the delamination lobe occur precisely in the direction of the fibers oriented at 0 degree. Furthermore, the overall pattern of damage were similar to that seen in carbon fiber reinforced composites used to for the experimental investigation, Fig. 4.21. Therefore, the material model provides a good prediction both of the delamination peanut shapes, who area characteristic of the interface damage caused by impact loading in fiber-reinforced composite laminates, and of their orientations.

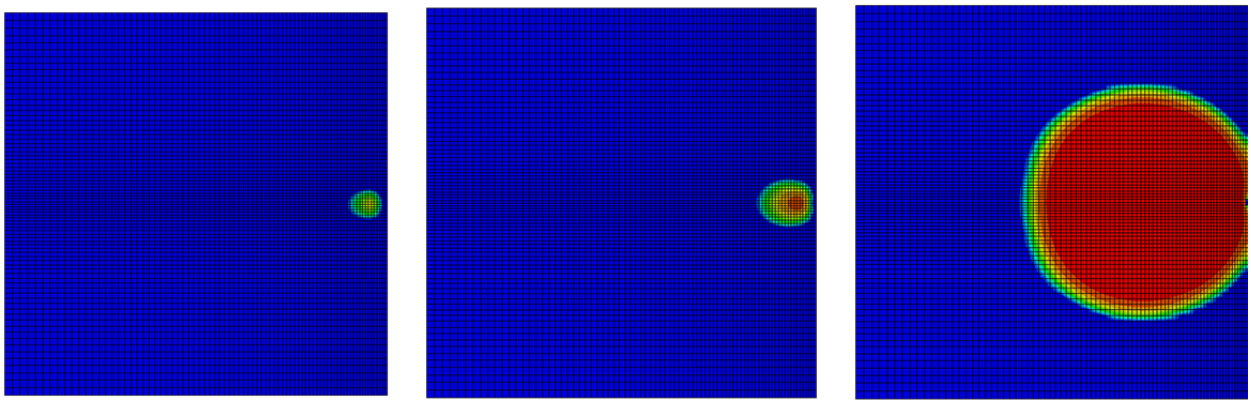

Fig. 4.20 – Development of delamination in the interface region [90/0].

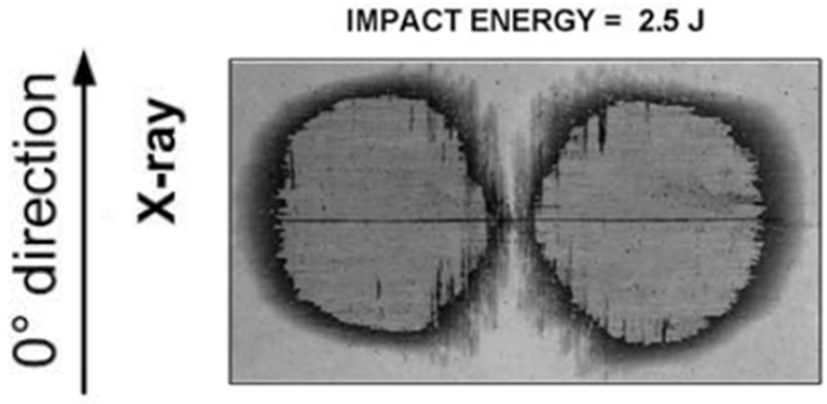

Fig. 4.21 – X-radiography of composite panel: peanut-shaped delamination on bottom interface in evidence.

Finally, in Fig. 4.22, a numerical experimental comparison about the delamination length is presented. Good agreement between the finite element results and experimental data was achieved. Furthermore from the two presented limiting cases it is possible to observe that until the energy of impact is low, the effect of friction is not visible. As the speed of the impactor increases (because the mass does not change) the delaminated area increases and therefore the friction between the damaged plies in contact becomes appreciable.

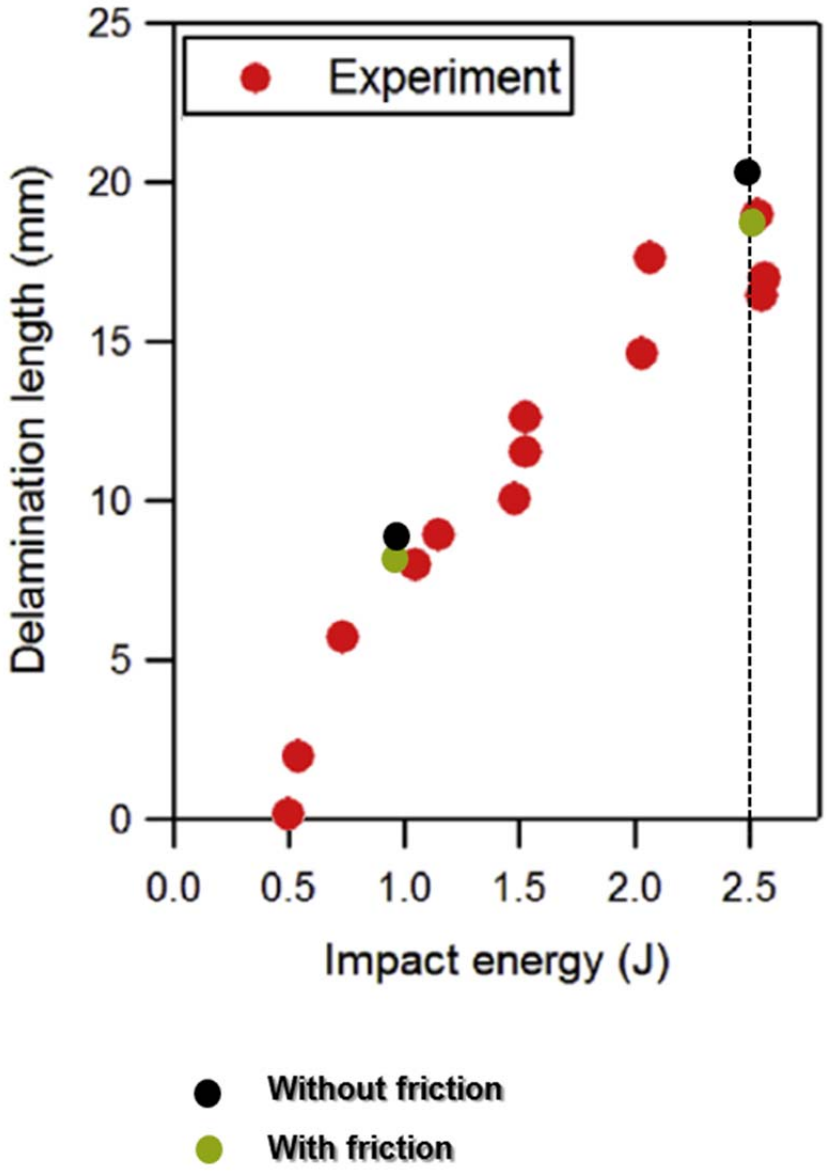

Fig. 4.22 – Numerical experimental comparison about the delamination length.

However, this study does not aim to extinguish all doubt but especially proposes the simple introduction of the frictional component in a model of cohesive zone always neglected in the formulation of the cohesive approaches designed to simulate impact tests and whose ability in the prediction of delamination is just demonstrated here. Furthermore the importance of friction component shall be demonstrated by means of targeted and detailed experimental investigations that this thesis aims to promote. For example, it is not possible to conduct important research on the effect of friction at the interface closest to the region of impact because of lack of data; in this interface it is expected that the frictional component play a more important role being the compression stresses of greater magnitude. Moreover, the response sensitivity to the friction coefficient it was not investigated leaving these studies to future works.

References

[1] Materiali Didattici Incollaggio/Adesivi, AVISA - Gruppo Adesivi e Sigillanti, Federchimica Confindustria.

[2] Z. Shi, "Crack Analysis in Structural Concrete: Theory and Applications", Butterworth-Heinemann, 2009.

[3] D. S. Dugdale, "Yielding of steel sheets containing slits", J. Mech. Phys. Solids, 1960, 8:100-104.

[4] G. I. Barenblatt, "The formation of equilibrium cracks during brittle fracture-general ideas and hypothesis, axially symmetric cracks", Prikl. Math Mekh., 1959, 23:434–444.

[5] A. Carpinteri, P. Cornetti, F. Barpi, S. Valente, "Cohesive crack model description of ductile to brittle size-scale transition: dimensional analysis vs. renormalization group theory, Eng. Fract. Mech., 2003, 70(14):31.

[6] A. Hilleborg, M. Modeer, P. E. Peterson, "Analysis of crack formation and growth in concrete by means of fracture mechanics and finite elements", Cement and Concrete Research, 1976; 6:773-782.

[7] T. L. Anderson, "Fracture Mechanics: Fundamentals and Applications", 2nd Ed. CRC Press LLC, 1995.

[8] H. Mei, "Fracture and delamination of elastic thin films on compliant substrates: modeling and simulations", Ph.D. thesis, The University of Texas at Austin, 2011.

[9] O. Van der Sluis, C.A. Yuan, W.D. van Driel, G.Q. Zhang, "Advances in delamination modeling", Nanotechnologies and Electronics Packaging, 2008, pp. 61–91.

[10] R. Krueger, "The virtual crack closure technique: history, approach and applications", NASA/Contractor, 2002, Report-2002-211628.

[11] J. Chen, M. A. Crisfield, A. J. Kinloch, E. P. Busso, F. L. Matthews, Y. Qiu, “Predicting progressive delamination of composite material specimens via interface elements”, Mechanics of Composite Materials & Structures, 1999; 6:301–317.

[12] P. P. Camanho, C. G. Dávila, M. F. S. F. de Moura, "Numerical Simulation of Mixed-Mode Progressive Delamination in Composite Materials," Journal of Composite Materials, 2003, 37(16):1415-1438.

[13] A. Turon, P. P. Camanho, J. Costa, C. G. Davila, "A Damage Model for the Simulation of Delamination in Advanced Composites under Variable-Mode Loading," Mechanics of Materials, 2006, 38(11):1072-1089.

[14] C. G. Dávila, P. P. Camanho, A. Turon, “Cohesive Elements for Shells”, NASA/TP-2007-214869.

[15] A. Rudawska, “Adhesive joint strength of hybrid assemblies: Titanium sheet-composites and aluminium sheet-composites-Experimental and numerical verification”, International Journal of Adhesion and Adhesives, 2010, 30(7):574–582.

[16] Abaqus/Standard User’s Manual version 6.5, Hibbit, Karlsson & Sorensen, Inc., 2005.

[17] R. Kregting, “Cohesive zone models towards a robust implementation of irreversible behavior”, University of Technology, Eindhoven, 2005.

[18] N. Valoroso, L. Champaney, “A damage-mechanics-based approach for modelling decohesion in adhesively bonded assemblies”, Engineering Fracture Mechanics, 2006, 73(18):2774-2801.

[19] Z. Hashin, “Failure criteria for unidirectional composites”, J. Appl. Mech., 1980;47:329–34.

[20] E. M. Wu, Jr. R.C. Reuter, “Crack Extension in Fiberglass Reinforced Plastics”, T&AM Report No. 275, University of Illinois, 1965.

[21] B. D. Davidson, W.Zhao, “An Accurate Mixed-mode Delamination Failure Criterion for Laminated Fibrous Composites Requiring Limited Experimental Input”, Journal of Composite Materials, 2007, 41(6):679-702..

[22] J.R. Reeder, “An evaluation of mixed-mode delamination failure criteria”, Technical Memorandum 104210, NASA, 1992.

[23] E. V. Gonzalez, P. Maimi, A. Turon, P.P. Camanho, J. Renart, “Simulation of delamination by means of cohesive elemnts using an explicit finite element code, CMC, 2009, 9(1):51-92.

[24] J. Li, J. K. Sen, “Analysis of Frame-to-Skin Joint Pull-Off Tests and Prediction of the Delamination Failure”, 42nd AIAA/ASME/ASCE/AHS/ASC Structures, Structural Dynamics and Materials Conference, Seattle, WA, USA, 2000.

[25] J. Li, “Three-Dimensional Effects in the Prediction of Flange Delamination in Composite Skin-Stringer Pull-Off Specimens”, 15th Conference of the American Society for Composites, Texas, USA, 2000.

[26] G. Marannano, A. Pasta, M. Terranova, “Analisi numerico-sperimentale sull’influenza dell’attrito nella delaminazione in Modo II”, AIAS, 2011, 140.

[27] G. Alfano, E. Sacco, “Combining interface damage and friction in a cohesive zone model”, International Journal for Numerical Methods in Engineering, 2006, 68:542–582.

[28] N. Valoroso, L. Champaney, “A Damage-Friction Formulation for the De-Cohesion Analysis of Adhesive Joints”, Proceedings of the Fifth International Conference on Engineering Computational Technology, 2006, 103.

[29] A. Bahtui, “Development of a Constitutive Model to Simulate Unbonded Flexible Riser Pipe Elements” ,Ph.D. thesis, Department of Mechanical Engineering Brunel University, 2008.

[30] L. A. Hagman. Measurements and Modelling of Microslip for Engineering Surfaces in Contact. PhD thesis, Department of Machine Design, Royal Institute of Technology, Stockholm, 1997.

[31] Abaqus User Subroutines Reference Manual, Version 6.8.

[32] C. Bouvet, S. Rivallant, J. J. Barrau, “Low velocity impact modeling in composite laminates capturing permanent indentation”, Composites Science and Technology, 2012, 72(16):1977-1988.

[33] S. Abrate, “Impact on composites structures”, Cambridge Univ. Press; 1998.

[34] F. Aymerich, F. Dore, P. Priolo, “Prediction of impact-induced delamination in cross-ply composite laminates using cohesive interface elements”, Composites Science and Technology, 2008, 68:2383–2390.

[35] Guidelines for Determining Finite Element Cohesive Material Parameters, Firehole Composites.

[36] A. Turon, C. G. Davila, P. P. Camanho, J. Costa, “An engineering solution for mesh size effects in the simulation of delamination using cohesive zone models”, Eng. Fract. Mech., 2007, 74(10):1665-82.

[37] R. Kruger, “Three dimensional finite element analysis of multidirectional composite DCB, SLB and ENF specimens”, 1994, ISD-Report No. 94/2.

[38] J. C. J. Schellekens, R. de Borst, “On the numerical integration of interface elements, International Journal for Numerical Methods in Engineering, 1992, 36:43-66.

[39] R. De Borst, J. J. C. Remmers, A. Needleman, “Computational aspects of cohesive zone models”.

[40] F. Aymerich, F. Dore, P. Priolo, “Simulation of multiple delaminations in impacted cross-ply laminates using a finite element model based on cohesive interface elements”, Composites Science and Technology, 2009, 69:1699–1709.

[41] D. Liu, “Impact-induced delamination - a view of material property mismatching”, J. Composite Materials, 1988, 22(7):674-691.

[42] D. Liu, M. Kokolakis, B. B. Raju, “Effects of Stacking Sequence on Perforation Resistance of Composite Laminates,” proceedings of the American Society for Composites, Fourteenth Annual Conference, Dayton, OH, 1999, pp. 121-130.

[43] S. Takeda, Y. Minakuchi, Y. Okabe, N. Takeda, “Delamination monitoring of laminated composites subjected to low velocity impact using small-diameter FBG sensors. Composites Part A 2004;36:903–8.

[44] H. Y. Choi, F. K. Chang, “A model for predicting damage on graphite/epoxy laminated composites resulting from low-velocity point impact”, J. Compos. Mater., 1992; 26(14):2l34-169.

[45] J. Schön, “Coefficient of friction of composite delamination surfaces”, Wear, 2000, 237(1):77–89.

[46] Y. Xiao, W. X. Wang, Y. Takao, T. Ishikawa, “The Effective Friction Coefficient of a Laminate Composite, and Analysis of Pin-Loaded Plates”, Journal of Composite Materials, 2000, 34(1):69-87.

CHAPTER 5

PROGRESSIVE DAMAGE MODEL

5.1 Challenging issue in designing composites

Composite laminates composed of fiber-reinforced plies are widely used in aerospace, civil, ship building and other industries because of their higher specific strength than those of metallic parts, and they can be engineered to obtain optimal material properties in desired directions. A challenging issue in designing composites is delineating various failure modes, such as fiber breakage, matrix cracking, fiber/matrix debonding, fiber kinking, and delamination between adjacent plies [1]. The difficulty of the problem was evidenced by the World Wide Failure Exercise, an international activity launched by Hinton, Kaddour and Soden [2] to establish the status of currently available theoretical methods for predicting material failure in fiber reinforced polymer composites materials in the course of which 12 of the leading theories for predicting failure in composite laminates have been tested against experimental evidence. This event revealed that very few theories successfully predicted failure of composite coupons deformed quasi statically.

In general, the load carrying capacity of a structure does not vanish as soon as either failure or damage ensues at a material point and the structure can support additional load before it eventually fails. Thus it is important to quantify damage caused by the initiation of a failure mode and study its development and progression and the eventual failure of a structure with an increase in the applied load. So, in many structural applications, the progressive failure analysis is required to predict composite structure mechanical response under various loading conditions.

Failure and damage in laminated structures can be studied by using a micro-mechanics approach [3] (see Ref. [1] for more information) but the damage studied at the constituent level is only

computationally expensive for a real size problem. The alternative is an approach based on continuum damage mechanics (CDM) in which material properties of the composite have been homogenized and failure and damage is studied at the ply/lamina level; e.g., see [4-9]. However a micromechanical approach can be used to deduce effective properties of a ply and CDM approach to study failure and damage at the lamina level.

5.2 The continuum damage mechanics

The issue of damage growth in fiber reinforced plastic (FRP) laminated composites has been addressed by an ever-increasing number of researchers through the use of Continuum Damage Mechanics (CDM). Usually it is recognized that CDM started with the papers by Kachanov (1958) and Rabotnov (1968). However the use of CDM for the simulation of composite behaviors has been popularized in the 1980s by Ladeveze [10] and Talreja [11]. The Continuum Damage Mechanics approach focuses on the effect of the presence of micro-failures in the material. In detail, it attempts to predict the effect of microscale defects and damage at a macroscale by making assumptions about the nature of the damage and its effect on the macroscale properties (e.g. elastic moduli) of the material. This damage theory describes the damage, i.e. the appearance of cracks, as a state variable that can be expressed as a scalar or as a tensor to quantify the isotropic or anisotropic damage. Therefore the CDM theories capture effects of microscopic damage by using the theory of internal variables.

Different models have been developed to permit the damage prediction in composite structures under loading. Ladeveze and Dantec [14] formulated mesomechanical damage model for single-ply laminate considering as composite damages fiber/matrix debonding and matrix microcracking; these damage modes are represented by two internal (damage) state variables; the damage evolution is then governed by a law assumed to be a linear function of equivalent damage energy release rate.

Xiao et al. [15,16] used this approach in modeling energy absorption of composite structures in crashworthiness applications or to study damage during quasistatic punching of woven fabric composites; Williams and Vaziri [17] used damage mechanics principles along with matrix and fiber failure criteria to model damage for low-velocity impacts; Yen and Caiazzo [18] implemented a damage model (MAT 162) in LS-DYNA by generalizing the layer failure model that exists (MAT 161); their damage model is based on damage mechanics approach due to Matzenmiller et al. [19] and it incorporates progressive damage and softening behavior after damage initiation. In the thesis work, this model will be analyzed in the next paragraph and then implemented as material subroutine for the commercial finite element software ABAQUS for single integration point brick elements only. It will be used in progressive failure analyses to predict composite structure mechanical response.

5.3 The damage constitutive model

The continuum damage mechanics theory allows to represent the damage state of a material in terms of properly defined state variable (or damage variables) and to describe the mechanical behavior of the damage material and the further development of the damage by the use of these state variables [21]. The term damage is used to indicate the deterioration of the material capability to carry loads. From a general point of view, damage develops in the material microstructure when non-reversible phenomena such as microcracking, debonding between the matrix and the second phase particles and microvoid formation take place [22]. Kachanov [12] pioneered the subject of damage mechanics by introducing the concept of effective stress. This concept is based on considering a fictitious undamaged configuration of a body and comparing it with the actual damaged configuration. The damage variable is defined in terms of both the damaged and effective cross-sectional areas of the body.

Kachanov [12] originally formulated his theory by using simple uniaxial tension. Following its work, a cylindrical bar subjected to a uniaxial tensile force F, as shown in Fig. 5.1, is now considered.

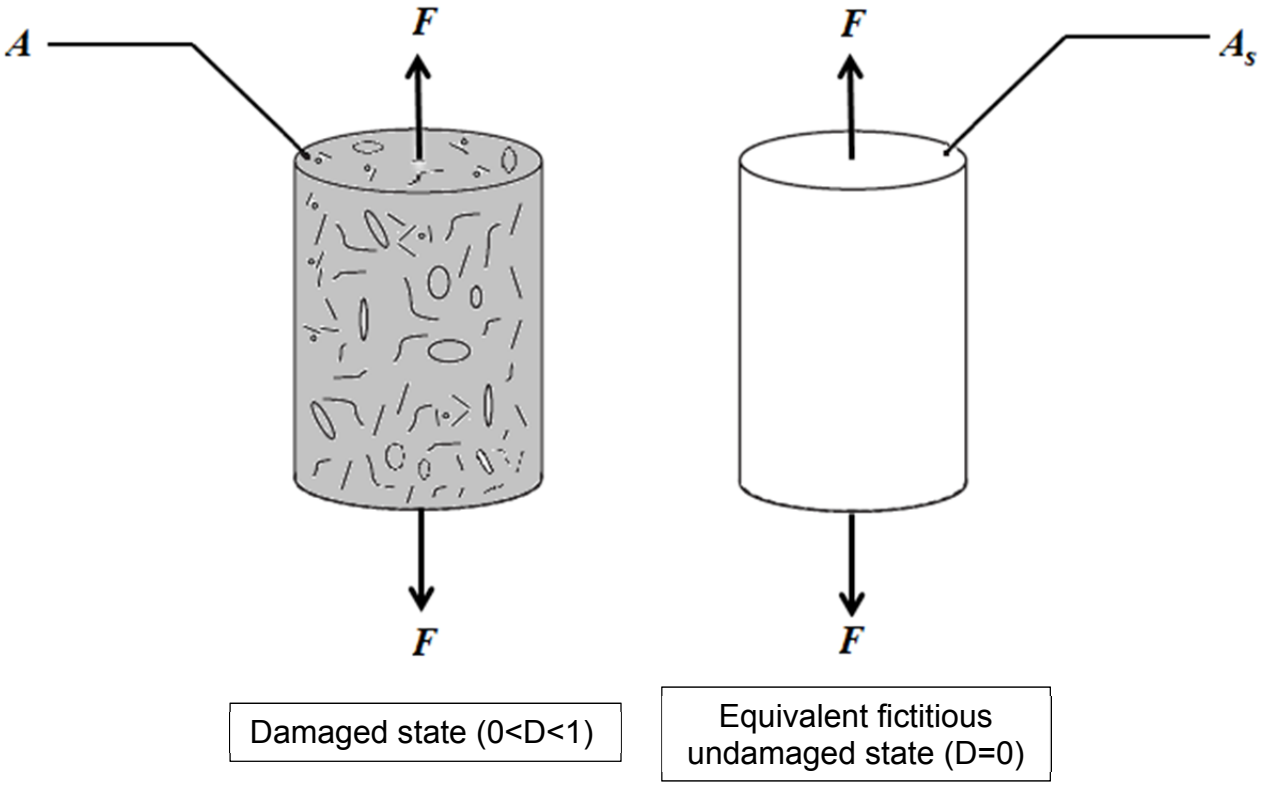

Fig. 5.1 – Cylindrical Bar Subjected to Uniaxial Tension.

The cross-sectional area of the bar is A and it is assumed that both voids and cracks appear as damage in the bar. The uniaxial stress σ in the bar is found easily from the formula $F = \sigma A$. In order to use the principles of damage mechanics, a fictitious undamaged configuration of the bar, as shown in Fig. 5.1, on the right.

In this configuration, all types of damage, including both voids and cracks, are removed from the bar. The effective cross-sectional area of the bar in this configuration is denoted by A and the effective uniaxial stress is σ. The bars in both the damaged configuration and the effective undamaged configuration are subjected to the same tensile force F. Therefore, considering the

effective undamaged configuration, we have the formula $F = \hat{\sigma} A_s$. Equating the two expressions of F obtained from both configurations, the following expression for the effective uniaxial stress $\hat{\sigma}$ is formed:

$$\hat{\sigma} = \frac{A}{A_s}\sigma \qquad (5.1)$$

Following Kachanov's work, the widely accepted definition in the macroscopic scale is the geometrical description of material damage in this way:

$$d = \frac{A_d}{A} = \frac{A - A_s}{A} \qquad (5.2)$$

where A is the nominal cross-sectional; A_s is the net area of the damaged specimen which excludes the area held by the damage entities (discontinuities) or in other words the effective resisting section area of the specimen reduced by the presence of microdefects and their mutual interaction and which carries the applied load; $A_d = A - A_s$ is the "damaged" cross section. Thus, the damage variable is defined as the ratio of the total area of voids and cracks to the total area; in its simplest form, it may be thought of as a reduction of area relative to the initial area of a specimen. Its value ranges from zero (for the case of an undamaged specimen) to one (for the case of complete rupture). The introduction of a damage variable, Eqn. 5.2, which represents a surface density of discontinuities, leads to the concept of *effective stress* that is stress calculated over the effectively resisting section. Lemaitre, using the effective stress definition proposed by Kachanov, determined the constitutive equations for ductile damaged material. According to *principle of strain equivalence* of Lemaitre [23,24], which assumes that the strain constitutive equations for a damaged material can be derived using the same formulations used for an undamaged material except that the stress is replaced by the effective stress. So, the mechanical behavior of a damaged material is usually described by using the notion of the effective stress, together with the hypothesis of mechanical equivalence between the damaged and the undamaged material.

The "effective" area is A_s or $(1-d)A$ and substituting this into Eqn. (5.1), one obtains the following expression for the effective uniaxial stress:

$$\hat{\sigma} = \frac{\sigma}{1-d} \qquad (5.3)$$

The Eqn. 5.3 represents the relationship between macroscopic stress σ and the corresponding effective stress $\hat{\sigma}$ in a damaged material and it is clear from this equation that the case of complete rupture (d =1) is unattainable, because the damage variable d is not allowed to take the value 1 in the denominator. The corresponding strain of an effective stress is called *effective strain*.

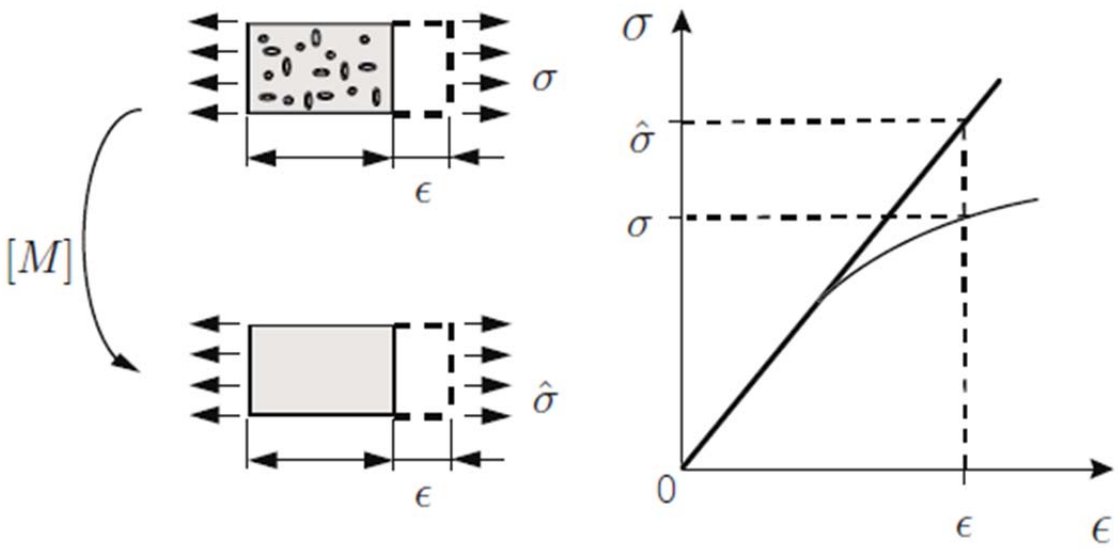

Fig. 5.2 – Hypothesis of effective stress (adapted from: Simo and Ju [25]).

It is important to note that the presence of cracks in the material diminishes the relative area of material capable of withstanding loads, thereby increasing the stress in the undamaged material under a given strain. This is also a further justification to the concept of effective stress, which implies that a damaged material subject to a load σ under a certain strain ϵ can be modeled as an equivalent undamaged material also subject to the same strain ϵ, but under a modified load or effective stress state $\hat{\sigma}$, see Fig. 5.2, and this can be expressed mathematically in tensorial form

simply replacing the scalar transformation between nominal and effective stress by a tensorial one as:

$$\{\hat{\sigma}\} = [M(d)]\{\sigma\} \qquad (5.4)$$

where $[M(d)]$ is a transformation tensor or damage effect tensor containing the damage variables which is a function of the damage state, d, and $\{\sigma\}, \{\hat{\sigma}\}$ are respectively the actual stress and equivalent stress tensors. The form of the $[M(d)]$ adopted in this model is:

$$[M(d)] = \begin{bmatrix} \frac{1}{(1-d_1)} & 0 & 0 & 0 & 0 & 0 \\ 0 & \frac{1}{(1-d_2)} & 0 & 0 & 0 & 0 \\ 0 & 0 & \frac{1}{(1-d_3)} & 0 & 0 & 0 \\ 0 & 0 & 0 & \frac{1}{(1-d_4)} & 0 & 0 \\ 0 & 0 & 0 & 0 & \frac{1}{(1-d_5)} & 0 \\ 0 & 0 & 0 & 0 & 0 & \frac{1}{(1-d_6)} \end{bmatrix} \qquad (5.5)$$

Note that here and throughout the paragraph the symmetric second order and fourth-order tensors are written in Voigt matrix notation. Using the effective stress–strain relationship:

$$\{\hat{\sigma}\} = [C^0]\{\varepsilon\} \qquad (5.6)$$

then the above equation becomes:

$$\{\sigma\} = [M]^{-1}[C^0]\{\varepsilon\} = [C(d)]\{\varepsilon\} \qquad (5.7)$$

where $[C^0]$ is the stiffness tensor of the undamaged material and $[C(d)]$ is the damaged or effective stiffness tensor (denotes the so-called “damaged” non-symmetric stiffness tensor).

The elements of matrix $[C(d)]$ are the elastic coefficients, which are functions of the undamaged (or initial) elastic material constants and the damage:

$$[C(d)]=\begin{bmatrix} \frac{1}{(1-d_1)\mathrm{E}_1} & \frac{-\nu_{21}}{E_2} & \frac{-\nu_{31}}{E_3} & 0 & 0 & 0 \\ \frac{-\nu_{12}}{E_1} & \frac{1}{(1-d_2)\mathrm{E}_2} & \frac{-\nu_{32}}{E_3} & 0 & 0 & 0 \\ \frac{-\nu_{13}}{E_1} & \frac{-\nu_{23}}{E_2} & \frac{1}{(1-d_3)\mathrm{E}_3} & 0 & 0 & 0 \\ 0 & 0 & 0 & \frac{1}{(1-d_4)G_{12}} & 0 & 0 \\ 0 & 0 & 0 & 0 & \frac{1}{(1-d_5)G_{23}} & 0 \\ 0 & 0 & 0 & 0 & 0 & \frac{1}{(1-d_6)G_{31}} \end{bmatrix} \qquad (5.8)$$

The extent of damage-induced stiffness loss is quantify by six damage variables d_j with $j=1,..,6$, one for each of the six elastic moduli. Therefore, the damaged stiffness tensor depends on six damage parameters, each associated to respective elastic constant. The elastic modulus reduction can be expressed in terms of associated damage parameter d in the following way:

$$E_{reduced}=(1-d)E_{initial} \qquad (5.9)$$

From Eqn. 5.9, it is evident that the post-failure mechanisms in a composite material is hence characterized by a reduction in material stiffness.

The role of a CDM model is to provide a mathematical description of the dependence of the elastic coefficients on the damage state and the change in the damage state with load state. For this purpose, similarly to the theory of plasticity, a *loading function* f, specifying elastic domain and the states at which damage grows, is introduced. In the damage theory, it is natural to work in the strain space and therefore the loading function is depending on the strain and on an additional

parameter r, which controls the evolution of the elastic domain and so describing the evolution of the damage. Physically, r is a scalar measure of the largest strain level ever reached in the history of the material. The loading function usually is postulated in the form:

$$f_i = F_i - r_i \qquad (5.10)$$

where i is the subscript which identifies the damage type (e.g. fiber and matrix tensile/compressive failure modes), F_i is a function adopted in the form of Hashin's failure criterion (e.g. function of the strain components, elastic moduli and strengths); r_i is the *damage threshold* corresponding to failure mechanism.

States for which $f < 0$ are supposed to be below the current damage threshold (i.e. the condition represents a set of states for which damage does not grow). Damage can grow only if current state reaches the boundary of elastic domain which is represented from condition $f = 0$ (*damage loading*). Therefore, the variable r describes the evolution of elastic domain. So it is possible to say that $f < 0$ is the elasticity criterion and $f = 0$ is the failure criterion [26].

According to the Hashin-type failure criteria, the loading functions for different failure mechanisms are given in Tab. 5.1.

$\left(\frac{E_1\varepsilon_1}{X_T}\right)^2 - r_1^2 \quad (\varepsilon_1 \geq 0)$	tensile fiber failure mode
$\left(\frac{E_1\varepsilon_1}{X_C}\right)^2 - r_2^2 \quad (\varepsilon_1 < 0)$	compressive fiber failure mode
$\left(\frac{E_2\varepsilon_2}{Y_T}\right)^2 + \left(\frac{G_{12}\varepsilon_{12}}{S_{12}}\right)^2 + \left(\frac{G_{23}\varepsilon_{23}}{S_{23}}\right)^2 - r_3^2 \ (\varepsilon_2 \geq 0)$	tensile/shear matrix failure mode
$\left(\frac{E_2\varepsilon_2}{Y_C}\right)^2 - r_4^2 \quad (\varepsilon_2 \geq 0)$	compressive matrix failure mode

Tab 5.1.– Examples of failure criteria. All the failure criteria are expressed in terms of stress components based on ply level strains (ε_1, ε_2, ε_3, ε_{12}, ε_{23}, ε_{31}) and associated elastic moduli (E_1, E_2, E_3, G_{12}, G_{23}, G_{31}).

For simplicity, rate effects on the values of the parameter in the loading function f are ignored. This limits the initial application of the model to rate insensitive materials such as CFRP and, to a lesser degree, glass fiber-reinforced plastic (GFRP) composites.

The function f and the rate of scalar variable $\dot{r}$ have to satisfy the Kuhn-Tucker loading-unloading conditions:

$$f \leq 0, \quad \dot{r} \geq 0, \quad f\dot{r} = 0 \qquad (5.11)$$

where the overdot denotes differentiation with respect to time.

The first condition means that r can never be smaller than F and the second condition means that r cannot decrease. Finally, according to the third condition, r can grow only if the current values of F and r are equal [27].

It remains to link the variable r to the damage parameter d. As both r and d grow monotonically, it is convenient to postulate an explicit evolution law:

$$d_j = g(r_i) \qquad (5.12)$$

In the Eqn. 5.12, the generic damage parameter may depend on several i types of damage.

The generic damage threshold, r_i, which controls the size of the damage surface and depends on the loading history, initially is taken to one.

The 3D damage model until now described may contain the formulation for different modes of failure, e.g. fiber breakage, fiber buckling or kinking, matrix cracking, matrix crushing etc. . These damage types are modeled by means of a combination of growth functions ϕ_i and damage coupling coefficients q_{ji} (vector components). In fact, as suggested in Matzenmiller et al. [19], the growth rate of generic damage variable $\dot{d}_i$ (or rate of damage evolution), is defined by the following type of evolution law:

$$\dot{d}_j = \sum_i \dot{\phi}_i q_{ji} \qquad (5.13)$$

where the scalar functions $\dot{\phi}_i$ define the growth rate of damage mode, i, and the coefficients q_{ji} (j associated to damage variable, i associated to damage mode) provide the coupling between the individual damage variables, d_j, and the various damage modes provided by the damage criteria f_i. In general, the damage increases ($\dot{\phi}_i$ will be non-zero) if deformation path crosses the corresponding loading surface (or damage surface, $f = F - r = 0$) or in other words, if the strain rate vector $\dot{\boldsymbol{\varepsilon}}$ forms an acute angle with the gradient $\nabla_{\varepsilon} f$ at the given state of strain $\boldsymbol{\varepsilon}$ on the loading surface:

$$\begin{aligned} f = 0 \quad , \quad & \frac{\partial f}{\partial \boldsymbol{\varepsilon}} \dot{\boldsymbol{\varepsilon}} > 0 \quad \textit{loading} \\ f = 0 \quad , \quad & \frac{\partial f}{\partial \boldsymbol{\varepsilon}} \dot{\boldsymbol{\varepsilon}} = 0 \quad \textit{neutral loading} \\ f = 0 \quad , \quad & \frac{\partial f}{\partial \boldsymbol{\varepsilon}} \dot{\boldsymbol{\varepsilon}} < 0 \quad \textit{neutral loading} \end{aligned} \qquad (5.14)$$

The prediction of damage growth thereby relies on obtaining the strain gradient when the strain path crosses the loading surface. In loading case (damage growth), the associated strain-vector increment has a positive component along the outward normal to the damage surface and in reference [28] it is shown that $\dot{\phi}_i$ can assume the form:

$$\dot{\phi}_i = \frac{1}{2}(1-\phi_i)\, f_i^{\frac{m}{2}-1} \dot{f}_i \ (\textit{no summation over } i) \qquad (5.15)$$

where ϕ_i is a variable representing the extent of mode-i damage, and m_i is a material constant that quantifies sensitivity of the material stiffness to the extent of damage. Integrating appropriately the above Eqn. 5.15, it follows that:

$$\phi_i = 1 - e^{\frac{1}{m_i}(1-r_i^{m_i})} \qquad (5.16)$$

from which, utilizing the damage coupling matrix, is derived the expression of the damage variable.

Therefore, the damage variable grows with the development of generic damage mode i according to equation that follows:

$$d_j = 1 - e^{\frac{1}{m_i}(1 - r_i^{m_i})}, \qquad j = 1,....,6 \qquad (5.17)$$

where d_j damage variable; m_i is the strain softening parameter and r_i is the damage threshold. The damage variable d_j varies from 0 to 1.0 as r_i varies from 1 to ∞, respectively.

The number of strain softening parameters can depend from number of damage modes and how these are connected in terms of material softening. These damage parameters provide the softening response in the post-failure regime of the stress-strain curve.

The effect of the exponent m on the stress-strain response of the element is such that high values of m result in brittle failure of the material; low values of m clearly indicate a ductile failure response resulting in more energy absorption prior to complete damage with a gradual loss of stiffness after failure.

The key to the success of all CDM models is to maintain a coherent link with the physical observations of damage growth and material response. So, it is important to note that in keeping with the thermodynamic constraints in damage mechanics, damage is considered to be an irreversible process; therefore the damage evolution rate should satisfy the following condition $\dot{d}_j \geq 0$, implicitly contained in Eqn. 5.11, and this leads to say that d_j is a monotonically increasing function of time t such that:

$$d_j = \max[d_j^\tau \mid \tau \leq t, d_j^t], \qquad j = 1,..,6 \qquad (5.17)$$

where d_j^t is the damage variable calculated from Eq. 5.17 for the current load state, and d_j^τ represents the state of damage at previous times $\tau \leq t$.

5.4 The constitutive response

In thesis work, the presented damage model will be enhanced with an nonlocal formulation to correct the mesh sensitivity problems due to strain localization in presence of material softening. The model has been implemented into ABAQUS/explicit within hexahedron solid elements and its ability to represent progressive damage is evaluated by simulating a tension test on one eight-node brick element.

Therefore, a single element uniaxial stress test, Fig. 5.3, was conducted to verify the constitutive response of the damage model. The predicted reaction/displacement curve of the cubic element subjected to monotonic tension is shown in Fig. 5.4.

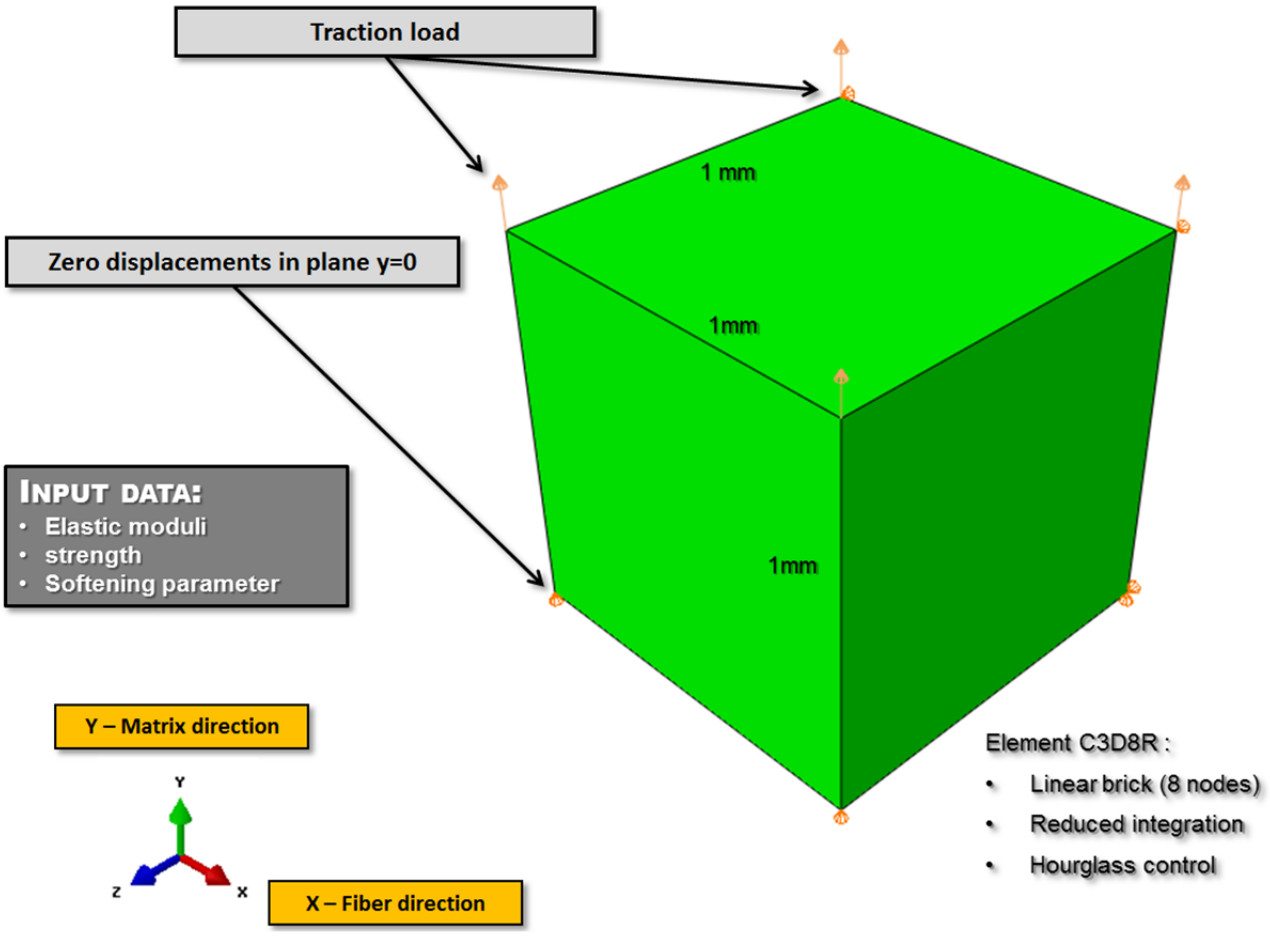

Fig. 5.3 – One-element test. Material data source in Ref. [29].

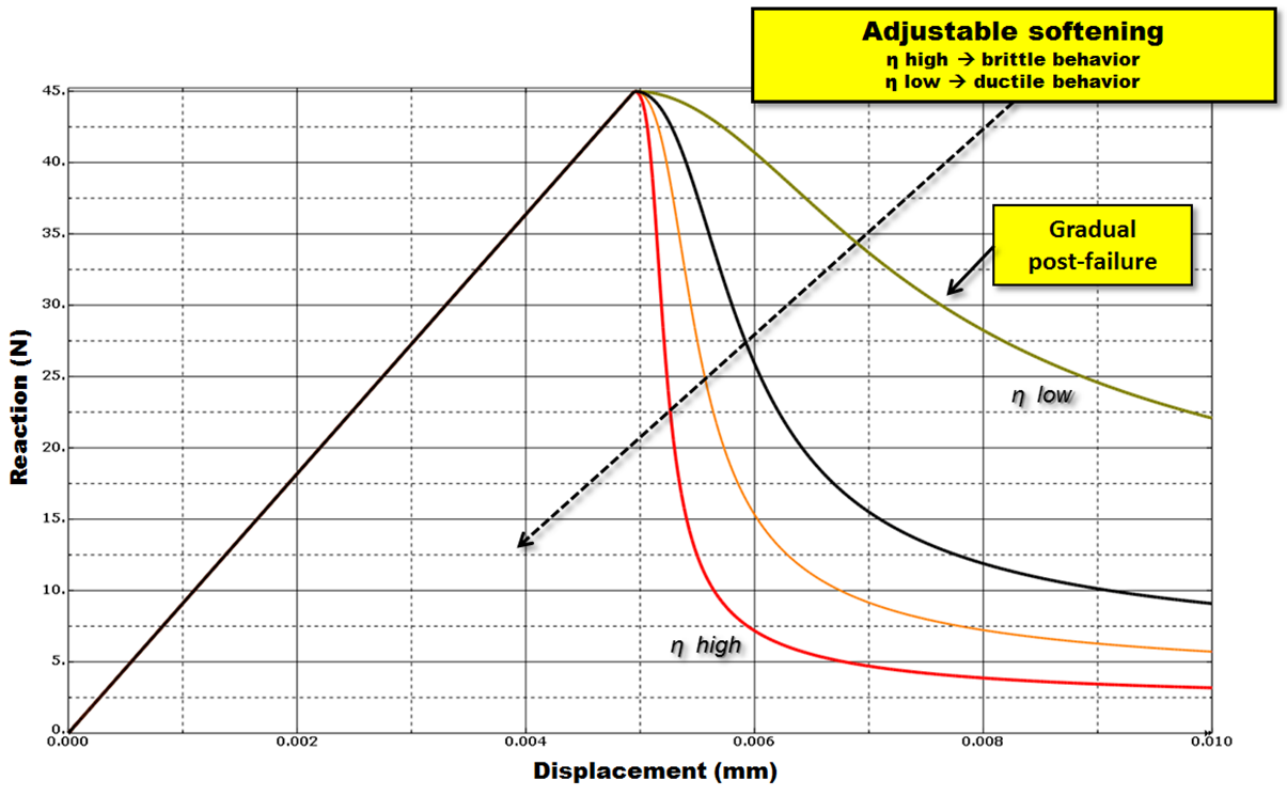

Fig. 5.4 – The constitutive response.

The one-element test is used to observe even the effect of the exponent m on the constitutive response. This exponent determines the brittle/ductile response of the element. In fact it can be seen that smaller values of m make the material more ductile that is a material that absorbs more energy prior to complete damage, with significant stiffness degradation prior to failure and a more gradual loss of stiffness after failure; conversely higher values give the material more brittle behavior with little or no loss in stiffness prior to failure and full damage corresponding to zero stiffness shortly after failure. These qualitative observations were used later as a guide in selecting values of the parameters m_i in Eqn. 5.17.

References

[1] R. C. Batra, G. Gopinatha, J. Q. Zheng, "Damage and failure in low energy impact of fiber-reinforced polymeric composite laminates", Composite Structures, 2012, 94:540–547.

[2] P. D. Soden, A. S. Kaddour, M. J. Hinton, "Recommendations for designers and researchers resulting from the world-wide failure exercise", Compos. Sci. Technol., 2004;64:589–601.

[3] A. M. Moncada, B. A. Bednarcyk, "Micromechanics-based progressive failure analysis of composite laminates using different constituent failure theories", Journal of Reinforced Plastics and Composites, 2012, 31(21):1467-1487.

[4] R. Maa, J. Cheng, "A CDM-based failure model for predicting strength of notched composite laminates", Composites Part B: Engineering, 2002, 33(6):479-489.

[5] P. Maimí, P. P. Camanho, J. A. Mayugo, C. G. Davila. "A continuum damage model for composite laminates: Part I – Constitutive model". Mechanics of Materials, Vol. 39, No. 10, pp 897-908, 2007.

[6] P. Maimí, P. P. Camanho, J. A. Mayugo, C. G. Davila. "A continuum damage model for composite laminates: Part II – Computational implementation and validation", Mechanics of Materials, 2007, 39(10):909-919.

[7] I. Lapczyk, J. A. Hurtado. "Progressive damage modeling in fiber-reinforced materials". Composites Part A: Applied Science and Manufacturing, 2007, 38(11):2333-2341.

[8] F. P. Van Der Meer, L. J. Sluys. "Continuum models for the analysis of progressive failure in composite laminates". Journal of Composite Materials, 2009, 43(20):2131-2156.

[9] X. Xiao. "Modeling energy absorption with a damage mechanics based composite material model". Journal of composite materials, 2009, 43(5):427-444.

[10] P. Ladeveze, "Sur une theorie de l'endommagement anisotrope", Report 34, Laboratoire de Mecanique et Technologie, Cachan, France, 1983.

[11] R.. A. Talreja, “Continuum mechanics characterization of damage in composite materials”, Proc. Royal Soc. London, 1985,399:195–216.

[12] L. Kachanov, “On the creep rupture time”, Izv Akad Nauk SSSR, 1958; 8:26–31.

[13] Y. Rabotnov, “On the equations of state for creep. Progress in applied mechanics”. Prager Anniversary vol. New York: Macmillan; 1963.

[14] P. Ladeveze P, E. Le Dantec, “Damage modeling of the elementary ply for laminated composites”, Compos. Sci. Technol. 1992;43:257–67.

[15] J. R. Xiao, B. A. Gama, J. W. Gillspie. Progressive damage and delamination in plain weave S-2 glass/SC-15 composites under quasi-static punch shear loading. Compos. Struct.; 2007; 78:182-96.

[16] X. Xiao, M. Botkin, N. Johnson, “Axial Crash Simulation of Braided Carbon Tubes Using LS-DYNA, Part 1: Material Model”, ACC TR EM03-02, September 2003.

[17] K. V. Williams, R. Vaziri, “Application of a damage mechanics model for predicting the impact response of composite materials”, Compos. Struct., 2001;79:997–1011.

[18] C. F. Yen, A. Caiazzo, “Innovative Processing of Multifunctional Composite Armor for Ground Vehicles; ARL-CR-484; U.S. Army Research Laboratory: Aberdeen Proving Ground, MD, 2001.

[19] A. Matzenmiller, J. Lubliner, R. L. Taylor. “A constitutive model for anisotropic damage in fiber composites”. Mechanics of Materials, 1995, 20(2):125-152.

[20] K. Gupta, B. P. Patel, Y. Nath, “Continuum damage mechanics approach to composite laminated shallow cylindrical/conical panels under static loading”, Composite Structures, 2012, 94(5):1703-1713.

[21] S. Murakami, “Continuum Damage Mechanics – A Continuum Mechanics Approach to the Analysis of Damage and Fracture”, Springer: Dordrecht, Heidelberg, London, New York, 2012.

[22] N. Bonora, “A nonlinear CDM model for ductile failure“,Engineering Fracture Mechanics, 1997, 58(1):11-28.

[23] J. Lemaitre, “Evaluation and dissipation of damage in metals submitted to dynamic loading”, Proceedings I.C.M.I. Kyoto, Japan, 1971.

[24] J. Lemaitre, “A continuous damage mechanics model for ductile fracture”, J. Eng. Materials and Technol., 1985, 107: 83–89.

[25] J. Simo, J. Ju, “Strain and stress based continuum damage models. Formulation”, *International Journal of Solids and Structures*, 1987, 23(7):821-40.

[26] A. Sluzalec, “Theory of thermomechanical processes in welding”, Springer, 2005.

[27] M. Jirásek, “Damage and Smeared Crack Models”, Numerical Modeling of Concrete Cracking CISM International Centre for Mechanical Sciences, 2011, 532:1-49.

[28] “A progressive composite damage model for unidirectional and woven fabric composites”, User manual version 10.0, Materials Sciences Corporation & University of Delaware Center for Composite Materials, 2011.

[29] H. Y. Choi, F. K. Chang, “A model for predicting damage on graphite/epoxy laminated composites resulting from low-velocity point impact”, J. Compos. Mater., 1992; 26(14):2l34-2169.

CHAPTER 6

NONLOCAL APPROACH

6.1 Strain softening and strain localization

In many heterogeneous materials such as concrete, rock, filled elastomers, wood, paper, and especially fiber reinforced composite which are object of study in this thesis, failure occurs by progressive damage which is manifested by phenomena such as microcracking and void formation. The scale of these phenomena, as compared to the scale of practical finite element meshes, is usually too small to be modeled and their effect must be incorporated in the numerical analysis through a macroscopic description of damage which can be captured by a constitutive model that exhibits a gradual decline of stress to zero at increasing strain (the so-called *strain softening*) beyond some critical strain [1]; essentially the softening behavior acts as a precursor to complete rupture.

Several studies [2,3,4] have shown that damage growth in a fiber reinforced polymer composite structure manifests itself in the form of overall strain softening of the material and that physical origin of softening is in the propagation and coalescence of defects such as voids or cracks. Strain-softening models have received a great deal of attention in the last decade for describing the fracture of concrete and other heterogeneous brittle materials.

Continuum Damage Mechanics (CDM) is one of the methods that can be used to capture the strain softening type behavior (material degradation). Continuum damage mechanics (CDM) is a constitutive theory that describes the progressive loss of material integrity due to the propagation and coalescence of the above said defects which lead to a degradation of material stiffness observed on the macroscale. In the framework of continuum mechanics, continuum damage models describe

the changes of material stiffness and strength, caused by the evolution of defects [5,6]. The density and orientation of microdefects can be approximated by certain internal variables whose number and character depend on the complexity of the model [7].

Unfortunately, numerical studies show that when strain softening behavior is introduced in a conventional local constitutive law then implemented in a finite element analysis software, the numerical result exhibits undesirable characteristics. It is well known that softening may lead to localization of inelastic strain into narrow process zone (this phenomenon is called *strain localization*). In detail, using a rate-independent strain softening material model, results dependent on the finite element discretization are obtained [8,9,10,11]; they show an extreme sensitivity with respect to the fineness and direction of the spatial discretization that is employed. Moreover upon refinement of the discretization, convergence is observed to a solution in which deformation is localized in an infinitely narrow band. This response is physically inappropriate in that with increasing mesh refinement the energy dissipated in the strain softening domain tends to zero; in other words, it does not allow for any energy dissipation in the fracture process [12].

The cause of this problem is the ill-posedness of the mathematical model. In fact, from the mathematical viewpoint, the underlying mathematical cause of the mesh dependence is that if softening is represented simply by a falling stress-strain curve in a rate-independent continuous material model, then the partial differential equations of motion or equilibrium which govern the deformation process locally will change characteristic type at the onset of softening, from hyperbolic to elliptic in dynamic problems and vice versa in static problems [8-12].

In either case, the problem will become ill-posed, as the boundary and initial conditions for one class of equations are not appropriated for the other (initial-boundary value problem ill-posed) [8]. For example, in static problems, in the localization zone, where strain-softening occurs, the differential equations, which result from equilibrium, are no longer elliptic, while in the other parts of the structure, which will unload elastically, the equations stay elliptic. As a result, the governing equations no longer have the same character throughout the structure [13].

Ill-posed problems can be regularized using different methods been presented in the open literature as discussed in [14]: including rate-dependence in the constitutive model [15,16,17]; by Cosserat or micro-polar models [18,19,20,21]; by higher-order gradient models [22,23,24,25]; by integral type nonlocal models [26,27,28,29,30]; changing the mesh topology in anticipation of material failure [31]; using a smeared cracking formulation [32].

Therefore, introducing higher temporal derivatives into the equations of motion or introducing higher special gradients into the equations of motion or using Cosserat theory or changing the mesh topology in anticipation of material failure or ensuring internal dissipation during failure by a smeared cracking formulation, it's possible resolve some of the issues of ill conditioning when softening behavior is numerically implemented in finite element analysis software. All these approaches explicitly or implicitly introduce a material characteristic length to control the width of the localization band, thus prevent strain from localizing into infinitely narrow zones. The introduction of an internal length is justified by the material heterogeneity. The microprocesses which are responsible for material damage usually extend over a band and the thickness of which is comparable to the characteristic microstructural length (e.g. long ranging mechanisms such as microcrack interaction severely influence the stress state at a material point). Detailed reasons of the nonlocality can be found in Ref. [30]

Out of all the methods presented here in order to avoid the discussed problem which afflicts continuum-based models expressed in terms of softening stress-strain relations, the nonlocal integral approaches are easy to program in the finite element method. Nonlocal integral formulation modifies damage models [29,30] by introducing nonlocal variables, which are space-weighted averages of local variables. The constitutive equation describing the strain localization phenomenon is nonlocal. In a nonlocal constitutive equation, typically, the stress in a material point not only depends on the strain in that point, but also on the strain in a neighbourhood of that point.

In conclusion, as above said, a non-local model is able to describe the large variations of strain in the localization zone. The size of this zone is controlled by additional parameters, which are incorporated in the constitutive model. The model has to be chosen such that the governing differential equations remain elliptic also when softening occurs. Then, the differential equations stay of the same type throughout the structure when localization of deformation occurs, and a localization zone containing more than one element can be obtained.

In this work, a simple and straightforward computational approach is presented for numerically integrating the non-local constitutive equations with little effort required to modify an existing finite element code.

The nonlocal damage model presented here is founded on references [33,34] and it has been implemented in commercial explicit Finite Element code Abaqus via the Vectorized User MaTerial subroutine VUMAT. In order to prevent strain localization and strong mesh sensitivity of the solution, an integral-type of nonlocal model based on the weighted spatial averaging of a local quantity controlling material softening or degradation is developed. The desired local variable is turned nonlocal at a new instant time using a penality coefficient based on the local and nonlocal variable values at the last converged incremental step which are available for calculations.

The effectiveness of the non-local model is assessed through the simulation of progressive damage growth around a notch in a composite laminate under different loading conditions.

6.2 Strain softening: the problem statement

To demonstrate that the pathological sensitivity of the numerical results to the discretization a simple one-dimensional localization problem is proposed by Jirásek [35] and here analyzed.

Consider a straight bar of constant cross section A and total length L under uniaxial tension, see Fig. 6.1).

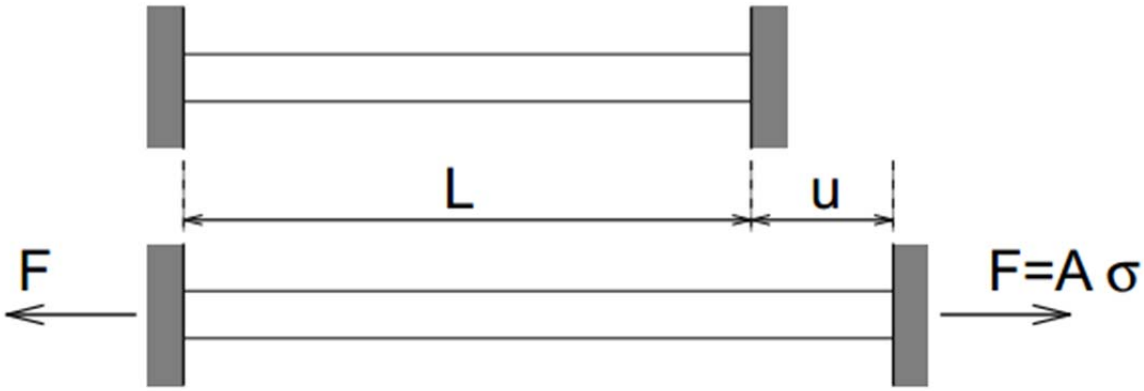

Fig. 6.1 – Bar under uniaxial tension (Jirásek) [35].

However, it's possible to have even a material layer under shear loading and all the results can be reinterpreted in terms of the shear problem, simply by replacing the normal stress by shear stress, normal strain by shear strain, Young's modulus by shear modulus, etc.

A bilinear stress-strain constitutive relation with linear elastic behavior up to the peak stress, f_t (damage-onset strength) followed by linear softening, see Fig. 6.2, is assumed to represent the material response.

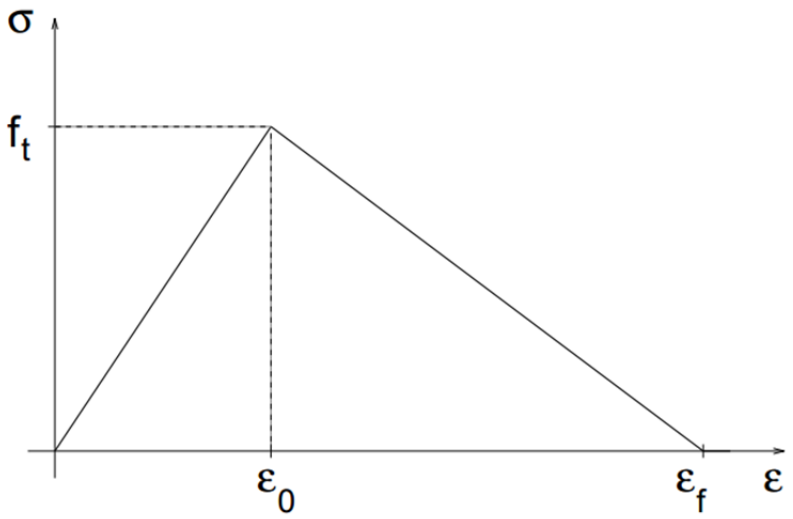

Fig. 6.2 – Stress-strain diagram with linear softening (Jirásek) [35].

If $\varepsilon_0 = f_t / E$, where E is Young's modulus of elasticity, the peak stress is attained. The tensile strain at which, after the damage onset, the transmitted stress completely disappears (tensile failure strain) is denoted by ε_f .

When an displacement u is applied at one of the supports, the response remains linear elastic up to peak stress $\sigma = f_t$. After the peak stress, the resistance of the bar starts decreasing and at each cross section, stress can decrease either at increasing strain (softening behavior) or at decreasing strain (elastic unloading). The equation of equilibrium implies that the stress profile must remain uniform along the bar. However, at any given stress level $\bar{\sigma}$ between zero and f_t there exist two values of strain ε_s and ε_u for which the constitutive equation is satisfied, Fig. 6.3, and so the strain profile does not have to be uniform.

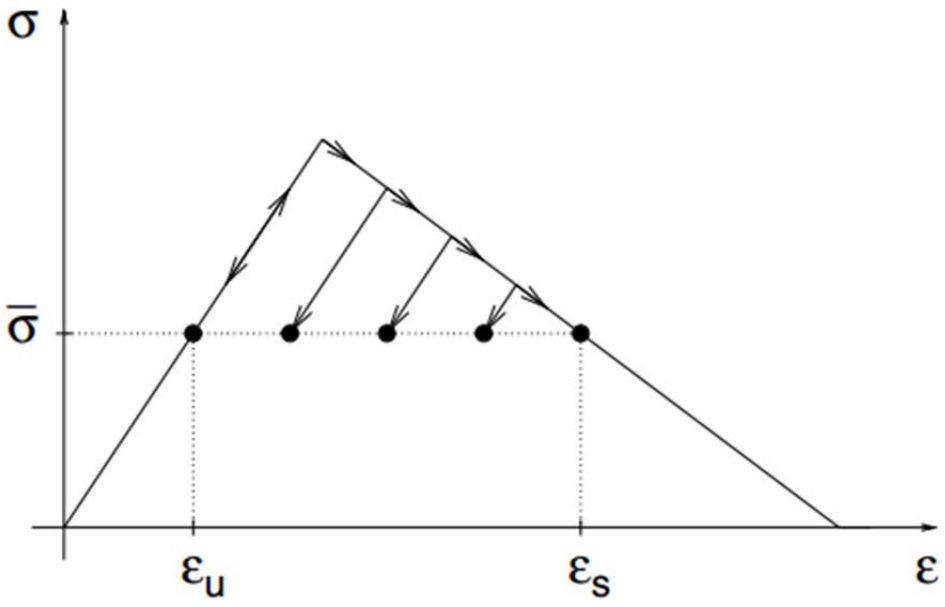

Fig. 6.3 –Two strain values corresponding to the same stress level (Jirásek) [35].

Denoting by L_s the cumulative length of the softening regions and by $L_u = L - L_s$ the cumulative length of the unloading regions, the material, for example, can be softening in an interval of length

L_s and unloading everywhere else in an interval of length L_u. When the stress is completely relaxed to zero, the strain in the softening region is $\varepsilon_s = \varepsilon_f$ and the strain in the unloading region is $\varepsilon_u = 0$; the total bar elongation is therefore $u = L_s\varepsilon_s + L_u\varepsilon_u = L_s\varepsilon_f$ but the softening region length L_s remains undetermined and it can take any value within the interval [0,L]. This means that the structural problem has infinitely many solutions, and the corresponding post-peak branches of the load-displacement diagram fill the fan shown in Fig. 6.4.

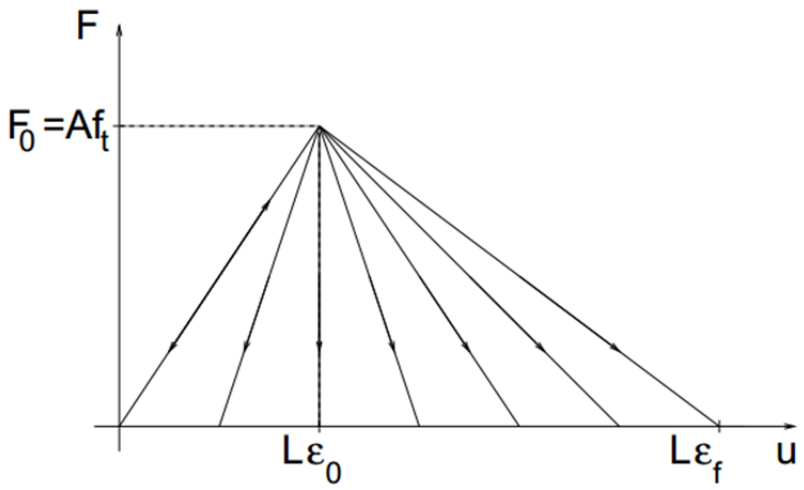

Fig. 6.4 – Fan of possible post-peak branches of the load-displacement diagram (Jirásek) [35].

The uncertainty in the length L_s of the softening regions is removed if imperfections are taken into account. The imperfections can be associated with the material (its properties are non-uniform) or the bar geometry (bar sectional dimensions are non-uniform). If the strength in a small region is supposed slightly lower than in the remaining portion of the bar, when the applied stress reaches the reduced strength, softening starts and the stress decreases; consequently, the material outside the weaker region must unload elastically, because its strength has not been exhausted. Therefore if the loading process is performed on a bar with geometric or material imperfections, the strain will localize in the weakest cross-section in combination with vanishing energy dissipation.

As stated above it's possible conclude that the softening region size cannot exceed the size of the region with minimum strength. However, the region with minimum strength can be arbitrarily small, and the corresponding softening branch can be arbitrarily close to the elastic branch of the load-displacement diagram. Therefore, as argued by Jirásek, the standard local damage model accounting for strain-softening leads to a solution that has several problems: (1) the region of material softening is infinitely small; (2) the load displacement diagram always exhibits snapback, independently of the structural size and of the material ductility; (3) the total amount of energy dissipated during the failure process is zero.

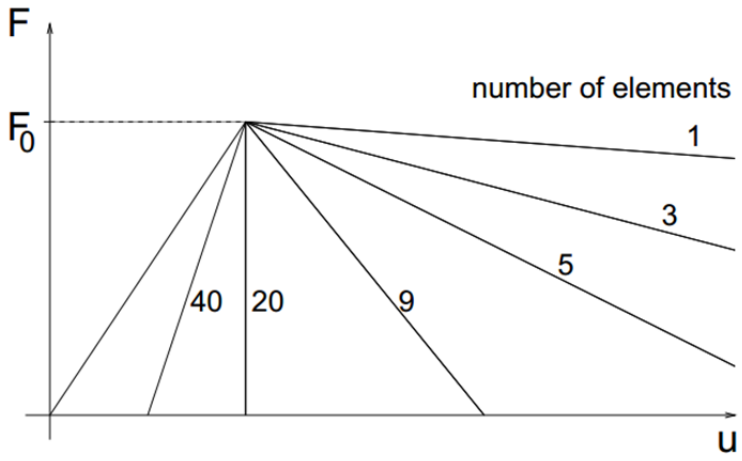

Fig. 6.5 – Effect of mesh refinement on the numerical results: load-displacement diagrams (Jirásek) [35].

From the mathematical point of view, these problems are related to the so-called loss of ellipticity of the governing differential equation which occurs when the tangent modulus, after peak-stress, ceases to be positive and the boundary value problem becomes ill-posed, i.e., it does not have a unique solution with continuous dependence on the given data. From the numerical point of view, ill-posedness is manifested by sensitivity of the results to the size of finite elements. If a bar is discretized by finite elements and if the numerical algorithm properly captures the localized solution, the softening region extends over one element and the slope of the post-peak branch depends on the number of elements, see Fig. 6.5 [35]

6.3 Strain softening: the numerical problem

The loss of uniqueness in the post-critical regime, from the numerical point of view, is manifested by pathological sensitivity of the results to finite element discretization (i.e. from size of finite elements). In this paragraph, the problems related to strain softening when a local constitutive model is used, are demonstrated by the example of a three-dimensional bar loaded in tension. The implemented local constitutive model in the software ABAQUS is that discussed in Chapter 5.

The bar, with length L = 10 mm, uniform square transverse cross section of 1mm x 1mm and with a fixed end (it is prevented from moving longitudinally), is divided into eleven elements initially, then fifteen and finally thirty-one elements and it is loaded by prescribing the displacement at x = L (at non-fixed end), see Fig. 6.6. The model is meshed with linear 8-noded hexahedral elements (ABAQUS element type C3DR8), which possessed 3 degrees of freedom per node. The ABAQUS automatic mesh generator is used to build the mesh. The discretization is done in such a way that in the center of the bar there is one element. The bar is made of generic isotropic material that can be damaged when the strain in the longitudinal direction satisfies the maximum strain criterion.

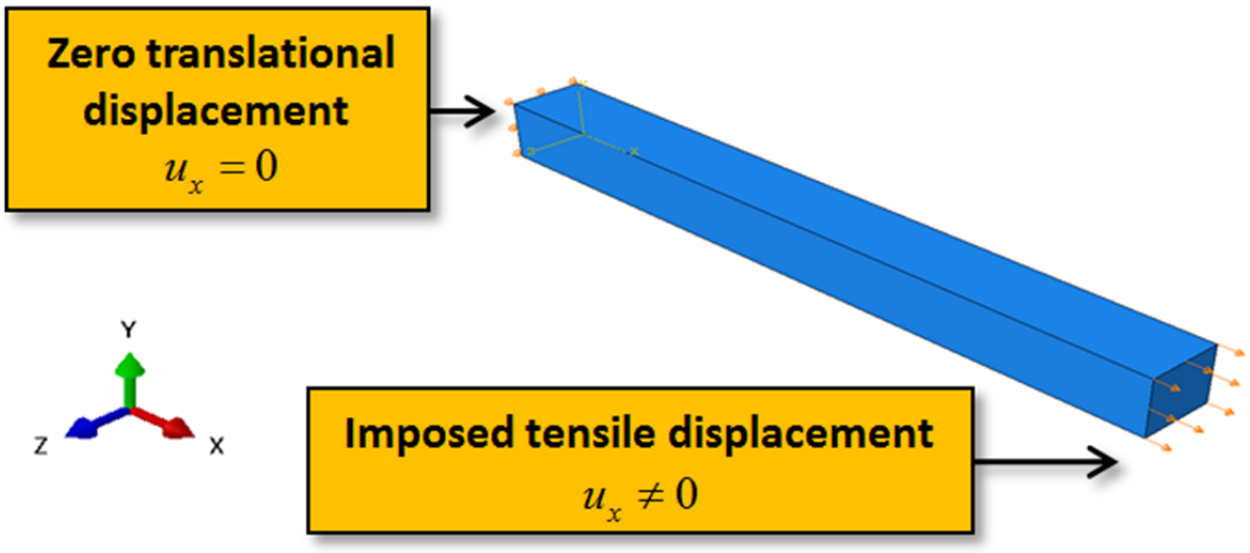

Fig. 6.6 – Bar loaded in displacement-controlled uniaxial tension.

Suppose the existence of a stress concentration in the center of the bar which is simulated by a marginally lower tensile strength for the central element, Fig. 6.7.

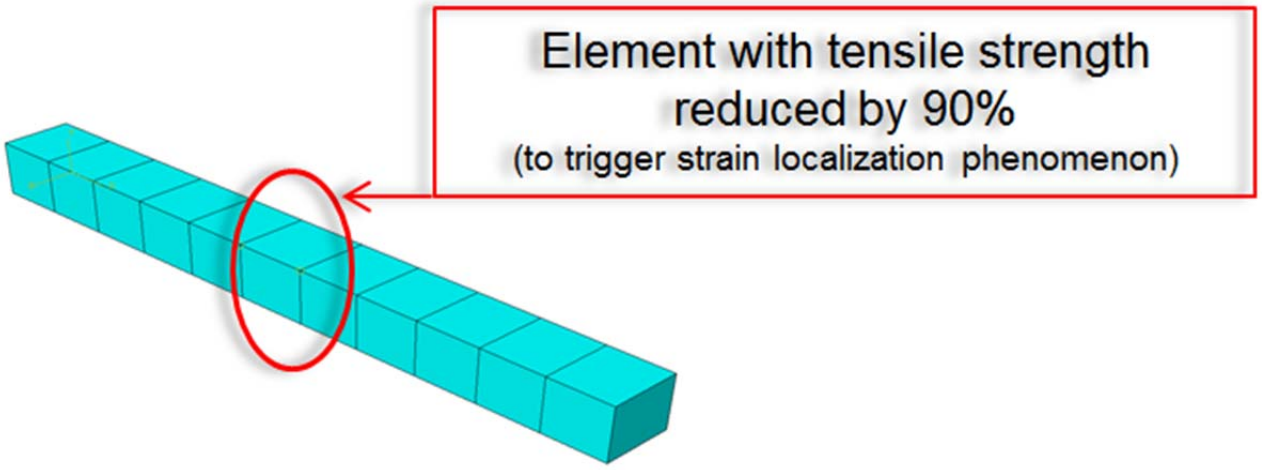

Fig. 6.7 – Discretized bar (eleven elements) with weak element in its center.

When the bar is subjected to-the prescribed displacement, the weakened element will reach its tensile strength first, and as a result the strain localizes into this element. In the other neighbouring elements, the tensile strength is not reached, and they will unload elastically.

The response curves in Fig. 6.8 show that the normalized reaction force versus imposed normalized displacement response of the bar is mesh dependent. Because of the strain concentration, localization occurs in one element, irrespective of its size.

Therefore if the numerical algorithm properly captures the most localized solution, the softening region extends over one element, and the length of the softening region is given by $L_s = L / N_e$. The slope of the post-peak branch therefore strongly depends on the number of elements, and it approaches the initial elastic slope as the number of elements tends to infinity.

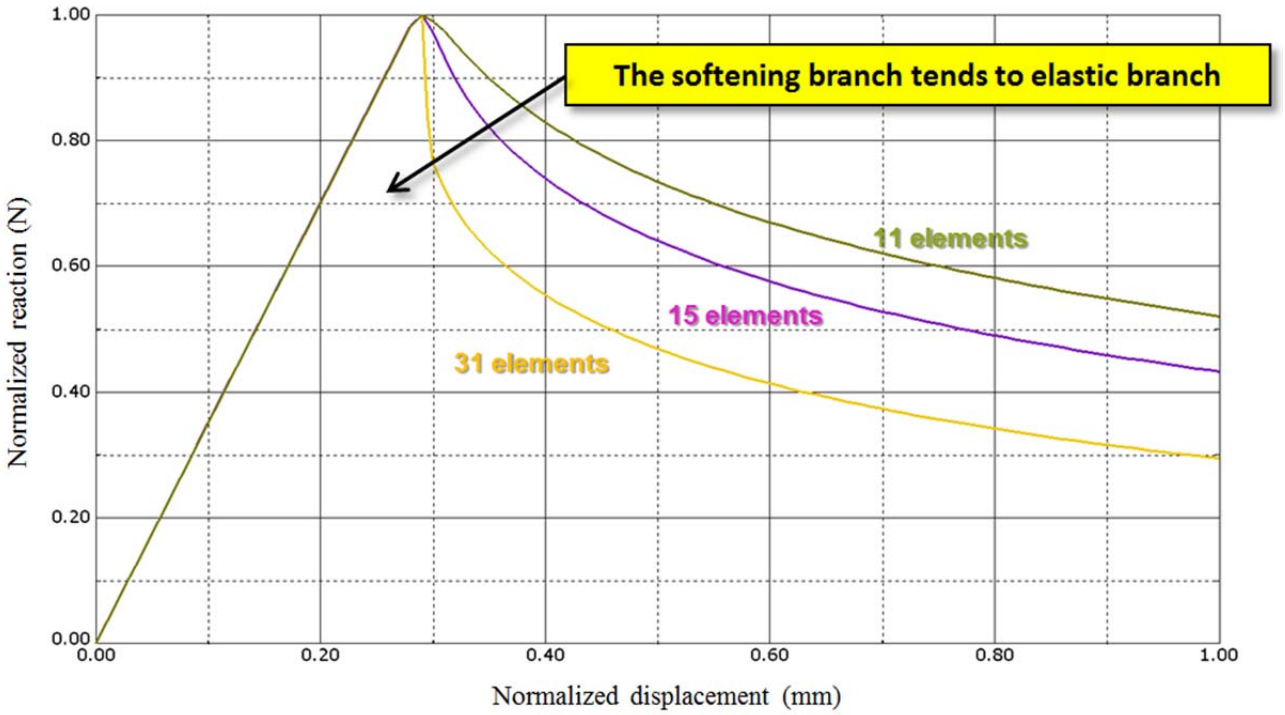

Fig. 6.8 – Normalized reaction force versus imposed normalized displacement at the right end of the bar. For an increasing number of elements, the contribution to the strain of the elements which unload increases and a more brittle post-peak response occurs. In the extreme case of an infinite number of elements, the post-peak behavior doubles back on the original loading curve (elastic branch) and the dissipated energy tends to zero [35].

6.4 Integral type nonlocal model

Nonlocal formulations have a regularizing effect on problems with strain localization. They can act as efficient localization limiters [7]. The nonlocal models of the integral type remove the classical assumption of locality and they assert that the material state at a point depends not only on the variables at that point but in general on the distribution of variables over the whole body, or at least on their distribution in a finite neighborhood of the point under consideration [35]. Details of the integral-type nonlocal models can be found in Ref. [30]

Consider a solid three-dimensional Euclidean space that occupies the domain V, consisting of damaging elastic material. Generally speaking, the nonlocal approach consists in replacing a certain variable or more variables (typically, state variables) by their nonlocal counterpart obtained by

weighted averaging over a spatial neighborhood of each point under consideration. If $f(\boldsymbol{x})$ is some "local" field in a domain V (the body of interest), the corresponding nonlocal field is defined as:

$$\bar{f}(\boldsymbol{x}) = \int_V \alpha(\boldsymbol{x}, \boldsymbol{\xi}) f(\boldsymbol{\xi}) d\boldsymbol{\xi} \qquad (6.1)$$

where $\alpha(\boldsymbol{x}, \boldsymbol{\xi})$ is a given nonlocal space weight function that has as its purpose the description of the interactions between nearby particles. Therefore, a non-local variable can be obtained by averaging the associated local quantity through the above integral. The integral introduces a diffusive effect in the constitutive model, which prevents the non-local variable to spuriously localise into a narrow band as the spatial discretization becomes finer [36].

For physically sound formulations, the weight function is required to be positive and symmetric $\alpha(\boldsymbol{x}, \boldsymbol{\xi}) = \alpha(\boldsymbol{\xi}, \boldsymbol{x})$ as it depends only on the distance $r = \|\boldsymbol{x} - \boldsymbol{\xi}\|$. It must have its maximum value for $r = \|\boldsymbol{x} - \boldsymbol{\xi}\| = 0$ (i.e. for $\boldsymbol{x} = \boldsymbol{\xi}$) and it must decrease monotonically and rapidly to zero for increasing r (i.e. the nonlocal interactions are effective only in a small, but finite, neighbour of the field point).

In an infinite domain, the space weight function depends only on the distance between the "source" point, $\boldsymbol{\xi}$, and the "receiver" point, $\boldsymbol{x}$. Indeed, in an finite body and in the vicinity of a boundary, the weight function is usually rescaled such that the nonlocal operator does not alter a uniform field [30]:

$$\alpha(\boldsymbol{x}, \boldsymbol{\xi}) = \frac{\alpha_o(\|\boldsymbol{x} - \boldsymbol{\xi}\|)}{\int_v \alpha_o(\|\boldsymbol{x} - \boldsymbol{\zeta}\|) d\boldsymbol{\zeta}} \qquad (6.2)$$

where $\alpha_0(r)$ is a monotonically decreasing non-negative function of the distance $r = \|\boldsymbol{x} - \boldsymbol{\xi}\|$.

In the one-dimensional setting, x and ξ are scalars and the domain of integration V reduces to an interval.

The weight function is often taken as the Gauss distribution function:

$$\alpha_0(r) = \exp\left(-\frac{r^2}{2l^2}\right) \qquad (6.3)$$

where l is a parameter representing the internal length of the nonlocal continuum. Another possible choice is the bell-shaped truncated quartic polynomial function:

$$\alpha_0(r) = \begin{cases} \left(1-\frac{r^2}{R^2}\right)^2 & if\ 0 \le r \le R \\ 0 & if\ R \le r \end{cases} \qquad (6.4)$$

where R is a parameter related to the internal length. Since R corresponds to the largest distance of point $\boldsymbol{\xi}$ that effects the nonlocal average at point $\boldsymbol{x}$, it is called the *interaction radius*.

It is noted that the Gauss function has an unbounded support, i.e., its interaction radius is $R = \infty$. In both cases l and R play the role of an internal length parameter which controls the nonlocal spatial spread of the local variable. However, for computational applications, it is more advantageous and efficient to use attenuation functions with a finite support as the polynomial bell-shaped function [30].

6.5 Approximate nonlocal approach

The implementation in a finite element software of a nonlocal regularisation method of integral-type is not straightforward due to presence of the integral in the constitutive evolution equations that prevents the model to have the consistency condition fulfilled locally [36]. In fact, the numerical implementation of a nonlocal model in a commercial finite element software ABAQUS

requires access to all integration points of finite elements constituting the mesh in order to proceed with the global integration scheme. Generally this is not a problem if it's possible have full access to the source code of the finite element software, or at least, if it's possible have access to the algorithm that assembles the internal force vector. Unfortunately, most of the commercial FE codes do not allow the user a lot of freedom and restrict the constitutive model defined by the user to only some calculations in Gauss points of each element. However the global integration can be avoided by using an alternative formulation that approximates the nonlocal theory. This approach comes from a study of Cesar De Sa et al. [36] based on that proposed by Tvergaard and Needleman [37] and it consists in transforming a local variable in one nonlocal at the same instant of time using just a product:

$$\mathrm{var}_{n+1}^{nonloc} = fact^{nonloc} * \mathrm{var}_{n+1}^{loc} \qquad (6.5)$$

where $fact^{nonloc}$ is a penality factor defined as:

$$fact^{nonloc} = \frac{\mathrm{var}_{n}^{nonloc}}{\mathrm{var}_{n}^{loc}} \qquad (6.6)$$

In the equation above, var_{n}^{loc} and $\mathrm{var}_{n}^{nonloc}$ are respectively the values of local and nonlocal at last incremental step convergent. The calculation is performed locally and the selected local variable at the new instant n+1, var_{n+1}^{loc}, is penalized with the coefficient $fact^{nonloc}$ in order to obtain the nonlocal value of the same variable at the same instant of time, $\mathrm{var}_{n+1}^{nonloc}$.

Therefore, with the nonlocal method, each integration point must query the surrounding integration points during the evaluation of material behavior. The limitation of this approach, as rightly stated by the authors in Ref. [36], is that the time step must be kept small enough to avoid instability in the solution. In explicit codes the size of the time step must be necessarily small in order to provide

stable solutions, so it's not a severe problem. The use of an approximate expression such as the one in Eqn. 6.5 is very attractive from a point of computational view because the update can be performed locally and the time step will be necessarily small.

The constitutive model which allows the material softening (damage) and in which the nonlocal approach is introduced is discussed in Chapter 5. The strain components that regulate the material softening after damage onset are the chosen local variables for nonlocal treatment above discussed. Alternatively, it's possible consider the damage variables as demonstrated in Ref. [38].

6.6 Nonlocal damage model assessment

To verify the effectiveness of the implemented nonlocal method, the bar in tension, with a weak part in the center, already used in paragraph 6.2 to demonstrate the mesh-size dependency problem associated with strain softening, is initially considered.

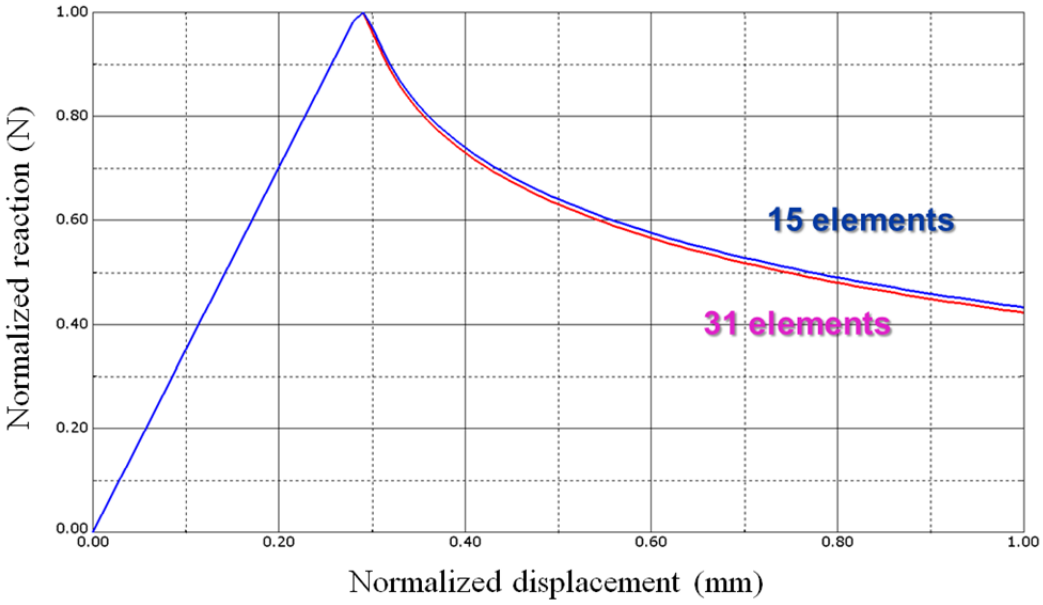

Fig. 6.9 – Predicted force-displacement responses for a bar subjected to an axial load. The bar was simulated with two different numbers of elements: 15 and 31 elements.

Two different spatial discretization using 15 and 31 elements are taken. An explicit dynamic analysis is then performed on this structure. The simulations is carry out under displacement controlled condition where one end of the bar was pulled under a constant rate. The Fig. 6.9 shows the predicted force versus elongation curves for the two mesh sizes. It can be noted that by refining the mesh, the response of the structure doesn't change significantly.

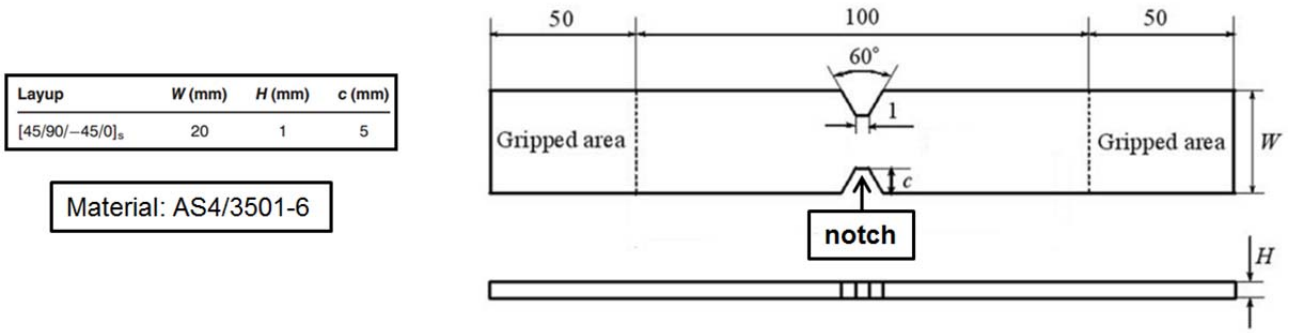

Fig. 6.10 – Specimen geometry of carbon/epoxy laminate (dimensions are given in mm).

In order to demonstrate the effectiveness of the proposed procedure for the treatment of strain localization, a laminate structures with geometric imperfections is taken into account. In detail the structural response of a double-notched carbon/epoxy composite laminate under uniaxial tension is numerically investigated by means of ABAQUS/Explicit commercial code in which the model is implemented. Abaqus/Explicit is particularly well suited for the simulation of discontinuous and unstable events. The problem of a double notched specimen under uniaxial tension was experimentally and numerically analyzed by Pham Dinh Chi in [39]. The material under study is the unidirectional AS4/3501-6 and its mechanical properties obtained from [39] are given in Tab. 6.1. The laminate is quasi-isotropic with layup $[45/90/-45/0]_s$. The finite element model is constructed with linear eight-node brick elements with reduced integration (C3DR8) and with a single element over the thickness of the ply. The boundary conditions of the model are shown in Fig. 6.11. Only half of the structure is modeled due to symmetry. The tensile loading is imposed by enforcing the longitudinal displacement of all nodes along the right edge.

Modulus in fiber direction E_1 (GPa)	147
Transverse moduli E_2= E_3 (GPa)	10.3
Shear moduli G_{12}=G_{13} (GPa)	7
Shear modulus G_{23} (GPa)	3.7
Poisson's ratios v_{12}= v_{13}	0.3
Poisson's ratio v_{23}	0.5
Longitudinal tensile strength X_T (MPa)	2280
Longitudinal compressive strength X_C (MPa)	1725
Transverse tensile strength Y_T (MPa)	57
Transverse compressive strength Y_C (MPa)	228
Out-of-plane tensile strength Z_T (MPa)	57
Out-of-plane compression strength Z_C (MPa)	228
Shear strength S_{12}=S_{13} (MPa)	75

Tab. 6.1 – Material properties of carbon/epoxy composite.

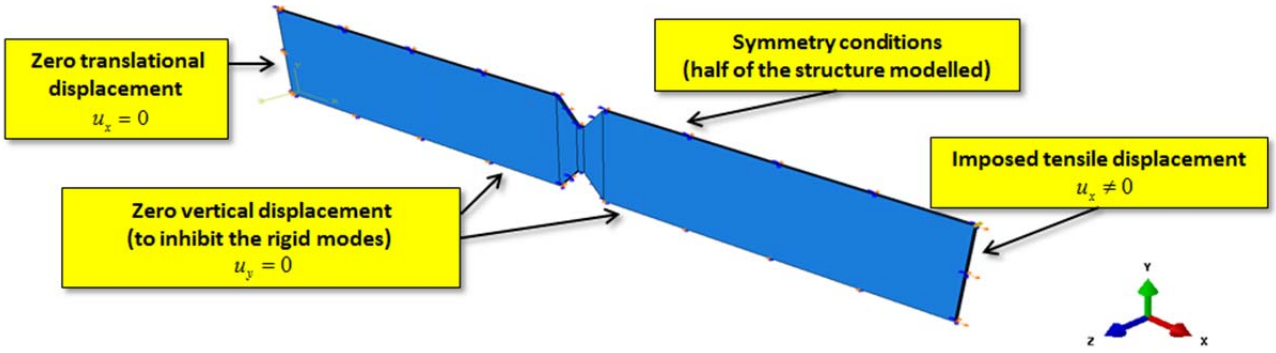

Fig. 6.11 - Boundary conditions for carbon/epoxy specimen.

The conditional stability for an explicit dynamic procedure requires the use of small time increments but this condition can be computationally impractical for the modeling of quasi-static events in their natural time scale (actual time taken for a physical process). Generally, it is safe to assume that performing an analysis in the natural time for a quasi-static process will produce accurate static results but to analyze quasi-static events in explicit solver event acceleration techniques must be employed to obtain an economical solution [40].

Two methods to obtain an economical quasi-static solution with an explicit dynamic procedure are to increase the loading rates and to perform mass scaling [40]. In the first method the event duration is reduced artificially by increasing the rate at which the loading is applied while the second method the material density is increased artificially which in turn carries to an increase of the stable time increment. Only the method based on loading rate is used for the present analysis so that the same physical event occurs in less time as long as the solution remains nearly the same as the true static solution and dynamic effects remain insignificant. One approach to determining the extent to which the loading rate can be increased is to study the natural frequencies of the structure using a traditional implicit finite element analysis (Abaqus/Standard). In a static or quasi-static analysis the lowest eigenmode of a structure usually dominates the response; knowing this frequency and the corresponding time period of the lowest structural mode, it's possible to estimate the time required to obtain a quasi-static response by explicit solver. One way to start the time setting is to specify a loading time greater than 10 times the period of the lowest eigenmode [41]. The application of loading must be as smooth as possible for reasons of quasi-static analysis accuracy and efficiency. In fact jerky movements cause stress waves, which can induce noisy or inaccurate solutions. Applying the load in the smoothest possible manner requires that the acceleration changes only a small amount from one increment to the next; if the acceleration is smooth, it follows that the changes in velocity and displacement are also smooth. In order to achieve this goal a displacement loading with SMOOTH STEP option (AMPLITUDE toolset in ABAQUS).

As regard to length, R (for *bell-shaped* curve *weight function)*, used in this work, or l_c (for *gaussian weight function)*, which denoted a characteristic internal length controlling the spread of the non-local weight function, the its determination is very complex since it is related to the fracture process zone with a certain volume. This parameter should be considered as a material property reflecting the internal length scale of the microstructure, but in this study its link to the actual material is not considered. The aim is only to show that the strain localization problem is solved using a approximated nonlocal model. Therefore, the characteristic length, in the zone of interest, is

assumed to be at least two times the smallest finite element size since otherwise the analysis is equivalent to the classical local continuum analysis [42]. Therefore in the notch of the structure where the strain/stress is localized the finite element size must be lower than the characteristic length to make the nonlocal approach active.

The Christensen failure criterion [43] is finally used in the material property degradation model to evaluate failure in an individual composite ply. This criterion identifies three distinct failure modes for a composite lamina: fiber tension, fiber compression, and matrix failure.

The numerical results obtained by finite element simulation are compared with those present in the literature [39]. The progressive damage patterns predicted by the approximated nonlocal model, see Fig. 6.12, follow those reported in reference document and shown in Fig. 6.13, resulting in very close output.

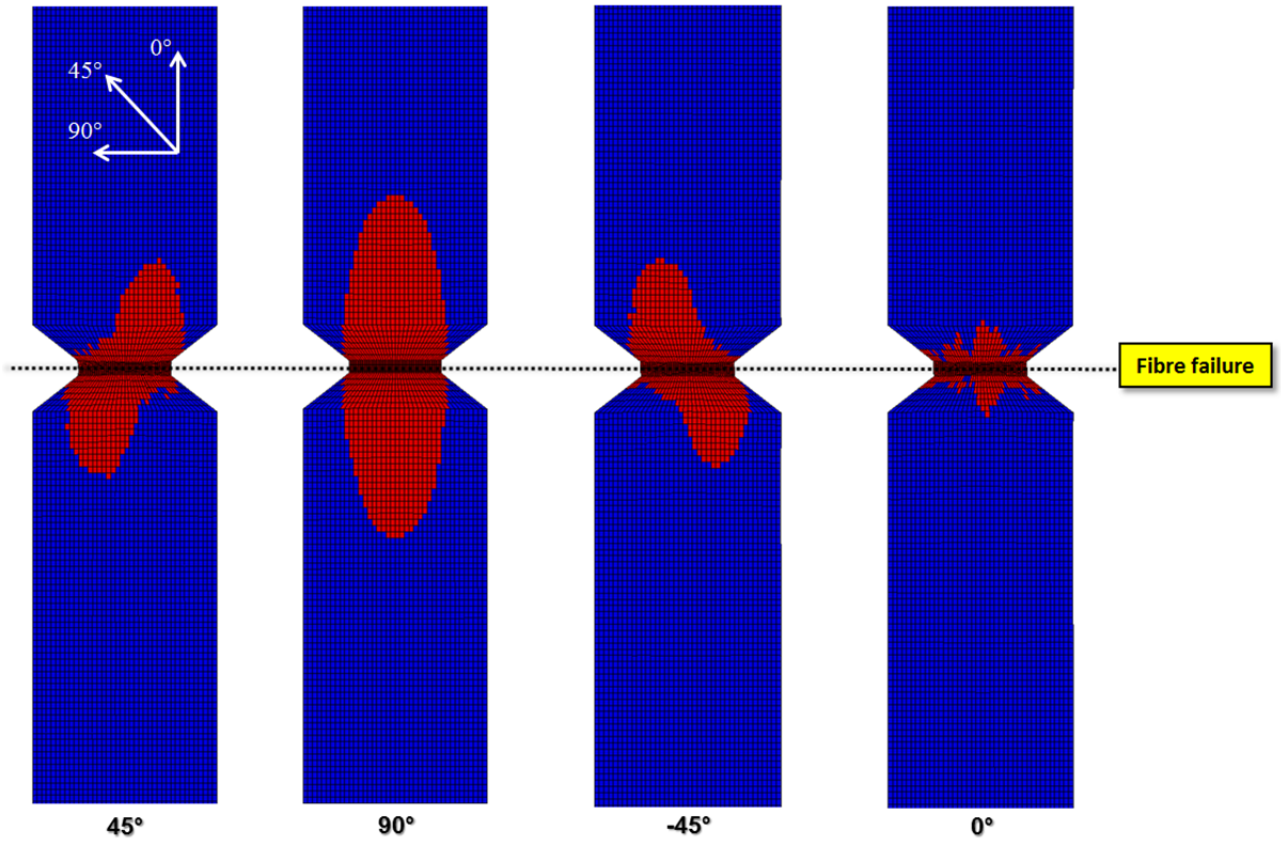

Fig. 6.12 - Predicted damage patterns for matrix and fiber failure. In red the elements that have verified the Christensen criterion. The final failure in these models is caused by fiber failures in the 0° and ±45°.

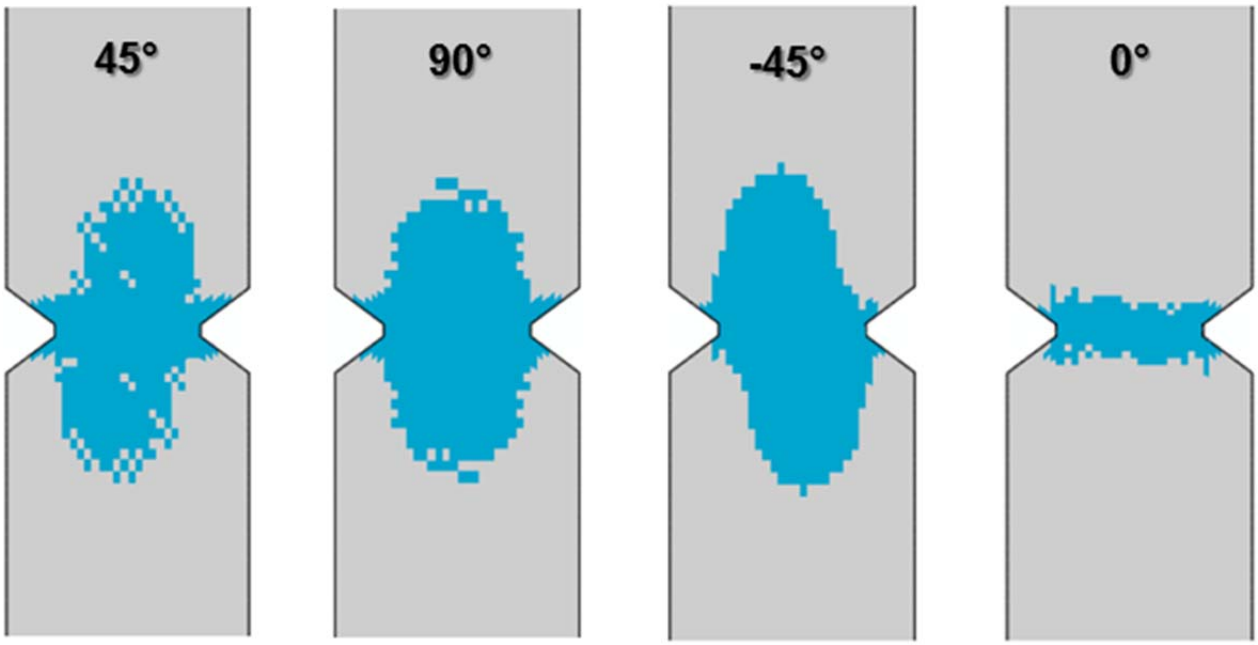

Fig. 6.13 - Predicted damage patterns for matrix and fiber failure from literature [39].

The ultimate load predicted by the implemented model, Fig. 6.14, is even very closely results obtained from experimental tests conducted on some specimens from author of Ref. [39].

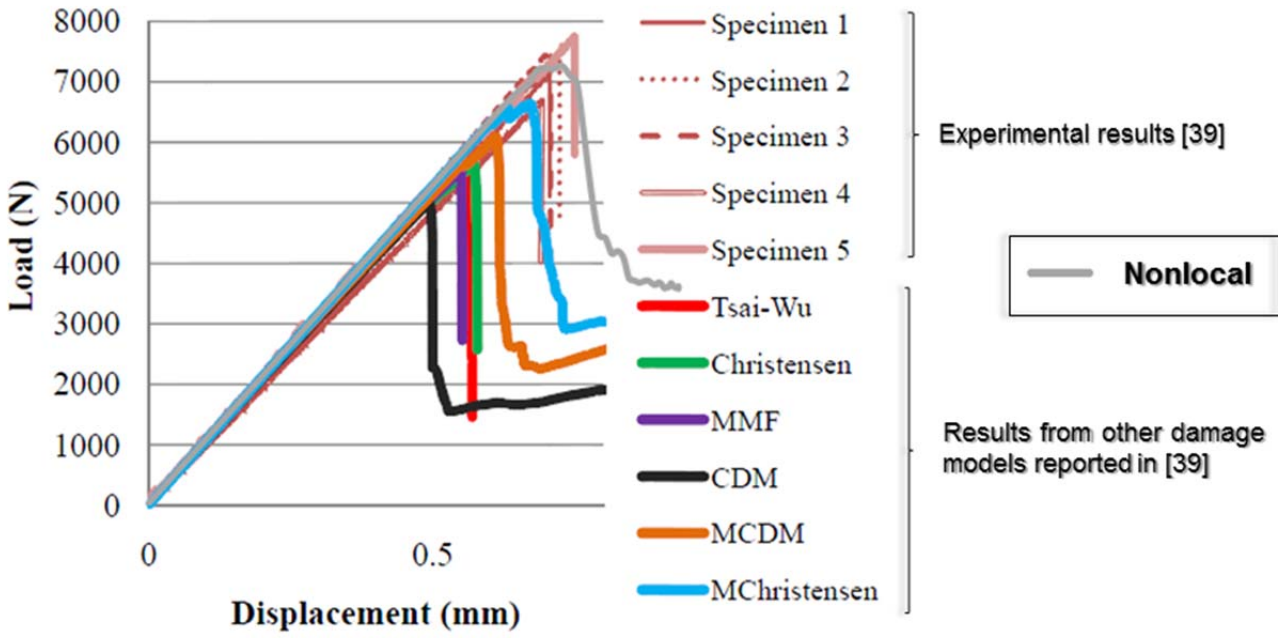

Fig. 6.14 - Predicted damage patterns for matrix and fiber failure from literature [39].

It is important to note that in the performed simulation no account was taken of the damage by delamination; so the result obtained through simulation in terms of ultimate load can overpredict the experimental results. Furthermore, the influence of the characteristic length on the force-displacement curve was not taken into consideration in this work nor the influence of parameters that in damage model regulates the nature of matrix and fibers (brittle or ductile nature). However the numerical result is presented exclusively for the qualitative purpose and to demonstrate the effectiveness of an approximated nonlocal approach.

Finally the problem of the strain localization in the absence of nonlocal approach is discussed. The strain localization is manifested by high strains in a narrow band, with a continuous transition to much lower strains in the surrounding parts of the body. A simulation was conducted to verify the problem. The damage model considered was always the same discussed in Chapter 5, but it was not enriched with nonlocal approach. Therefore the formation of strain localization bands near the notch root was numerically observed in the case examined if the local damage model was used. In Fig. 6.15 the damage which results from this localization is shown.

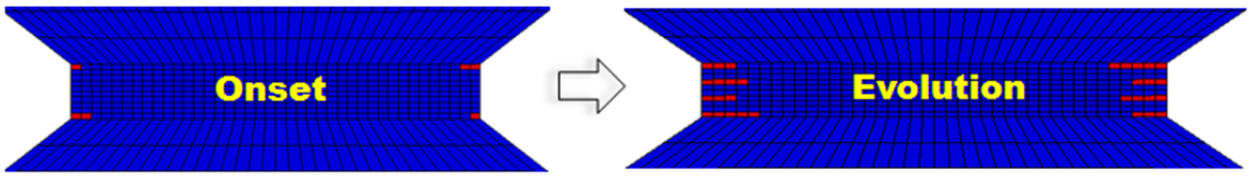

Fig. 6.15 - Notch detail : damage in the absence of nonlocal approach.

In conclusion, an approximated nonlocal approach introduced in a damage local model constitutes an regularization technique that allows to describe strain localization properly, preserve the well-posedness of the boundary value problem, obtain finite element results free from spurious discretization sensitivity and capture the correct damage pattern.

A last application of the damage model is presented in order to demonstrate the effectiveness of the proposed procedure for the damage prediction in laminate structures with geometric imperfections. In detail the structural response of a polymer matrix composite open-hole specimen under tensile loading is numerically investigated by means of ABAQUS/Explicit. This investigation was concerns with determining the response, type and extent of damage in composite structure as a function of applied load. The problem of a laminated composites containing an open hole was analyzed by Tai in [44]. The material under study is the unidirectional IM7/5250-4 and its mechanical properties obtained from [44] are given in Tab. 6.2. The laminate is quasi-isotropic with layup $[45/0/-45/90]_s$. The diameter of the hole is 12.7 mm and the width of the plate is 76.2 mm. The boundary conditions of the model are shown in Fig. 6.16. The finite element model is constructed with linear eight-node brick elements with reduced integration (C3DR8) and with a single element over the thickness of the ply, see Fig. 6.17. The tensile loading is imposed by enforcing the longitudinal displacement of all nodes along an edge.

Modulus in fiber direction E_1 (GPa)	172.4
Transverse moduli E_2= E_3 (GPa)	10.3
Shear moduli G_{12}=G_{13} (GPa)	5.52
Shear modulus G_{23} (GPa)	3.45
Poisson's ratios v_{12}= v_{13}	0.32
Poisson's ratio v_{23}	0.4
Longitudinal tensile strength X_T (MPa)	2826.5
Longitudinal compressive strength X_C (MPa)	1620
Transverse tensile strength Y_T (MPa)	65.5
Transverse compressive strength Y_C (MPa)	248
Out-of-plane tensile strength Z_T (MPa)	65.5
Out-of-plane compression strength Z_C (MPa)	248
Shear strength S_{12}=S_{13}=S_{23} (MPa)	122

Tab. 6.2 – Material properties of carbon/epoxy composite system.

The failure criteria in [45] are used in the material property degradation model to evaluate the damage onset in an individual composite ply. The criteria identify four distinct failure modes for a composite lamina: fiber tension, fiber compression, matrix tension, matrix compression failure.

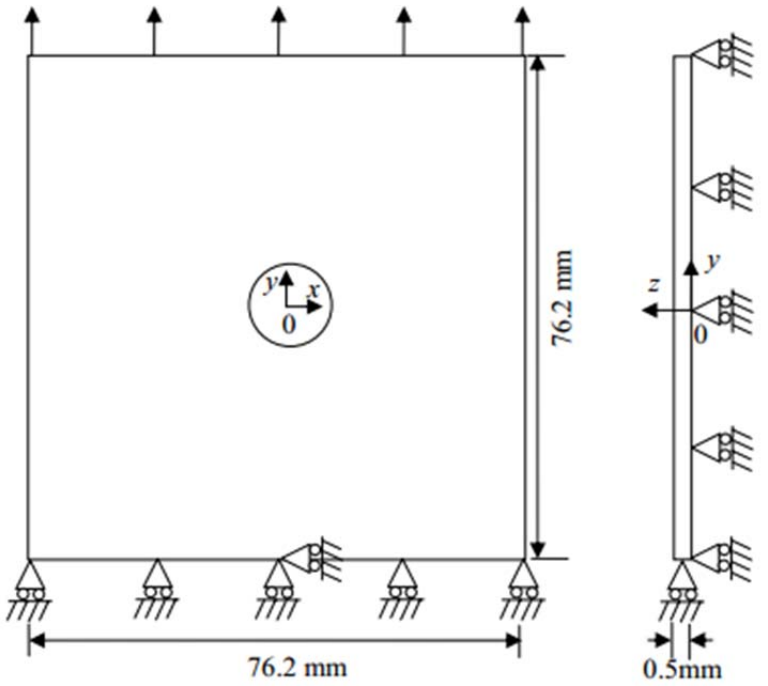

Fig. 6.16 – Geometry, dimensions and boundary conditions of open-hole specimen [44].

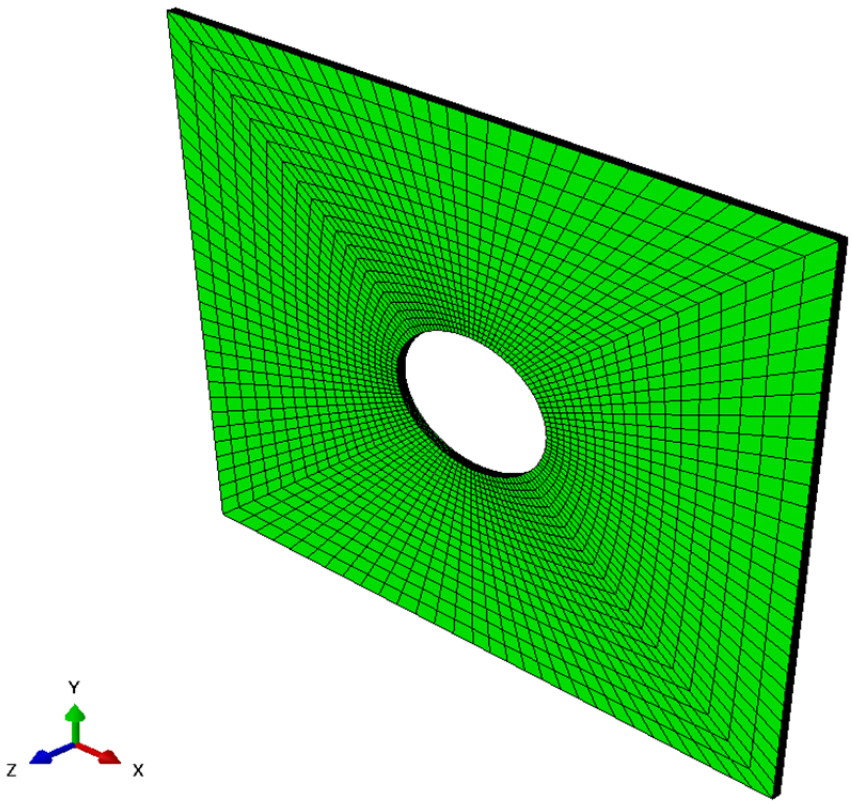

Fig. 6.17 – Finite element mesh for open-hole model.

The numerical results obtained by finite element simulation are compared with those present in the literature [44]. The ultimate load predicted by the implemented model, Fig. 6.18, is very closely results obtained both from experimental tests conducted on some specimens from author of the reference document and numerical simulation performed by the same through the use of a code based on “Element Failure Method” [46,47] and “Multi-continuum theory” [48].

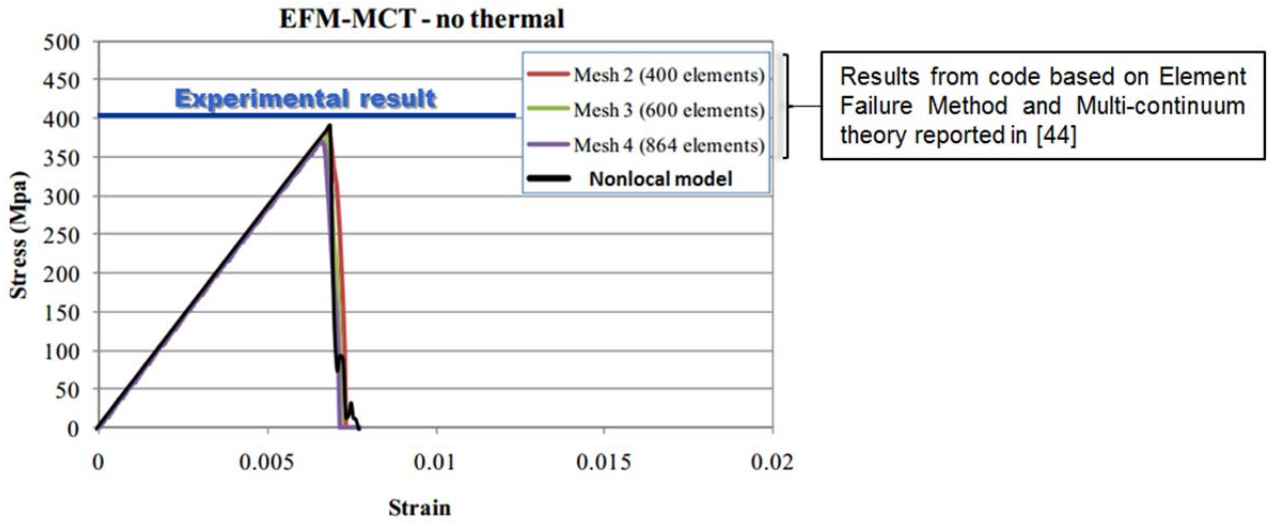

Fig. 6.18 – Comparison with experimental results and another damage model.

An example of progressive damage pattern predicted by the approximated nonlocal model is shown in Fig. 6.19; it is possible to note the development of tensile damage in the inner lamina when the load is transverse (90°) to the fiber direction.

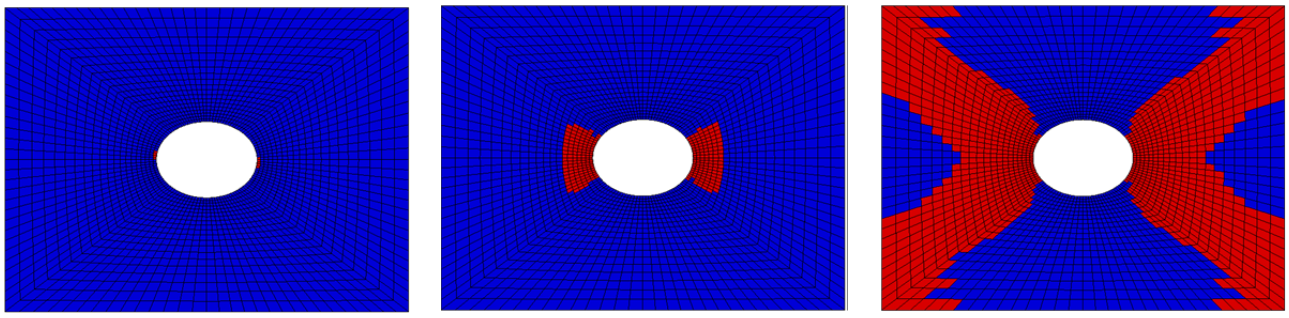

Fig. 6.19 - Development of matrix tensile damage for 90° ply.

References

[1] T. Belytschko, Z. P. Bazant, H. Y. Woong, T. P. Chang, “Strain softening materials and finite element solutions”, Computers & Structures, 1986, 23:163-180.

[2] K. V. Williams, A. M. Floyd, R. Vaziri, A. Poursartip, “Numerical Simulation of In-Plane Damage Progression in Laminated Composite Plates”, 12th International Conference on Composite Materials, Paris, France, 5-9 July 1999.

[3] L. B. Ilcewicz, T. H. Walker, D. P. Murphy, “Tension Fracture of Laminates for Transport Fuselage, Part 4: Damage Tolerance Analysis”, Fourth NASA/DOD Advanced Composite Tech. Conference, NASA CP-3229, 1993, pp. 265-298.

[4] I. Kongshavn, A. Poursartip, “Experimental Investigation of a Strain Softening Approach to Predicting Failure in Notched Fibre Reinforced Composite Laminates”, Composites Science and Technology, 1999, 59(1):29-40.

[5] D. Krajcinovic, “Continuum Damage Mechanics”, Applied Mechanics Review, 1984,37(1):1-6.

[6] J. L. Chaboche, “Continuum Damage Mechanics. I. General Concepts”, Journal of Applied Mechanics, 1988, 55(1): 59-64.

[7] S. Marfia, M. Jirásek, Regularized damage model based on nonlocal displacement field.

[8] M. V. Donadon, L. Iannucci, “An objectivity algorithm for strain softening material models”, The 9th International LS-DYNA Users Conference, 2006, Pages:15-43.

[9] E. Bittencourta, A. Needleman, “Rate-dependent nonlocal crystal plasticity: implementation and boundary layers”, Mecánica Computacional, Fracture, Fatigue and Damage Material Modeling, 2008, 27(16): 1177-1192.

[10] L. J. Sluys, R. De Borst, “Wave propagation and dispersion in a gradient-dependent medium”, Int. J. Solids & Structures, 1993, 30: 1153-1171.

[11] R. De Borst, “Damage, material instabilities and failure”, Encyclopedia of Computational Mechanics, Wiley, Chichester, 2004, 2(10), 2004.

[12] R.H.J. Peerlings, R. de Borst, W. A. M. Brekelmans, J. H. P. de Vree, I. Spee, “Some observations on localization in non-local and gradient damage models”, Eur. J. Mech., A/Solids, 1996, 15(6):937-953.

[13] J.D. Janssen, P.J.G. Schreurs, P.H.J. Vosbeek, “A non-local constitutive model describing localization of deformation based on micromechanics”, WFW-report: 93.114, 1993.

[14] X. Lua, J. P. Bardet, M. Huang, “Numerical solutions of strain localization with nonlocal softening plasticity”, Comput. Methods Appl. Mech. Engrg., 2009, 198:3702–3711.

[15] A. Needleman, “Material rate dependence and mesh sensitivity in localization problems”, Comp. Meth. in Appl. Mech. and Engineering, 1988, 63:69-85.

[16] H. L. Schreyer, M. K. Neilsen, “Analytical and numerical tests for loss of material stability, Int. J. Numer. Methods Engrg.”, 1996, 39(10):1721–1736.

[17] L. J. Sluys, R. D. Borst, “Wave propagation and localization in rate dependent crack medium, model formulation and one-dimensional examples”, Int. J. Solids Struct., 1992, 29:2945–2958.

[18] E. Cosserat, F. Cosserat, “Theorie des Corps Deformable”, Hermann, Paris, 1909.

[19] A. Khoei, S. Yadegari, M. Anahid Three-dimensional modeling of strain localization in Cosserat continuum theory, IJCE, 2006; 4:176-191.

[20] M. I. Alsaleh, “Numerical modeling of strain localization in granular materials using Cosserat theory enhanced with microfabric properties”, Ph.D. thesis, 2004.

[21] M.I. Alsaleh, G.Z. Voyiadjis, K.A. Alshibli, Modelling strain localization in granular materials using micropolar theory: mathematical formulations, Int. J. Numer. Anal. Methods Geomech, 2006, 30:1501–1524.

[22] E. C. Aifantis, “The physics of plastic deformation”, Int. J. Plasticity, 1987, 3:211-247.

[23] Z. Bažant, “Mechanics of distributed cracking”, Appl Mech Rev, 1986, 39:675-705.

[24] R. de Borst, H.B. Mühlhaus, “Gradient-dependent plasticity: formulation and algorithmic aspects”, Int. J. Numer. Methods Engrg., 1992,35:521–539.

[25] C. Comi, “Computational modelling of gradient-enhanced damage in quasibrittle materials”, Mech. Cohesive Frict. Mater. 1999, 4(1):17–36.

[26] L. Strömberg, M. Ristinmaa, “FE-formulation of a nonlocal plasticity theory”, Comput. Methods Appl. Mech. Engrg., 1996,136:127–144.

[27] C. Comi, A non-local model with tension and compression damage mechanisms, Eur. J. Mech. A/Solids, 2001, 20:1–22.

[28] Z. P. Bažant, M. Jirásek, Nonlocal integral formulations of plasticity and damage: survey of progress, J. Engrg. Mech., ASCE, 2002, 128(11):1119–1149.

[29] Z. P. Bažant, T. Belytschko, T.P. Chang, Continuum theory for strain softening, J. Engrg. Mech., ASCE , 1984,110(1):1666–1692.

[30] Z. Bažant, M. Jirásek, ”Nonlocal Integral Formulations of Plasticity and Damage: Survey of Progress”, J. Eng. Mech., 2002, 128(11):1119–1149.

[31] A. Hillerborg, et al, “Analysis of crack formation and crack growth in concrete by means of fracture mechanics and finite elements”, Cement and Concrete Research, 1976, 6:773-782,.

[32] Z. Bazant, “Crack band theory for fracture of concrete”, Materiaux et Constructions, 1983, 16(93).

[33] J. M. A. Cesar de Sa, F. X. C. Andrade, F. M. Andrade Pires, “Theoretical and numerical issues on ductile failure prediction - An overview”, Computer Methods in Materials Science, 2010, 10(4):279–293.

[34] V. Tvergaard, A. Needleman, “Analysis of cup-cone fracture in a round tensile bar”, Acta Metallurgica, 1984, 32:157–169.

[35] M. Jirásek, “Damage and Smeared Crack Models”, Numerical Modeling of Concrete Cracking, CISM International Centre for Mechanical Sciences, 2011, 532:1-49.

[36] J.M. A. Cesar de Sa, F. X. C. Andrade, F. M. Andrade Pires, “Theoretical and numerical issues on ductile failure prediction - An overview”, Computer Methods in Materials Science, 2010, 10(4):279–293.

[37] V. Tvergaard, A. Needleman, “Effects of nonlocal damage in porous plastic solids”, International Journal of Solids and Structures, 1995, 32(8/9):1063-1077.

[38] G. Borino, B. Failla, F. Parrinello, “Un modello di danno non locale per l’analisi a collasso di strutture di materiale quasi fragile”, Dipartimento di Ingegneria Strutturale & Geotecnica, DISeG.

[39] D. C. Pham, X. S. Sun, V. B. C. Tan, B. Chen, T. E. Tay, “Progressive Failure Analysis of Scaled Double-Notched Carbon/Epoxy Composite Laminates”, International Journal of Damage Mechanics November, 2012, 21(8):1154-1185.

[40] F. Pan, J. Zhu, A. O. Helminen, R. Vatanparast, NOKIA Inc., “Three Point Bending Analysis of a Mobile Phone Using LS-DYNA Explicit Integration Method”, 9th International LS-DYNA Users Conference.

[41] Simulia, Dassault Systèmes , “Automobile Roof Crush Analysis with Abaqus”, Abaqus Technology Brief, 2007.

[42] J. T. Ozbol, R. Eligehausen, “Analysis of reinforced concrete beams without shear reinforcement using non-local microplane model”, RILEM proceedings 13, 1991, ISBN 0-419-15870-7, S. 919-930.

[43] R. M. Christensen,“Stress Based Yield/Failure Criteria for Fiber Composites,” Int. J. Solids Structures, 1997, 34:529-543.

[44] T. E. Tay , “MCT-EFM for Composite Structural Failure Analysis”, National University of Singapore, 2010.

[45] A. Satyanarayana, A. Przekop, “Predicting Failure Progression and Failure Loads in Composite Open-Hole Tension Coupons”, NASA/CR–2010-216700, Hampton, Virginia.

[46] T. E. Tay, G. Liu, V. B. C. Tan, “Damage Progression in Open-hole Tension Laminates by the SIFT-EFM Approach”, Journal of Composite Materials, 2006, 40(11):971-992.

[47] T. E. Tay, S. H. N. Tan, V. B. C. Tan, J. H. Gosse," Damage progression by the element-failure method (EFM) and strain invariant failure theory (SIFT)", Composites Science and Technology, 2005, 65(6):935–944.

[48] A. C. Hansen, M. R. Garnich, "A multicontinuum theory for structural analysis of composite material systems", Composites Engineering, 1995, 5(9):1091–1103.

CONCLUSIONS

In this research are examined and developed some of the most recent studies in the field of damage prediction and the issues associated to the application of these methods to composite structures are discussed. In detail the objective of the conducted research program is to enhance the damage prediction model capabilities for unidirectionally reinforced continuous carbon fiber reinforced polymers.

For this purpose, a cohesive-frictional model for the prediction of interlaminar damage and a non-local constitutive model for intralaminar progressive damage simulation in composite laminated structures are defined. The proposed constitutive models are then implemented in the commercial finite element software ABAQUS which has demonstrated to be a powerful tool for implementation of FORTRAN Vectorized User-Material (VUMAT) and for the simulation of discontinuous and unstable events.

The results obtained from research concern mainly the interfacial damage from low energy impact in the presence of friction and the numerical solution to the problem of the strain localization in the presence of material softening. They have helped to highlight the following aspects: a) the importance of a cohesive-frictional model used to predict the interlaminar damage induced by impact in composite laminates; b) the importance of a constitutive model based on the assumption of nonlocal continuous for the correct prediction of the damage pattern for matrix and fibers in the various geometric and loading conditions of the structure in composite material; c) a numerical procedure for the implementation of a non-local model for the explicit solver of the commercial software of finite element analysis ABAQUS.

The activity of the thesis also introduces additional objectives to be achieved by future research as a detailed study of the delamination phenomenon at interfaces closer to the region of impact typically little discussed; a rigorous study of friction in laminated composite structures supported by a wide

experimental campaign; the investigation on the characteristic length which play important role in the proposed nonlocal damage model and in general the enhancement of the discussed damage models to make them capable of simulating a wider range of damage propagation problems in laminated composites. The tools to achieve the above remarks are provided in this thesis and look forward to new uses.

ACKNOWLEDGEMENTS

I wish to express my sincere acknowledgement first of all to my tutor Prof. Lecce, inspiring professor, mentor, and advisor. It has been an honor to work for him.

My grateful thanks also go to my friends and people in my department for their support throughout my academic life.

Finally, a much deserved acknowledgement of my parents, whose encouragement and personal sacrifices laid the foundation for my education.

Last but not least I gratefully thank my uncles and my prospective wife Isa for their everlasting and unconditional love.